Initial Radiobiological Experiments with Accelerated Nitrogen Ions at the Bevatron

Donner Laboratory and
Lawerence Berkeley Laboratory
University of California
Berkeley, California

LBL-529
C.1

DISCLAIMER

LBL-529

INITIAL RADIOBIOLOGICAL EXPERIMENTS WITH ACCELERATED NITROGEN IONS AT THE BEVATRON

prepared for

Committee of Space Biology and Medicine

and

Radiobiological Advisory Panel of the
Space Science Board of the
National Academy of Sciences

December 1971

Donner Laboratory and
Lawrence Berkeley Laboratory
University of California
Berkeley, California 94720

Work done under the auspices of the
U.S. Atomic Energy Commission and the
National Aeronautics and Space Administration

INITIAL RADIOBIOLOGICAL EXPERIMENTS WITH ACCELERATED NITROGEN IONS AT THE BEVATRON

Contents

INITIAL RADIOBIOLOGICAL EXPERIMENTS WITH ACCELERATED NITROGEN IONS AT THE BEVATRON

INTRODUCTION

In a four-week period during August, 1971, nitrogen 7+ ions were accelerated to energies of up to 39 BeV for physics research and to about 3.8 BeV for biomedical research. These experiments and parallel work at the Princeton accelerator proved the feasibility of reproducing at ground level a significant part of the spectrum of cosmic rays with the same energies as most of them occur in space. At Berkeley, we plan to accomplish this goal by using the existing Super-Hilac as pre-accelerator and injecting its low-energy heavy ion beams for synchrotron acceleration into high kinetic energies (the Bevalac project).

The heavy ion beams will allow exploration of the biological effects of cosmic ray particles needed for longterm manned space flights to other planets. The use of the particles, as earlier suggested by us, will perhaps lead to improved methods of cancer therapy. Most important, heavy ion radiobiology could permit fundamental contributions to many diverse fields, including our understanding of functions of the nervous system, of differentiation and development, of carcinogenesis and mutagenesis, and the general interaction of radiation with matter.

Initial reports on the method of acceleration and on particle and radiological physics were published in the December 10, 1971, issue of Science magazine and in Lawrence Berkeley Laboratory Report No. 345.

Some of the biological studies are presented in the following pages. The reader should bear in mind that results are preliminary and must be re-studied in more detail. The accelerator time available for these studies was about one week at a relatively-low beam intensity of about 10^5 particles per beam pulse; several of the experiments were planned with this low beam intensity in mind.

The biological studies described here were made possible through the cooperation of several specialized groups and individuals. These include: Edward Lofgren and the Physics and Engineering Groups at the Bevatron; Herman Grunder, who led the Accelerator Development Group; and Walter Hartsough in charge of beam operations. Albert Ghiorso originally suggested the "Bevalac" approach, and for several years biological research was carried out with the low-energy heavy ion beams at the HILAC, which have led directly to the current work. A cosmic ray physics group led by Harry Heckman has aided the radiological physics effort. Fred Goulding and Frank Upham were responsible for much of the instrumentation developed for radiological physics.

Since 1947 biophysical research has been carried out with proton and helium beams of the 184-in. cyclotron, with the cooperation of Robert Thornton and his group. Under leadership from John H. Lawrence, Donner Laboratory's Director Emeritus, and James Born, current Director, a medical group has developed experience with radiobiologic aspects and special therapeutic approaches. Finally, Edwin McMillan, Director of LBL gave full support to this project and cooperated in the first biological work with the accelerated heavy

nitrogen ions by being the first subject exposed to beam particles in the "light flash" experiments reported here.

It is a pleasure to acknowledge the support of the Atomic Energy Commission and of the National Aeronautics and Space Administration.

December, 1971 The Authors

EXPERIMENTAL SETUP AND PHYSICAL MEASUREMENTS OF A HEAVY ION BEAM FOR INITIAL BIOLOGICAL IRRADIATIONS AT THE BEVATRON

by

J. T. Lyman, J. Howard, H.D. Maccabee, M.R. Raju, J. Sperinde, R. Walton
G. P. Welch and C.A. Tobias

Abstract

The recent acceleration of nitrogen-14 ions to a very high energy at the Bevatron, several hundred MeV/amu (1-3) has for the first time provided an opportunity to use heavy ion beams capable of deep penetration within a biologic object for investigations ranging from fundamental radiobiology to radiation therapy. Described here is the physical layout of the beam transport system, as well as the experimental area at the Bevatron during initial experiments. Also included are results of the initial dosimetry measurements.

A schematic plan view of the Bevatron is shown in Figure 1. The nitrogen ions were produced in the ion source and then accelerated through the LINAC with a +5 charge. The beam, then with an energy of 5 MeV/amu, was passed through a stripping foil in order to obtain ions with a +7 charge (fully stripped). These fully stripped ions were then injected into the Bevatron synchrotron ring and accelerated to an energy of several hundred MeV/amu. The beam was then extracted from the machine and passed through channel 2 of the EPB (external proton beam) transport system. Channel 2 is shown in detail in Figure 2. The beam was focused by quadrapole magnets and steered to the correct position by the bending magnets. The beam passed out of the EPB vacuum system through the center port of X2M7 and passed down the axis of a 6-foot optical bench. The

optical bench, which was constructed from an 8-inch-wide piece of steel channel, was used to support the dosimetry equipment and the biological samples which were irradiated.

A 12 x 24-ft modular room to be used as a counting and control room by experimenters and a 12 x 12-ft room to be used as an animal preparation area were set up just outside the door to the experimental cave. This location was about 100 ft from the optical bench.

The primary beam monitor, which was supplied by Dr. Heckman's group for the benefit of the operators in the main control room and for all the experimenters, was a 1/4-in.-thick plastic scintillator 2 in. square and was connected to a RCA 8575 photomultiplier tube. The number of particles detected by this scintillator was displayed in the main control room and in the experimental counting area.

Additional monitoring of the beam was in many instances accomplished with ionization chambers. Three types of parallel plate ionization chambers were used at various times. The usefulness of the ionization chambers was at times limited by the inherent leakage current of the chambers. A quadrant ionization chamber with its collecting electrodes connected to four Keithley picoammeters was used to monitor beam position. An output which was derived from the appropriate sums and differences of current detected was displayed on an x-y oscilloscope. Because of the very low beam current, this device was only able to provide a qualitative indication on a pulse basis of the beam position. This was unfortunate, because, on occasions, the beam did shift its position due to inadequate

regulation of some magnet power supplies, while samples were being irradiated. Large area, parallel plate, ionization chambers were useful as total beam monitors, since these detectors respond to ionization caused by all charged particles, while the monitor scintillator gain was set so that it would not count particles that lost an insufficient amount of energy. At times, this threshold may have been as high as 120 MeV for the 1/4-in.-thick scintillator. The third type of ionization chamber used was one which had a small collector area (1.27 cm diameter) surrounded by a large guard ring. This chamber was used to monitor the total beam that passed through its collector electrode. The chamber was positioned on the optical bench, so that its axis coincided with the beam axis.

Beam alignment was accomplished by exposing type 57 Polaroid film to the beam and then either making the necessary adjustments by changing magnet currents or by moving the optical bench axis to a more appropriate position. Film exposures were obtained with very low doses at times by using a Polaroid XR-7 Land Diffraction Cassette #57-1. This cassette contains a high-speed, high-resolution phosphor-coated intensifying screen. Other intensifying screens which were less grainy were also used in another specially constructed cassette, and exposures were made at higher dose levels with the film exposed in its paper envelope, unintensified.

Beam profile determinations were made by exposing DuPont Cronex 4 x-ray film to the beam and subsequently processing the film in a Corsair automatic film processor. The film could then be immediately scanned with a MacBeth Quantalog Densitometer with a 1 mm resolution.

The optical density profiles along a horizontal and a vertical axis are shown in Figure 3 for films exposed at the high-energy portion of the beam at F2 and at the Bragg peak position of the beam (about 1 mm from F2). The beam size as determined by the optical density (FWHM) was 0.3 by 2.0 cm and 1.0 by 2.0 cm at the two respective locations.

The beam was degraded in energy for the different experiments by a variable-thickness water absorber. The water was contained in an aluminium cylinder with Lucite end windows. One of the windows was the end of a piston which was moved remotely from the counting area, an encoder providing a position readout to the nearest 0.25 mm. The diameter of the Lucite windows was 15 cm , and the total travel of the piston was 30 cm.

A Bragg curve is a plot of the relative specific ionization of a beam of particles, plotted as a function of the thickness of the absorber that the beam has traversed (4). It can be obtained experimentally by taking the ratio of current from two ionization chambers. The first chamber, called the monitor chamber, is placed before a variable absorber, and the second chamber behind the absorber. The current from the two chambers for this measurement was integrated and measured with two E-H electrometer systems connected to digital readouts. The Bragg curve obtained for the nitrogen beam is shown in Figure 4. It was determined that the total water equivalent thickness of all the materials between the Bevatron machine vacuum and the center of the second ionization chamber when the water absorber was set at its minimum thickness was 1.91 ± 0.05 g/cm^2 *

*The data given here only differ from those in Ref. (3) in amount of absorber interposed between the vacuum of the Bevatron and the second ionization chamber. Recently, we were able to estimate this more accurately than in Ref. (3). The curves given here indicate abt. 0.7 g/cm^2 less penetration of the particles than indicated in Ref. (3). The theoretical calculations are new in this paper.

(see Table I). This thickness has therefore been added to variable-absorber values before plotting the data.

Integral and differential range curves were also obtained with a three-scintillator system and its associated electronics. It was determined that, for these measurements, the total nonvariable water equivalent thickness before the third scintillator (S1) as well as the number of S1-S2 coincident events and the S1-S2-S3 coincident events were recorded. Figure 5 is a plot of some of the data obtained. The data were normalized and corrected for the additional absorber thicknesses. Discriminator settings were set so that most of the particles that cannot produce a pulse height as high as that produced by the full energy beam will not be counted. But a stopping carbon ion for an example can produce a pulse larger than a high-energy nitrogen ion, so there is some ambiguity as to the identity of the stopping particle, since the incoming nitrogen particle may fragment in flight. It was originally intended that these measurements would be made with a 16-channel silicon detector counter telescope which would have provided particle identification, but an unexpected time structure of the beam spill along with the telescope response time and the limited available beam time made it necessary to postpone these measurements.

From a comparison of the position of the Bragg peak, its height and the rapid falloff of dose beyond the peak with the predictions of the shape of the Bragg curve using the computer programs BRAGG (5) and BRSEC, which are based upon Dr. Steward's range-energy predictions for heavy ions (6), it would appear that the nitrogen ions were

accelerated to about 266 MeV/amu and probably with an energy spread less than 0.5MeV/amu. The total dose curve calculated by the BRSEC program is the summation of the primary ion Bragg curve (as is calculated using BRAGG), and Bragg curves for secondary ions, the type and number of which are chosen by the programmer.

Figure 6 shows the Bragg curve data plotted with calculated curves of the primary, secondary and total dose. The total dose curve was fitted to the data by the choice of energy, energy spread and the cross section for an interaction of the primary ions, plus the type and number of fragments produced in an interaction. The fragments were all assumed to have the same velocity as the incoming nitrogen ion. Added to the primary curve is an energy of 30 MeV per interaction to account for some locally deposited dose at the interaction site. It is also assumed that the secondary particles do not have nuclear interactions. Table 2 gives the types of fragments included in the calculation and the number of each type per interaction. Protons were not included in the calculation, because they would have the same range as the Helium-4 ions; therefore, their inclusion would have only added to the computation time. The choice of parameters used is not the only possible choice which would give a satisfactory solution, but it is in reasonable agreement with particle identification measurements made with a total of about 7 g/cm^2 water-equivalent thickness of material (5 g/cm^2 of water plus 2 g/cm^2 water-equivalent thickness). The assumptions of the velocity of the fragments is in agreement with the fragmentation measurements of nitrogen at 2 GeV/amu by Heckman (2).

If the assumption is made that the scintillators must absorb 60 MeV before a countable pulse is obtained (the incoming full-energy nitrogen ion will lose about 70 MeV in the scintillator), then carbon ions should be countable for most of their path. The efficiency for counting particles with smaller charges will increase as the particles slow down. In Figure 7, the integral range data have been plotted with the calculations for the primary ion flux, for the flux of all particles with z (nuclear charge) greater than 3, 4, 5 and 6.

The above data were obtained during August, 1971, a few days after the acceleration of N^{7+} beams became possible. The data should be viewed as preliminary: the radiological properties of the heavy particles will be explored in much more detail in the future. It is clear, however, that our previous estimates for particle penetration and ionization properties were nearly correct, and that heavy ion beams will be useful for basic and applied biomedical research.

Acknowledgments

We wish to thank Drs. H. Heckman and D. Greiner and Messrs. F. Bieser and P. Lindstrom for their beam diagnostics and instrumentation and general assistance. We are indebted to the Physics Group at the Bevatron, particularly to Ed Lofgren, H. Grunder and W. Hartsough for making these experiments possible.

REFERENCES

1. Grunder, H.A., Hartsough, W.D. and Lofgren, E.J., Acceleration of heavy ions at the Bevatron, Science 174, 1128-1129 (1971).

2. Heckman, H.H. et al, Fragmentation of nitrogen-14 nuclei at 2.1 GeV per nucleon, Science 174, 1130-1131 (1971).

3. Tobias, C.A. et al, Radiological physics characteristics of the extracted heavy ion beams of the Bevatron, Science 174, 1131-1134.

4. Raju, M.R., Lyman, J.T., Brustad, T. and Tobias, C.A., Heavy charged particle beams, in Radiation dosimetry, v. 3, 151-193 (1969).

5. Litton, G.M., Penetration of high-energy heavy ions with the inclusion of coulomb, nuclear and other stochastic processes, Ph.D. Thesis, UCRL-17392 (1967).

6. Steward, P.G., Stopping power and range for any nucleus in the specific energy interval 0.01 to 500 MeV/amu in any nongaseous material, Ph.D. Thesis, UCRL-18127 (1968).

Table 1

Absorber	Thickness (inches)	Material	Water equivalent
Bevatron exit window	.005	aluminum	.027
F1 air gap	22	air	.063
EPB entrance window	.002	Al	.011
EPB vacuum system	1457.5	air at (10^{-F} Torr)	<.001
EPB channel II exit window	.010	Al	.053
Scintillator and light-tight wrapping	.250	plastic	.734
	.002	Al	.011
	.012	paper	.045
Ionization chamber	.012	Mylar	.040
Miscellaneous paths	26	air	.074
Windows of water absorber (2)	25	Lucite	.734
Minimum water path	.040	water	.102
One-half ion chamber	.006	Mylar	.020

Table 2

Secondary particles	No. per interaction
Nitrogen-13	.06
Carbon-12	.24
Boron-11	.06
Beryllium-9	.06*
Helium-4	1.5**

*Not included in dose calculation.

**Not included in integral range calculation.

FIGURE CAPTIONS

Fig. 1. Schematic plan view of the Bevatron.

Fig. 2. Schematic plan view of EPB channel 2.

Fig. 3(a). Optical density profiles at the high energy portion of the beam. Fig. 3(b). Optical density profiles in the stopping region of the beam.

Fig. 4. Bragg curve of the nitrogen ion beam as measured in water. The inset shows diagramatically the experimental setup.

Fig. 5. Integral and differential range curves measured in water. The inset shows diagramatically the experimental setup.

Fig. 6. The experimental Bragg curve data plotted with computer calculated curves showing estimates of the dose due to the primary ions, the secondary ions and the total dose.

Fig. 7. The experimental integral range data plotted with the computer calculated primary ion flux, the total of all particles with a charge greater than four.

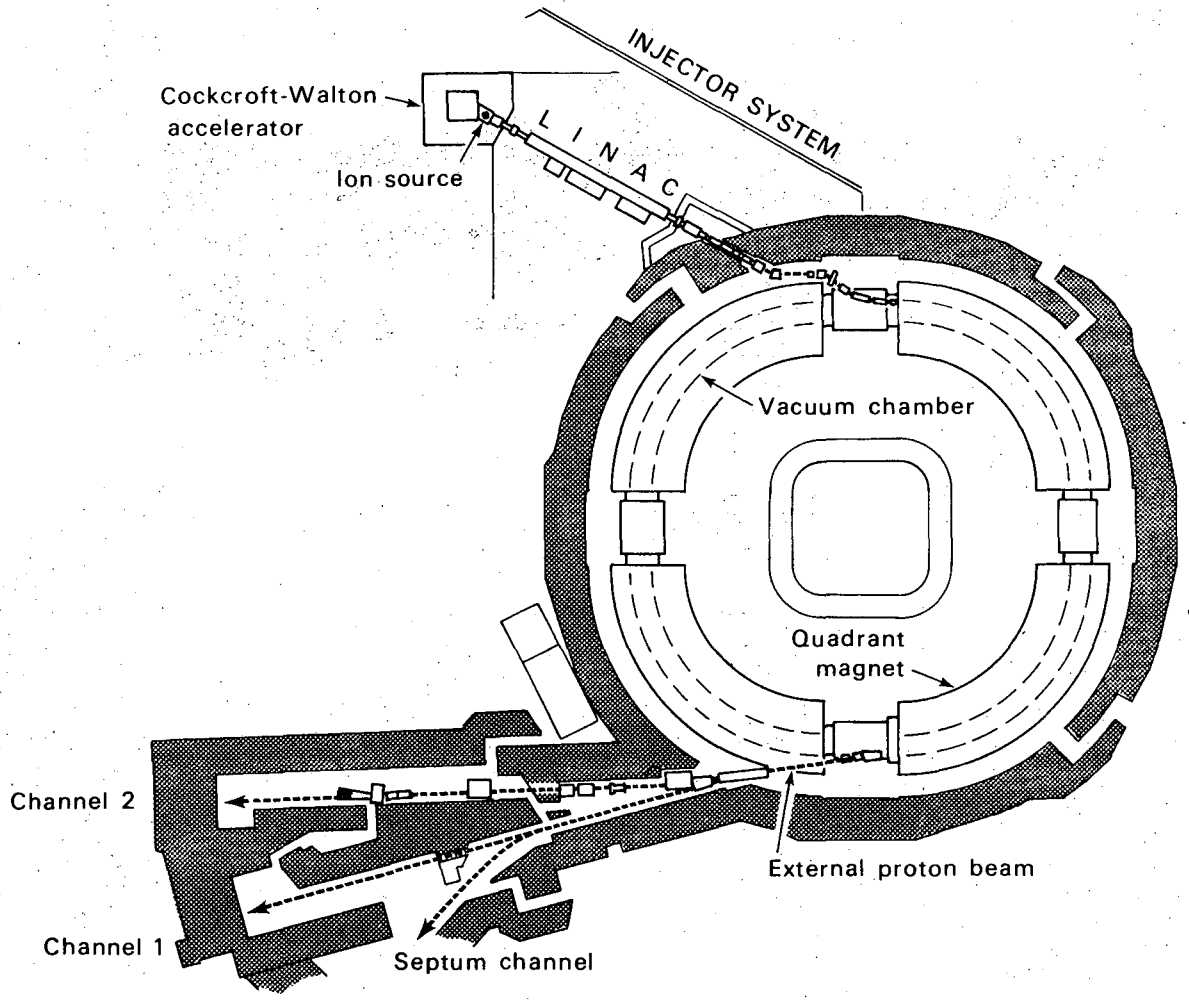
INJECTOR SYSTEM
Cockcroft-Walton accelerator
Ion source
L I N A C
Vacuum chamber
Quadrant magnet
Channel 2
External proton beam
Channel 1
Septum channel
DBL 721 5108

Fig. 1

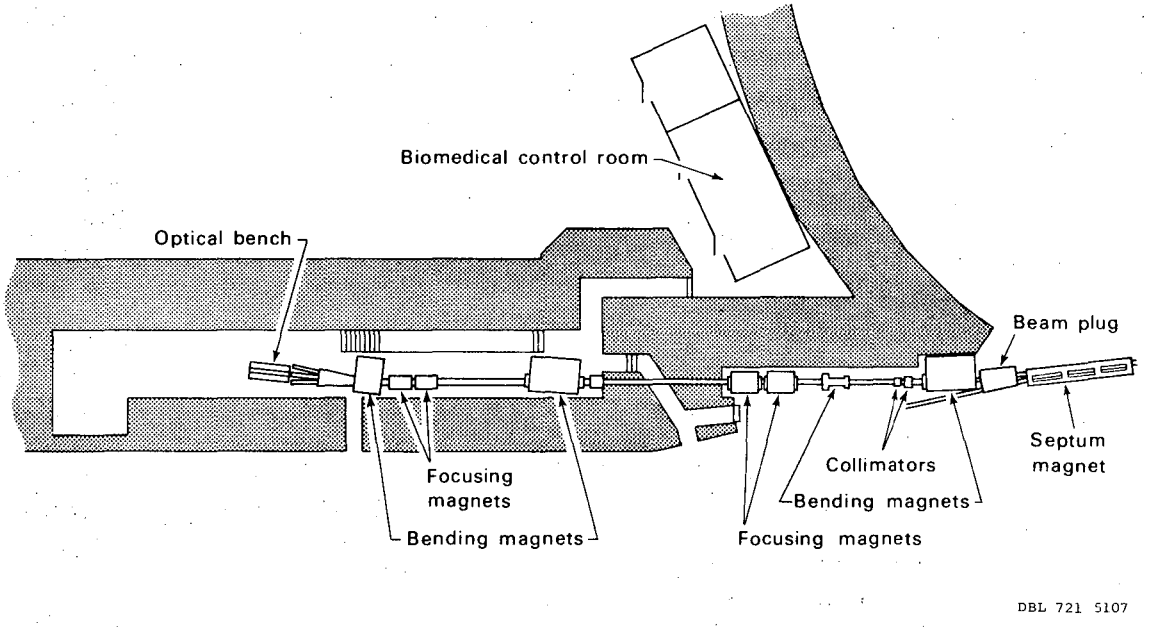
Biomedical control room
Optical bench
Beam plug
Septum magnet
Collimators
Bending magnets
Focusing magnets
Focusing magnets
Bending magnets
DBL 721 5107

Fig. 2

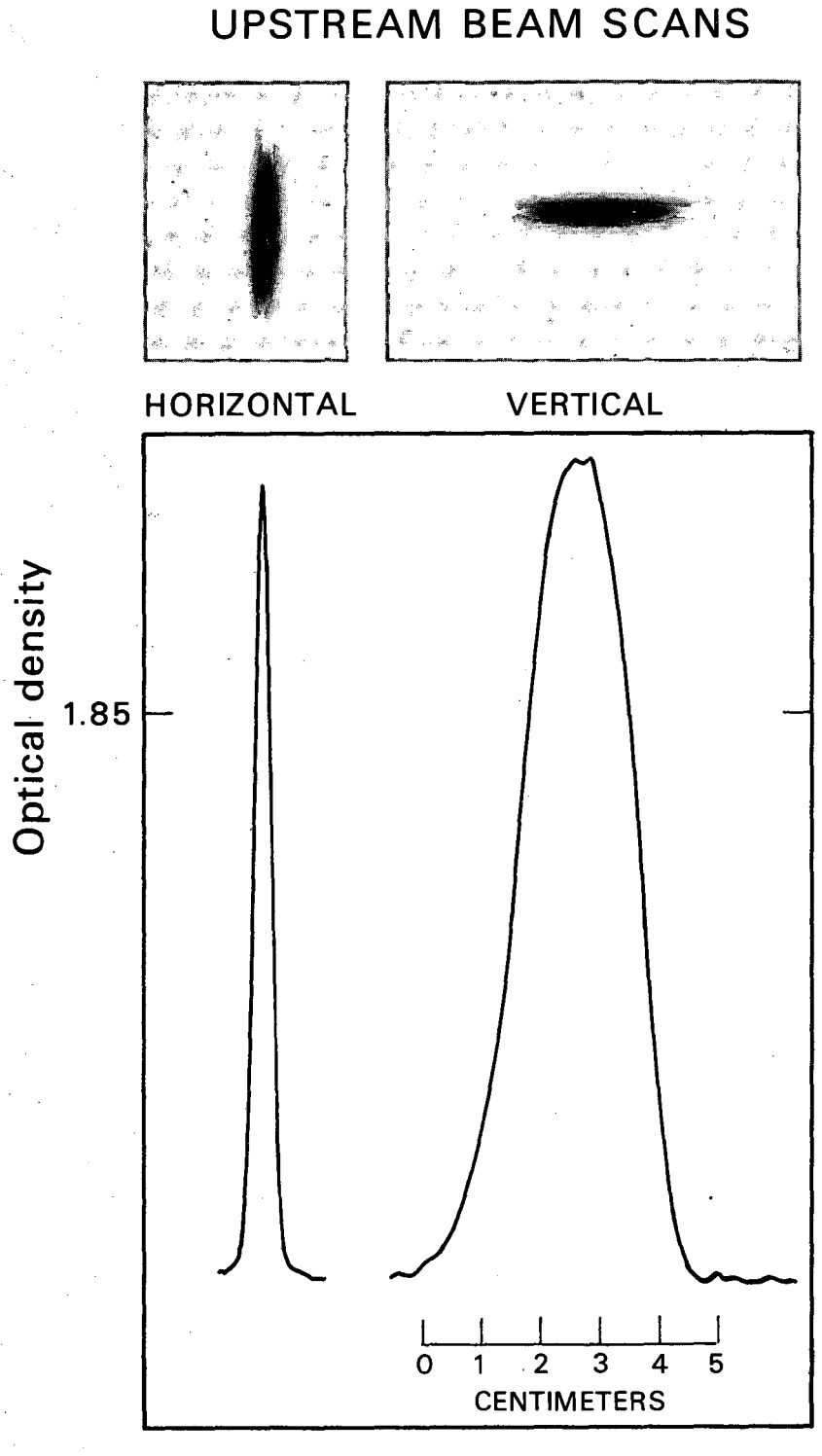
UPSTREAM BEAM SCANS
HORIZONTAL
VERTICAL
Optical density
1.85
0 1 2 3 4 5
CENTIMETERS
DBL 721 5106

Fig. 3(a)

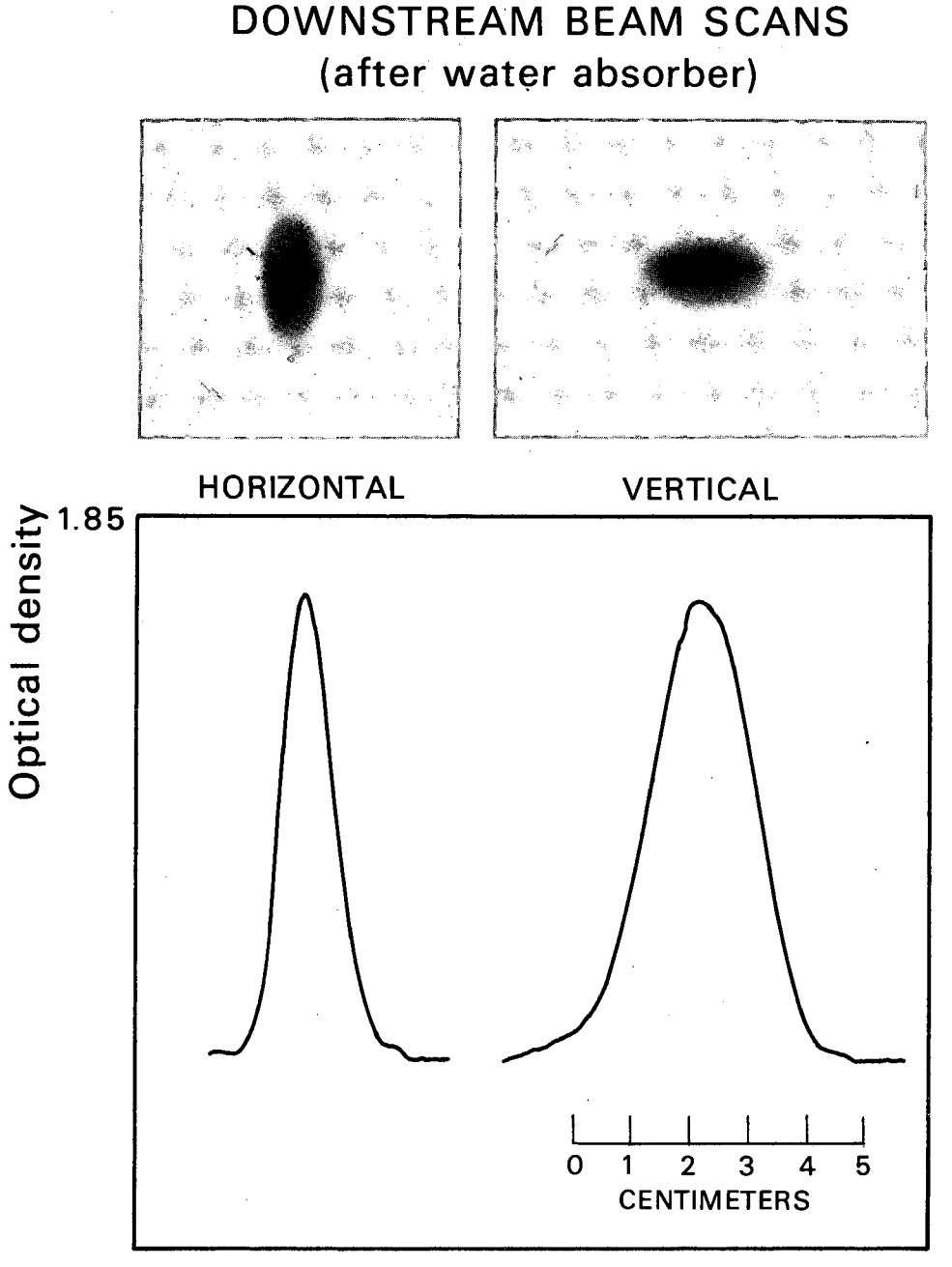
DOWNSTREAM BEAM SCANS
(after water absorber)
HORIZONTAL
VERTICAL
Optical density
1.85
0 1 2 3 4 5
CENTIMETERS
DBL 721 5105

Fig. 3(b)

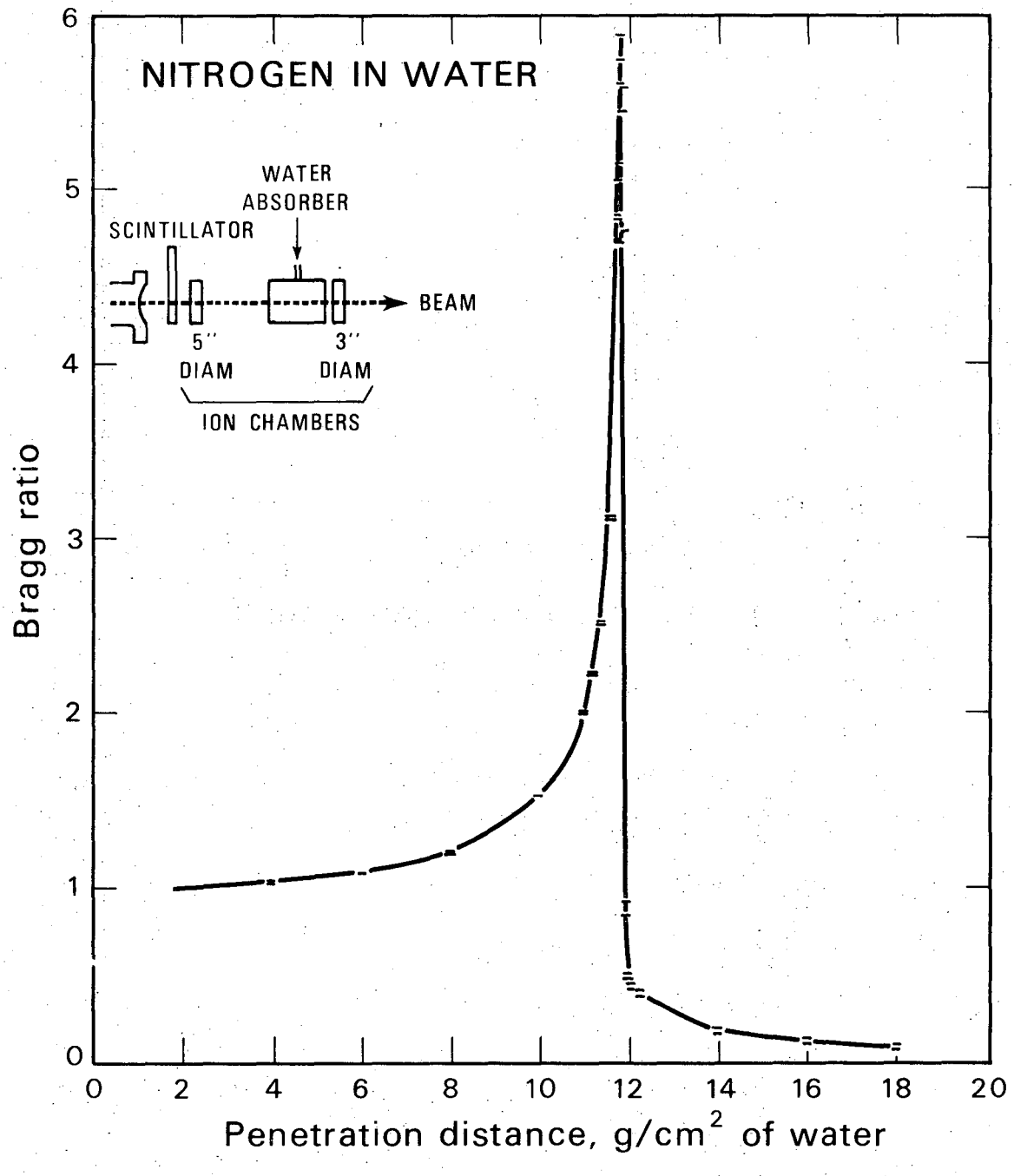

DBL 721 5109

Fig. 4

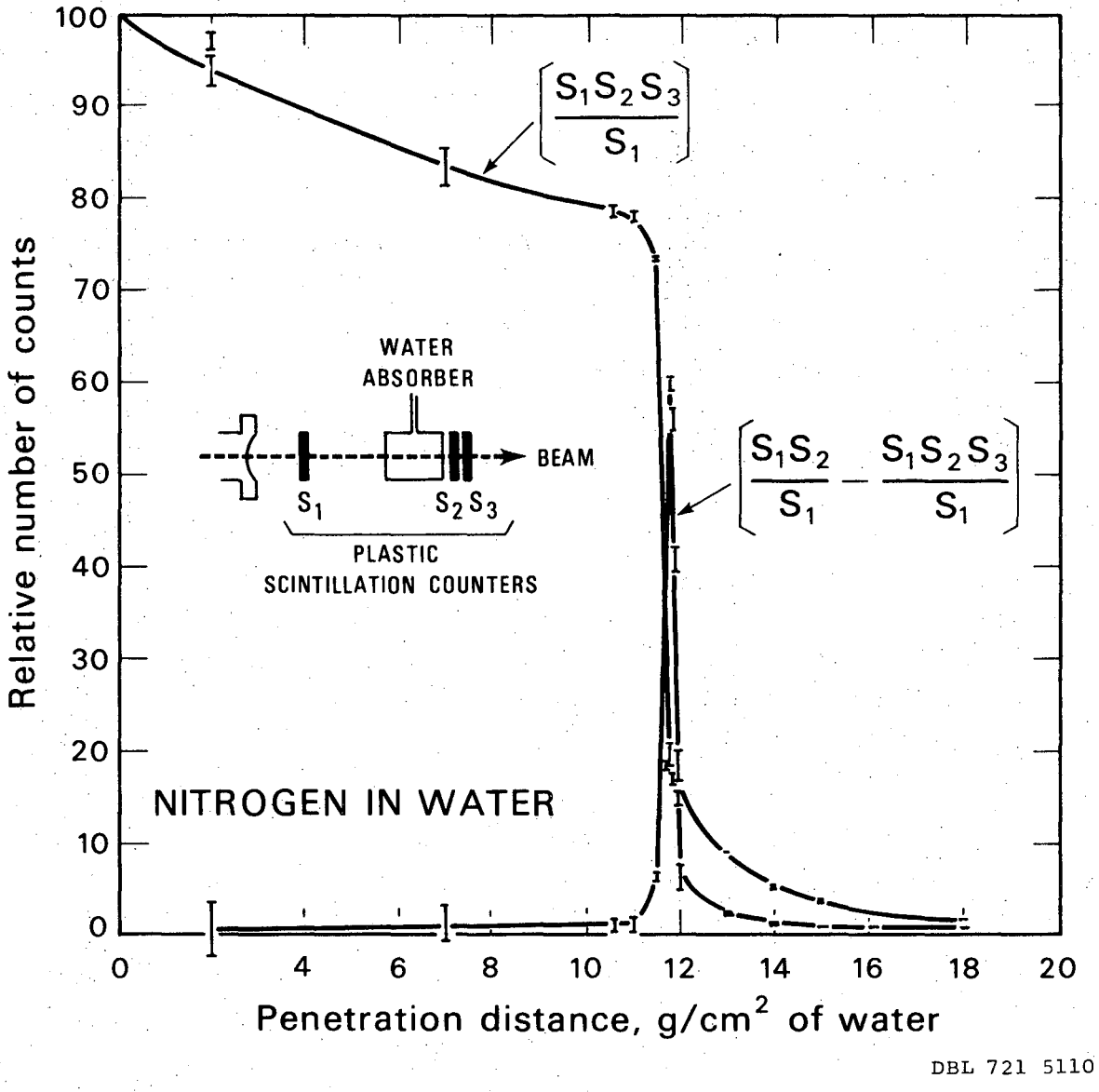
Relative number of counts
100
90
80
70
60
50
40
30
20
10
0
0
4
6
8
10
12
14
16
18
20
Penetration distance, g/cm² of water
$\left[\frac{S_1S_2S_3}{S_1}\right]$
$\left[\frac{S_1S_2}{S_1} - \frac{S_1S_2S_3}{S_1}\right]$
WATER
ABSORBER
BEAM
S_1
S_2S_3
PLASTIC
SCINTILLATION COUNTERS
NITROGEN IN WATER
DBL 721 5110

Fig. 5

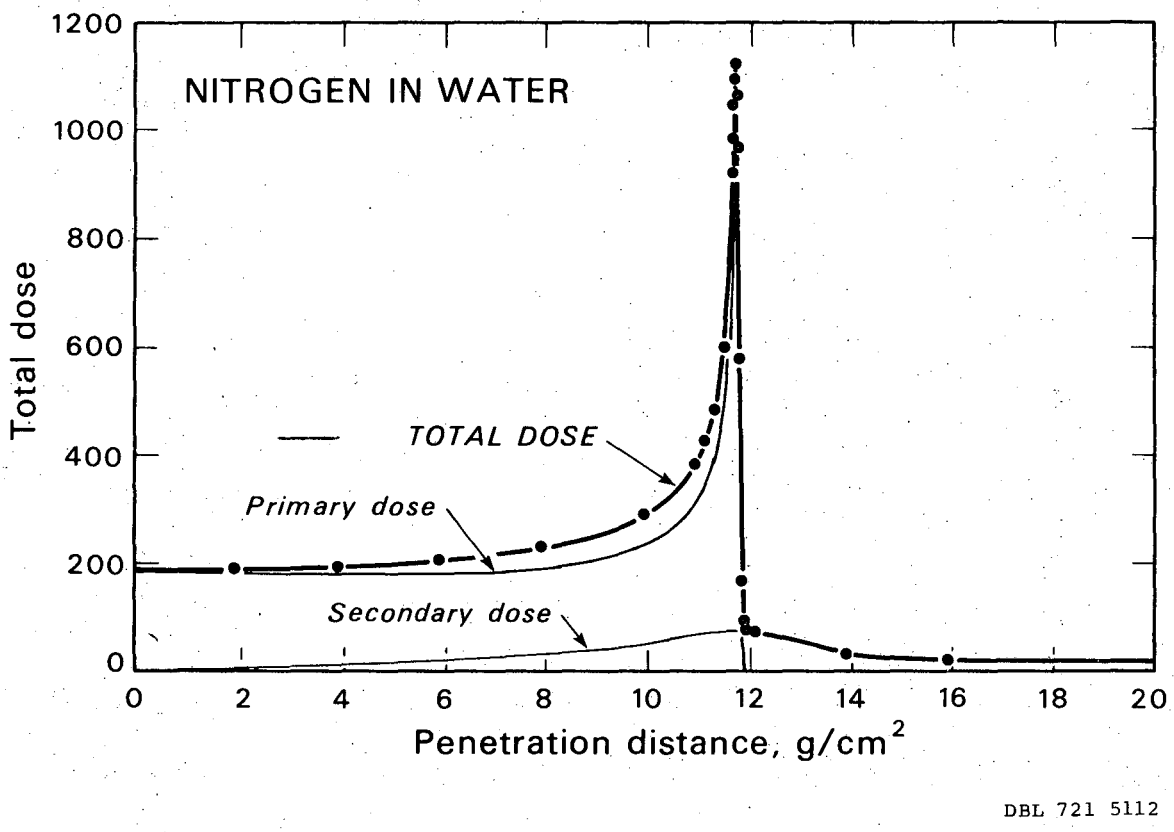
NITROGEN IN WATER
TOTAL DOSE
Primary dose
Secondary dose
Total dose
Penetration distance, g/cm²
1200
1000
800
600
400
200
0
0
2
4
6
8
10
12
14
16
18
20
DBL 721 5112

Fig. 6

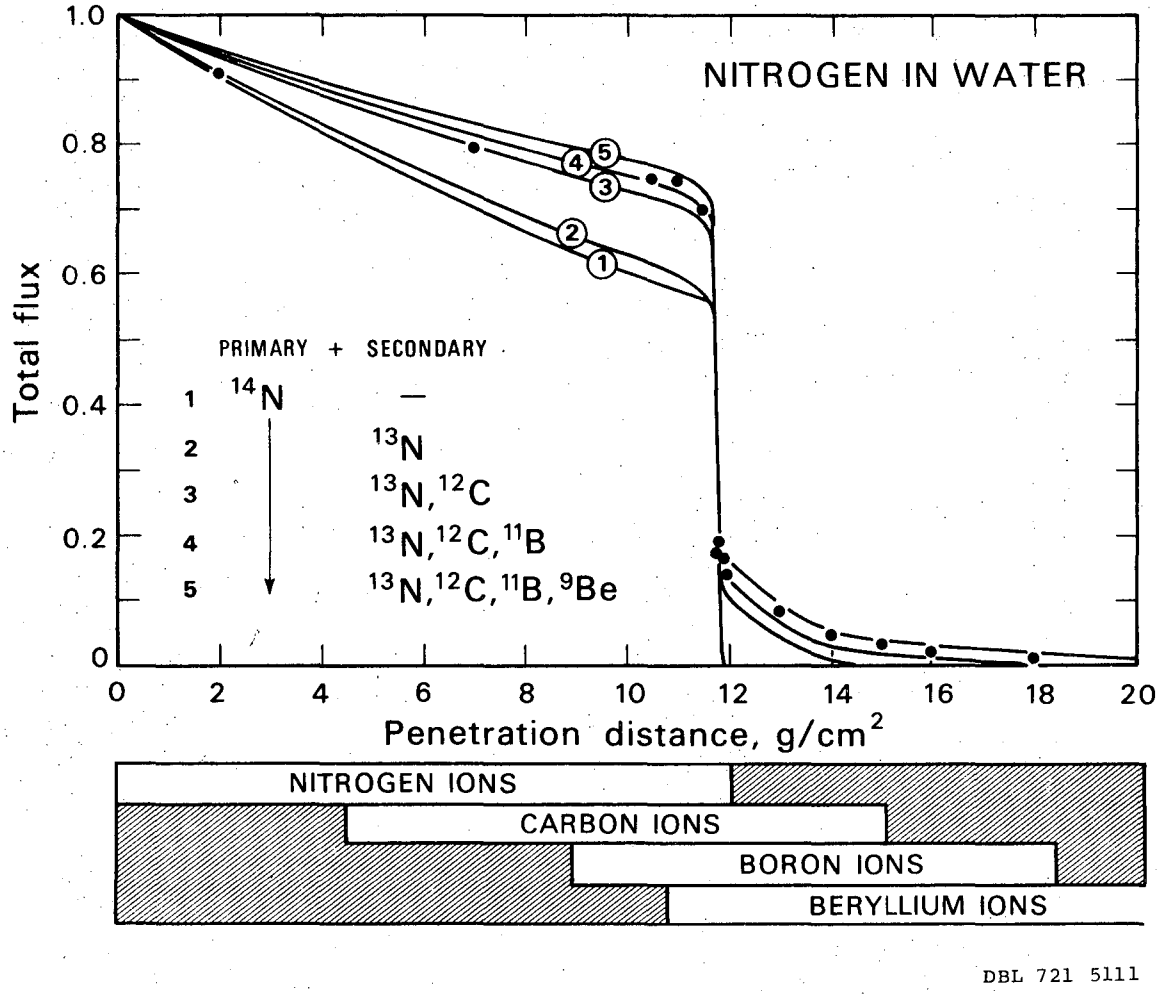

Fig. 7

RADIOACTIVE FRAGMENTATION OF NITROGEN ION BEAM IN A BERYLLIUM TARGET

by

C.A. Tobias, A. Chatterjee and A.R. Smith

Abstract

Using a 250 MeV/nucleon nitrogen beam on a beryllium target, we have obtained evidence that some of the fragments of the projectile nitrogen nuclei are radioactive nuclides as a result of the inelastic nuclear collision. This is irrespective of the changes the target nuclei may undergo. We call this phenomenon "autoactivation".

Among the various possible radioactivation products of the fragmentation of nitrogen nuclei, we have found $^{11}_{6}C$ (half-life 20.34 min.) and $^{13}_{7}N$ (half-life 10.1 min.). The beryllium target acts as a degrading absorber for the nitrogen beam and a catcher for the autoactivated nuclei. Activity-versus-depth measurements have also been performed.

Study of the phenomenon of autoactivation may lead to some interesting biomedical applications; geophysical implications of autoradioactivation are self-evident: streams of heavy cosmic ray nuclei are sources of short and long half life isotopes, which add to the radioactivity on the surface of the moon and planets.

Introduction

A very significant feature of nuclear collisions involving primary heavy nuclei and target nuclei is the frequency with which a fast secondary heavy nucleus emerges from the encounter (1,2,3). As pointed out by Fowler et al (1), nuclei with $Z \geq 2$ are never emitted at relativistic velocities from disintegrations due to fast protons. This fact immediately leads to the reasonable assumption that any fast heavy secondary particles formed as a result of a nuclear collision are part of the incoming nucleus. Production of a compound nucleus (involving the incident and the target nuclei) and subsequent ejection of a fast secondary heavy nucleus can be ruled out, considering the time of interaction (10^{-22} sec) at such high velocities. It has also been assumed by several workers (1,4) that the fast fragments of incident primary nuclei travel with a velocity little different from that of the incoming nucleus, and their direction of propagation, as well as ejection angle, is almost the same as that of the parent nucleus.

Prior to the experiment reported on here, the various assumptions mentioned above could not be verified, and quantitative detail could not be obtained due to nonavailability of very high energy heavy ion beams in the laboratory. The only data available are those from direct evidence of cosmic ray (heavy ion) tracks recorded in photographic emulsion (1) and in gelatin and cellulose acetate (3). These data do confirm the fragmentation of incident heavy nuclei into secondary heavy nuclei.

In August, 1971, fully stripped nitrogen ions were successfully accelerated in the Berkeley Bevatron (5) to various energies up to a maximum of 2.57 GeV/nucleon.

By using a special counting technique, Heckman, et al (8) immediately obtained measurements of the fragmentation of 2.1GeV nitrogen and identified some fragment nuclei, including those of $^{7}_{4}Be$.

In the present experiment, we have used 250 MeV/nucleon nitrogen ions as the incident beam, with beryllium used as a target. Beryllium acts as an absorber for the nitrogen beam and also as a catcher for the radioactive Carbon-11 ($^{11}_{6}C$; half life = 20.34 min) which is formed as a fragmentation product of the incident nitrogen nucleus. In particular, the object of the experiment was to study the formation in flight of the radioisotope $^{11}_{6}C$, a positron emitter, and also to verify some of the assumptions mentioned earlier.

The purpose of selecting solid beryllium was to use a lower atomic number than carbon as a target. It is very unlikely that a beryllium nucleus could capture a sufficiently large fragment of fast nitrogen to become $^{11}_{6}C$, and, thus, any formation of $^{11}_{6}C$ would be a result of fragmentation of the nitrogen nucleus with a certain cross section.

We call the phenomenon of formation of radioactive nuclides emerging from the incident nucleus "autoactivation". Through autoactivation, we have been able to measure the depth-activation distribution which may have important biomedical applications, as discussed in the final section of this paper. Also, the phenomenon of autoactivation may prove to be useful with respect to irradiation with radioactive beams.

Theoretical considerations

The impact parameter is of great importance for collisions involving complex nuclei. In peripheral collisions in which the impact parameter is larger than the nuclear radius (see Fig. 1a), only a few of the nucleons of the primary fast particle, or of the target nucleus, are involved in the collision. The projectile nucleus may therefore be split into a large multiply-charged fragment, along with a few singly-charged and neutral particles. In such a collision, it may happen that most of the nucleons of the interacting nuclei are not sufficiently disturbed to change their momentum significantly. Thus, a heavy nuclear fragment emerges with almost the same velocity as that of the incoming nucleus, while a fragment of the struck nucleus is given little velocity in the laboratory frame of reference. The fragments of the target nucleus disperse in various directions that may very well overlap with paths of the projectile fragments. According to this model, one obtains a characteristic spatial pattern of the particle trajectories as shown in Fig. 1b.

In the "head-on" collision between two nuclei (i.e., impact parameter $\lesssim$ nuclear radius), both of them may be completely dispersed into their component nucleons (1). Production of a large number of mesons and other secondary particles is generally associated with this kind of collision. The total nuclear interaction cross section, (within $\pm$15%) first proposed by Bradt and Peters (6), can be written empirically as

$$\sigma_{total} = \pi R_0^2 (A_t^{1/3} + A_i^{1/3} - 1.7)^2 \qquad \text{Eq.(1)}$$

where A_t and A_i are, respectively, the mass numbers of the target and incident nuclei, $R_o = 1.45 \times 10^{-13}$ cm. From cosmic ray data on heavy ions, the empirical relation given by Eqn. 1 is approximately valid in all cases where both A_i and A_t are greater than or equal to 4. A knowledge of the production cross section for a particular fragment (with atomic number Z, mass number A) is of paramount importance. Symbolically, one can write this as

$$\sigma_{Z,A} = \rho_{Z,A}\, \sigma_{total} \qquad \text{Eq. (2)}$$

where $\rho_{Z,A}$ is the probability of obtaining a fragment with atomic number Z and mass number A in a given collision, and $\sigma_{Z,A}$ is the corresponding cross section. So far, no theory exists for the determination of $\sigma_{Z,A}$ or $\rho_{Z,A}$, but experimental determination is possible (See Section on Results).

Assuming that the velocity of the fragments remains the same as that of the moving nucleus (this is not strictly correct), one can estimate the local region within which a particular fragment ($^{11}_{6}C$ in the present case) should get caught in the target (beryllium in the present case). It is obvious that a fragment produced deeper in the absorber will have a shorter range than a fragment produced earlier in the target. Also, a fragment (with smaller charge but the same velocity) will have a range longer than the residual range of the incident particle by the ratio of its mass over charge squared. Thus, C-11 produced right at the point of entrance will travel a distance

which is equal to ϕR_N , where

$$\phi = \frac{(Z^2/A)_{Nitrogen}}{(Z^2/A_{Fragment}} \qquad \text{Eq. (3)}$$

and R_N is the range of the nitrogen beam of incident energy. For nitrogen, Z = 7 and A = 14, whereas, for C-11, Z = 6 and A = 11. C-11 fragments, which are produced right at the end of the range of the incident nitrogen beam, will not be able to penetrate at all. Thus, one expects all the C-11 to be deposited between R_N and ϕR_N. The distribution of C-11 deposition will not be uniform, with a maximum deposition at R_N and a minimum at ϕR_N . This distribution is also tempered by range straggling effects.

Materials and methods

Nearly parallel beams of 2.7×10^6 nitrogen particles of energy of about 270 MeV/nucleon from the Bevatron were allowed to be stopped by a slab of spectroscopically pure beryllium metal (impurities less than 0.1%). The exposure time was 13 minutes. C-11 is a positron emitter. Gamma-ray spectra from the irradiated beryllium sample were studied with a scintillation spectrometer. The scintillation spectrometer consisted of an 8-inch diameter by 4-inch thick NaI (Tl) crystal and a digital-gain-stabilized 400-channel pulse height analyzer. The very low and constant background of the spectrometer system (48 counts/minute in the 511 KeV peak region) enabled precise measurement of the small counting rate encountered. A detailed description of the spectrometer is given elsewhere (7).

The depth-activation distribution for C-11 was measured in another experiment where the nitrogen beam was allowed to impinge on a stack of beryllium absorbers, each 0.5 cm thick. Activity was measured with each disc from the stack of absorbers.

We also irradiated a stack of polyethylene (C_2H_4) absorbers, rich in C-12, with the nitrogen beam at 250 MeV/nucleon. The idea was to look for C-11 activity all along the path of the beam.

Finally, we induced $^{13}_{7}N$ (half-life 10.1 minutes) and $^{11}_{6}C$ activities in a target that contained three aluminium discs each 1.27 cm thick, followed by a stacked set of beryllium discs. The beryllium discs were analyzed for $^{11}_{6}C$ and $^{13}_{7}N$ activation.

Results

No appreciable radioactivity was detected in the irradiated slab of spectroscopically pure beryllium metal, except in the channels set to measure annihilation radiation at 0.51± 0.01 MeV. The data obtained in these channels were analyzed into two components with a half-life of 20.34 minutes and 10.1 minutes, respectively. These correspond to the radioisotopes $^{11}_{6}C$ and $^{13}_{7}N$. The data are plotted in Figure 2.

In order to verify the hypothesis that the radioactive fragments are formed as a result of the splitting of the nitrogen nucleus, depth-activation distribution of $^{11}_{6}C$ activity was measured in each 0.5 cm-thick beryllium disc. Out of the two radioisotopes, $^{11}_{6}C$ was chosen because it has a longer half-life than the other one. No measurable radioactivity was detected at all in the first 10 gm/cm^2 of beryllium. The radioactivity in the .51 MeV channel was at background level, and, if there is any activity, it is less than 10^{-3} of the peak. Most of the $^{11}_{6}C$ activity was concentrated in a fairly sharp peak near the range of nitrogen particles in beryllium, as is shown in Figure 3. The range of 250 MeV/nucleon in beryllium is 13.0 gm/cm^2. Again, no activity was found beyond 16 gm/cm^2.

The cross section for production of $^{11}_{6}C$ and $^{13}_{7}N$ from incident nitrogen beams directed at the beryllium target was obtained by analysis of the data. We find that

$$_{6,11} = 17 \text{ millibarns and } \rho_{6,11} = 0.03;$$

$$_{7,13} = 6 \text{ millibarns and } \rho_{7,13} = 0.01.$$

Analysis of the data concerning the irradiated stack of polyethylene absorbers agreed with our expectation that radioactivity would appear all along the path of the beam. The reason for this was that resting carbon nuclei were expected to give rise to slow $^{11}_{6}C$ nuclei. However, near the range of nitrogen ions, there was a small peak (see Figure 4) in the carbon-11 activity, which we believe is principally an effect of autoactivation.

In the final experiment, in which three aluminium discs were followed by beryllium discs, radioactivity measurements were also taken as before (see Materials and Methods section). It is interesting to note that, in this sample, the $^{13}_{7}N$ activity was found to have different depth distribution than $^{11}_{6}C$ activity, more of the former being deposited at a lesser depth in the beryllium absorber.

Discussion

The phenomenon of autoactivation appears to have promise from the point of view of various information relating to physical as well as biological applications.

Physical

1. Cross sections. From the measurements of activation of the fragments produced in the present experiment, we have been able to calculate the cross section of production of a particular fragment (see Results section). Because of the uncertainty in the measurement of the flux of the initial nitrogen beam, the absolute cross sections may not be very accurate compared to the relative cross sections. However, it is interesting to note that, when Heckman et al (8) used hydrogen as a target, they obtained cross sections for production of C-11 and N-13 such as 10.4 millibarns and 3.6 millibarns respectively, compared to that of 17 millibarns (for C-11) and 6 millibarns (N-13) obtained in the present experiment using beryllium as a target (see Results section). Qualitatively, there is an agreement between the two results and also, one does expect the cross sections to be somewhat smaller using hydrogen as a target compared to a beryllium target. As might be predicted for autoactivation products, the ratio of the cross sections of C-11 to those of N-13 is the same in both cases (ratio = 2.8).

2. Dome distribution. As indicated earlier, the production of a given fragment depends on probability, $\rho_{Z,A}$, for that particular fragment. Using the simple rule for relative range of fragment to

whole nucleus, it is obvious that a fragment produced deeper in a target will have a lesser range. The secondary particle flux, N_f, may be described in a relatively simple manner as:

$$N_f = N_0(1-e^{-\mu X}), \text{ for } X \leq R, \qquad \text{Eq. (4)}$$

and

$$N_f = N_0[\,1-e^{-(\mu/(\phi-1))(R_f-X)}\,], \text{ for } X \geq R_0, \qquad \text{Eq. (5)}$$

where

N_o ..... initial particle flux;

μ ..... inverse of the mean free path of production of a particular fragment, which is assumed to be constant over the energy region considered;

R_f ..... range of the fragment in the target;

X ..... the distance of the point of consideration of the flux.

In the above two equations, no loss of the fragment due to nuclear collisions has been considered. Equations (4) and (5) give rise to a kind of distribution (see Figure 5) which we call "dome distribution", for its dome-like shape. Any deviation of the secondary flux distribution from idealistic dome distribution will give some understanding of the validity of the assumption made regarding the velocity of the fragment being the same as that of the incident particle at the point of production. Furthermore, if the assumption is not true, a detailed analysis similar to that of Heckman, et al, can be made for velocity spectrum, by applying a magnetic field and then subsequent recording.

3. Isotopes. Various short-lived and long-lived isotopes can be produced by means of autoactivation. The phenomenon of autoactivation presents a definite possibility of detecting short-lived isotopes in flight measurements.

Biological

1. Localization of the Bragg ionization peak in tissue during radiotherapy. Autoradioactivity of accelerated particles appears as a localized peak of radioactivity in the region where the primary particles stop, in exact, measurable relationship to the location of the Bragg ionization peak. It should be possible to apply coincidence counting techniques to localize the Bragg peak by measuring the auto-radioactivity induced during actual radiotherapy procedures in humans. Measurements would be carried out during therapy, at periods between beam pulses. (Currently there are 10-20 beam pulses per minute, of duration of 1 msec to 1 sec) The lack of exact diagnostic knowledge of the position of the Bragg peak has hindered therapeutic procedures in the past. Exact calculation is impractical because of intervening bone tissues and, in some locations, of air. ^{13}N and ^{11}C may be suitable; however, shorter lived radioactivities and prompt gamma rays will also be explored. The planned use of neon beams in therapy will increase the possibility of finding appropriate isotopes for this purpose.

2. Radioactive beams. Since the charge to mass ratio of radio-active fragments is often different from that of the particles of the primary beams, radioactive fragments can be separated from the main beam by deflection in appropriate magnetic channels. This principle has already been used by H. Heckman and group in physical studies of the properties of fragments (2). It is expected that, when sufficient circulating beam intensities have been reached in the Bevatron, relatively intense "carrier-free" radioactive (and nonactive) fragment

beams will also be available to be used in biologic study and therapy. Localization of such beams inside of the human body by counting radioactivity would be much more efficient than that of unseparated beams, perhaps by a factor of fifty. In practice, this means that measurement of the localization of the stopping region can be carried out at much lower dose levels.

The deposited radioactive particles may remain localized and deliver additional dosage to tissue as it decays. This dose is small compared to the initial dose delivered by the beam. Some of the radioactive atoms may translocate and some might be exhaled or excreted.

3. Diagnostic application in vascular disease. We anticipate that the use of radioactive beams will find important medical diagnostic applications. For example, a single pulse of a monoenergetic beam may be brought to a stop in a small region inside the human heart. The time required might be as little as one millisecond. A radioactive bolus is formed; some part of this will be carried with the streaming blood. Appropriate counting arrangement, observing passage of the radioactivity, could result in measurement of blood flow and heart valve action. Such techniques could also be applied in the carotid artery to measure cerebral blood flow and perhaps elsewhere. The autoradioactive beam technique might eliminate the necessity of arterial puncture and catheterization, and could keep the injection time shorter than with currently used techniques.

4. Hot atom interactions. The atoms in an autoradioactive beam are first, at high velocity, stripped of all of their electrons. In

the process of slowing down, they gradually pick up electrons; just before stopping, they form a locally hot column. Chemical reactivity in such a column is high, and one may expect that a fraction of the hot atoms would interact with molecules of the absorbing medium. Hot atom chemistry using ions accelerated in a mass spectograph (10) is already an important tool in organic chemistry. The autoradioactive beam adds the convenience of allowing tracing of some of the reactions that occurred and thus aiding in the identification of products. The process is equivalent to accelerating a radioactive species in a mass spectroscope for hot atom chemistry, except that the Bevatron beams allow deep penetration as well.

Interactions of hot atoms in living tissues is an almost entirely unknown domain. We know, however, that ^{11}C atoms produced by protons from ^{12}C, N, and O in a process of "target activation" show anomalous behavior. They rapidly translocate in the mammalian body from the site of production and an appreciable fraction of the activity (10%) was found in CO-Hemoglobin.

5. Origin of organic compounds. It is well known that a milieu of ultraviolet, or heavily ionizing radiation results in primary synthesis of bio-organic compounds in an atmosphere rich in compounds containing carbon, hydrogen, nitrogen, and oxygen. The possible role of heavy primary cosmic rays in this process has not been evaluated, however. Autoradioactivity might be helpful in this regard.

One of the problems with the origin of organic compounds is that of the initial formation of molecules with catalytic properties: molecules that eventually evoluted into today's enzymes. It is

interesting to note that some of the most important biological substances, e.g., chlorophyll and hemoglobin, use atoms of magnesium and of iron, respectively--atoms that are prominent in primary cosmic rays. Perhaps initial formation of metallo-organic compounds does occur in planetary atmospheres, and possibly some of these have catalytic properties.

6. Contribution of autoradioactivity to the radioactivity of planetary atmospheres and of surfaces. Atmospheric radioactivity is usually thought of as due to "target" activation by primary protons and secondary neturons produced in collisions with atmospheric atoms and subsequently slowed down, and to remnant radioactivity of the earth.

Autoradioactivity of primary cosmic rays is making a contribution; this contribution is as yet unevaluated. Short-lived radioactivities decay rapidly (on a geological scale). Longer-lived activities, such as ^{10}Be or ^{40}K remain and add to the radioactivity which was produced at the time the elements originated. Evaluation of the contribution of autoradioactivity in the course of the history of the solar system necessitates measurements of production cross-sections (which can be performed at the Bevatron), and this radioactivity also depends on the intensity of the heavy primary component of cosmic rays.

It is of interest to note that already many heavy ion tracks (e.g., 10^{11} per cm^2) were measured in lunar surface rock samples (11). Initial measurement of radioactivity in shallow surface layers of the moon is higher than expected.

The authors' primary purpose in discussing these very interesting cosmic ray phenomena is that, eventually, their relationship with life phenomena can be studied.

REFERENCES

1. Powell, C.F., Fowler, P.H. and Perkins, D.H., The study of elementary particles by the photographic method (Pergamon Press, New York, 1959).

2. Rajopadhye, V.Y. and Waddington, C.J., Phil. Mag. 3, 19 (1958).

3. Noon, J.H. and Kaplon, M.F., Physical Rev. 97, 769 (1955).

4. Curtis, S.B., Semiannual report, Donner Laboratory, UCRL-18347, 171-174 (1968).

5. Grunder, H.A., Hartsough, W.D. and Lofgren, E.J., Acceleration of heavy ions at the bevatron, Science, 174, 1128-1129 (1971).

6. Bradt, H.L. and Peters, B., Physical Rev. 77, 54 (1950).

7. LBL Health Physics Staff, Experiment 10 in Laboratory Manual, Accelerator Health Physics Training Manual, LBL 18222 (to be published).

8. Heckman, H.H. et al, Fragmentation of Nitrogen-14 nuclei at 2.1 GeV per nucleon, Science 174, 1130-1131 (1971).

9. The cross section for N-13 production as measured by Heckman et al was total cross section, but for C-11, the result may be 50% off. The value of 10.4 millibarns was obtained after doubling the partial cross section which was measured.

10. Lin, Tz-Hong and Lemmon, Richard M., Reactions of accelerated carbon-14 with benzene. Degradation of toluene and its mechanism of formation, The Journal of Physical Chemistry 75, 3524, (1971).

11. Borg, J., Dran, J. C., Durrieu, L., Jouret, C., Maurette, M., Earth Planet. Sci. Lett. 8, 379 (1970).

Figure Captions

Fig. 1. (a) The overlapping portions of the two nuclei are likely to be fragmented during a fast collision. The collision time is of the order of 10^{-22} or 10^{-23} sec.

(b) A schematic representation of the spatial distribution of fragments in a collision of a moving and a resting nucleus. The fragments of the moving particle are within a narrow cone. The secondary fragments, in the laboratory frame, are scattered more or less isotropically. The thickness of the line is an indication of the rate of energy loss.

Fig. 2. A semi-log plot of intensity (counts/5 min) against time (min) is shown. The slope of the line corresponds to the ^{11}C activity resulting when 250 MeV/nucleon nitrogen ions are stopped in a beryllium target. A similar plot for ^{13}N confirmed its formation also.

Fig. 3. Activity of ^{11}C vs depth curve. It shows that ^{11}C resulting from the fragmentation of nitrogen ions impinging on a beryllium target is deposited mostly at a particular depth corresponding to the range of the 250 MeV/nucleon nitrogen beam.

Fig. 4. A 250 MeV/nucleon nitrogen beam was stopped in polyethylene absorber. The ^{11}C activity appeared all along the path of the beam. However near the range of nitrogen ions there is a small peak which is an effect of autoactivation.

Fig. 5. Schematic diagram of dome distribution. Theoretically all the fragments should be deposited between R_N and corresponding ϕR_N.

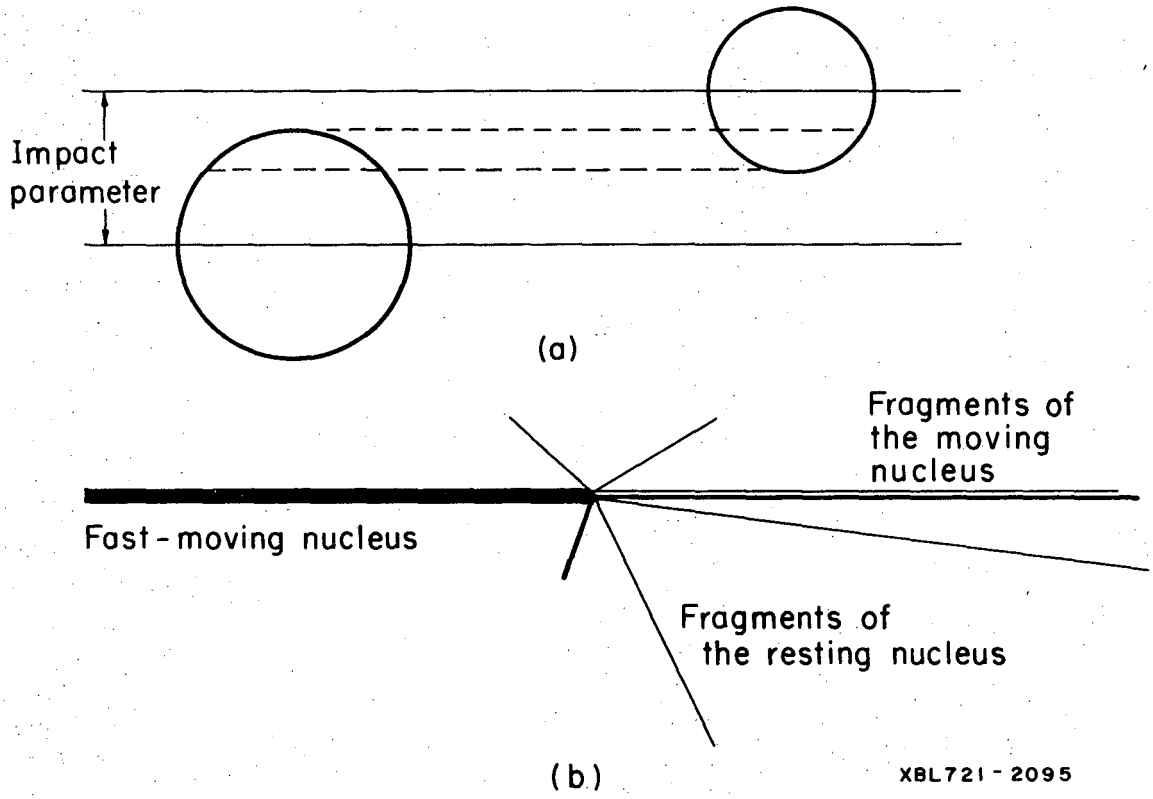

Fig. 1

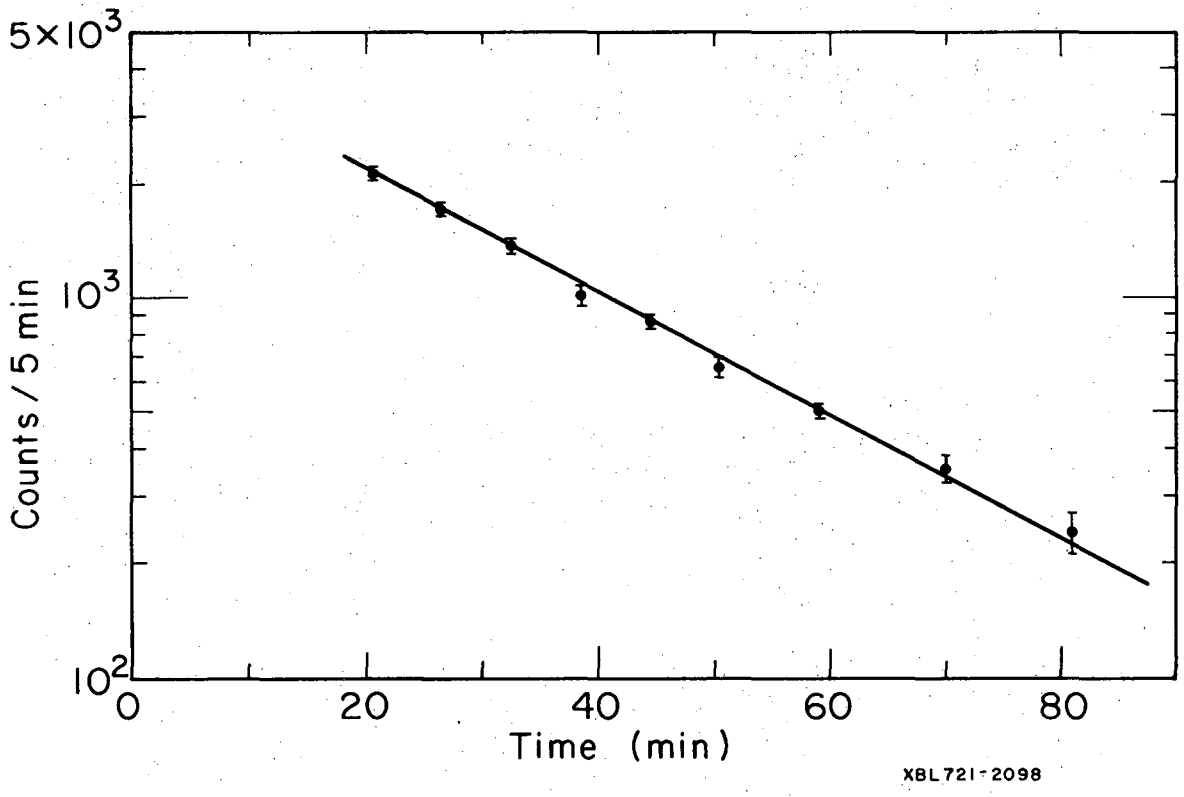

Fig. 2

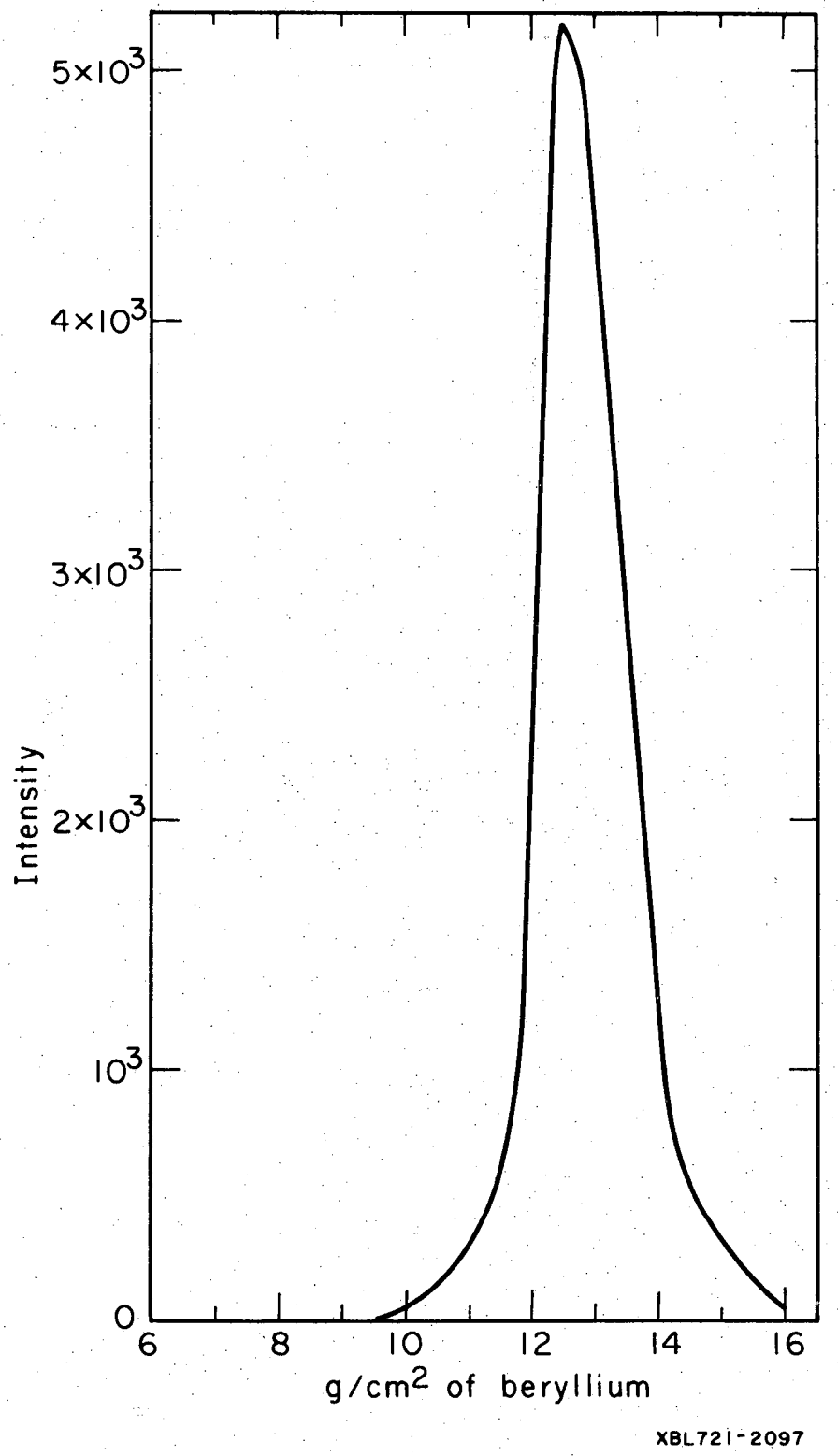
5×10³
4×10³
3×10³
2×10³
10³
0
Intensity
6
8
10
12
14
16
g/cm² of beryllium
XBL721-2097

Fig. 3

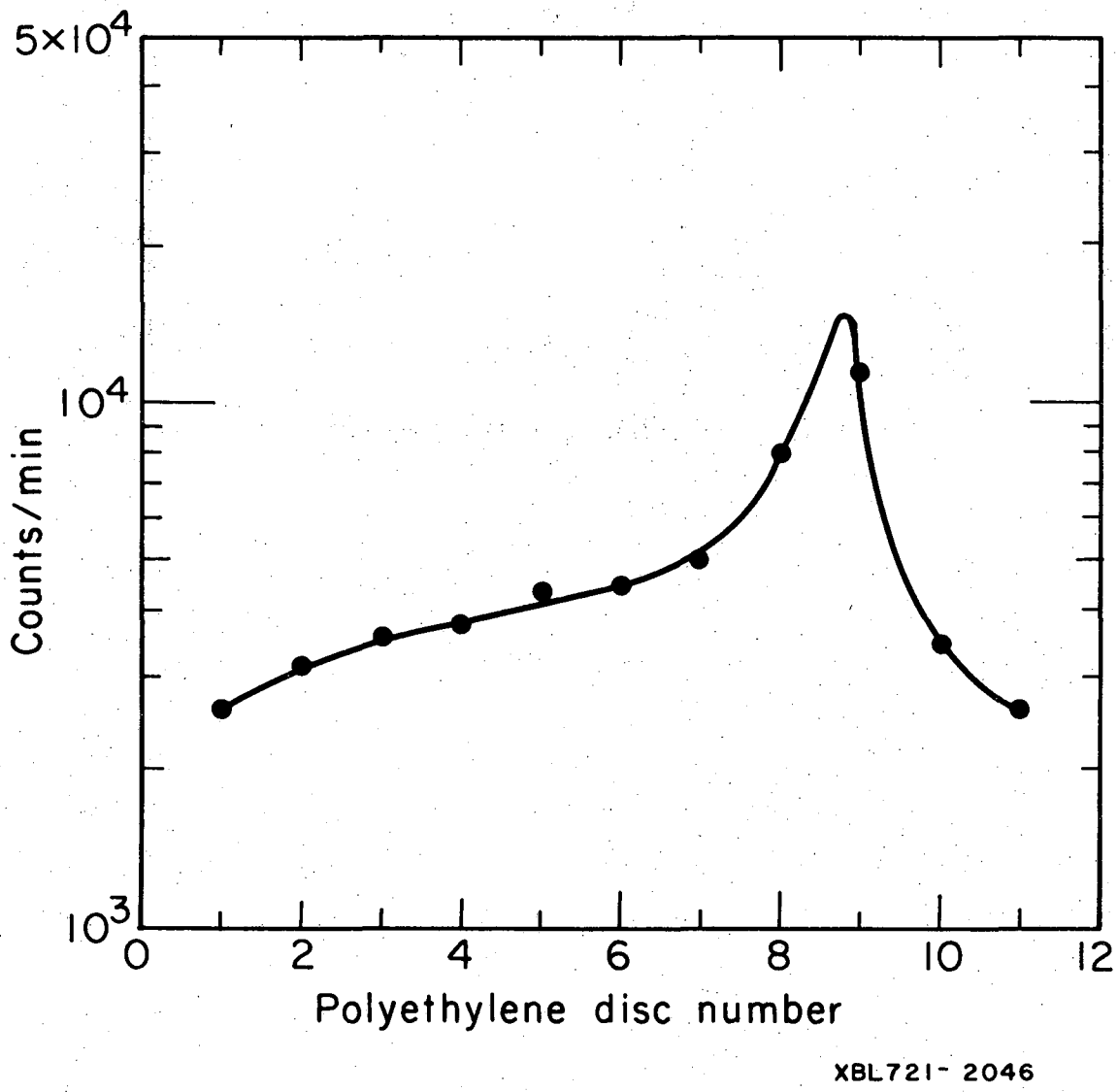
5×10^4
10^4
10^3
Counts/min
0
2
4
6
8
10
12
Polyethylene disc number
XBL721-2046

Fig. 4

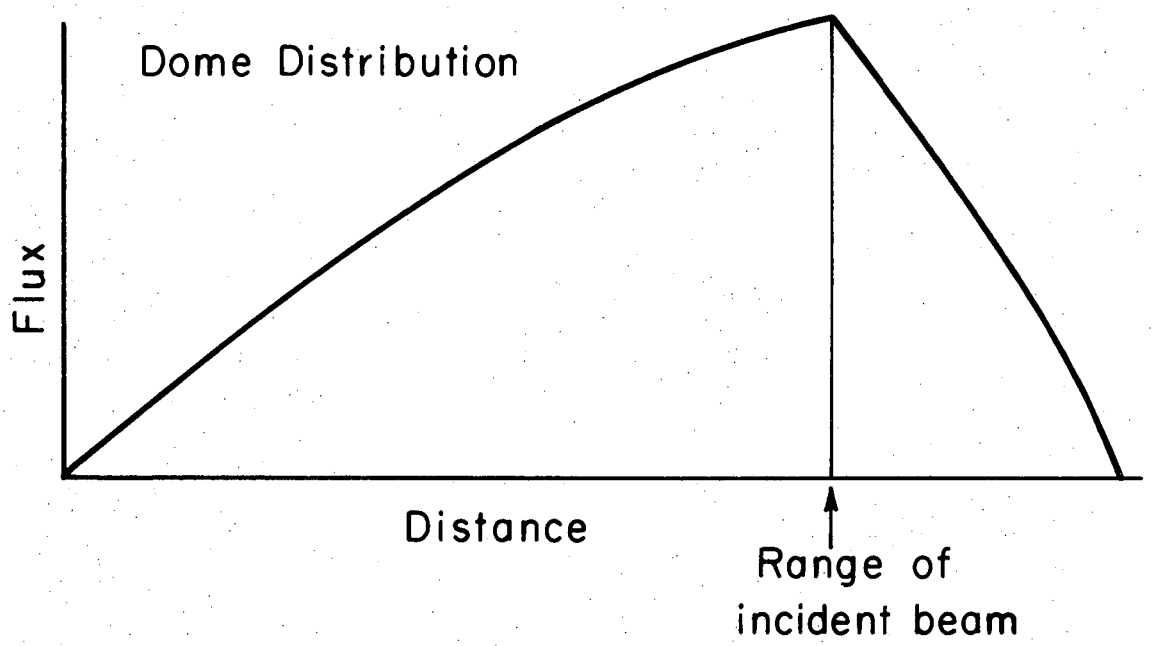

Fig. 5

MEASUREMENTS WITH PLASTIC NUCLEAR TRACK DETECTORS*

by

E. V. Benton, R. P. Henke, and H. D. Maccabee

Abstract

Measurements of the ^{14}N ion Bevatron beam were made, utilizing tissue equivalent plastic nuclear track detectors. Preliminary results are presented.

Layers of cellulose nitrate (CN) and Lexan detectors assembled into stacks were exposed normally to the incident 280 MeV/nucleon, ^{14}N ion beam. The experimental objectives included: the measurement of particle range straggling at the Bragg peak, the measurement of the highly ionizing secondaries, and the determination of the response of the detectors as a function of particle LET.

To date, most of the effort in the analysis has gone into establishing the response of the CN detector as a function of particles' LET. That is, measurement of the track etch rate V_T, has been performed as a function of the particle residual range, R.

The incident 280 MeV/nucleon, ^{14}N beam was stopped, using a 28-layer CN stack (with individual layer thickness of approximately 270 microns) after having been degraded in energy by a 10.6 g/cm^2 stack of Lexan. Lexan thickness

*A portion of the work was performed under NAS8-26758. Dr. Benton is with the Physics Department, University of San Francisco, Calif.

was based on the initial expectation of a 250 MeV/nucleon energy beam. Thus, only a few straggling particles rather than the expected Bragg peak were stopped in the CN layers.

The detector layers were individually etched at 40°C in 100 ml of 6.25N NaOH. The layer used for locating the stopping point for the particle was etched for five hours. The immediately adjacent layer was etched for 2.5 hours, the next for 30 hours, and the last for 48 hours.

The stack configuration and etched track parameters (1) are shown in Figure 1, which is not to scale. The average residual range for each track, $\bar{R}$, is the distance from the stopping point to the center of the etch length, L.

The tracks produced by eleven different particles were measured in the four detector layers. Knowing the original thickness of the layers and L allows the calculation of $\bar{R}$, as shown in Figure 1. For each track, the track etch rate, V_T, is given by

$$V_T = \frac{L}{t_e} , \qquad (1)$$

where t_e is the etch time for that layer.

For all the tracks measured, V_T has been plotted as a function of $\bar{R}$, as shown in Figure 2. Two groups of points are apparent. One curve has been drawn through the measured points attributed to ^{14}N particles. The second group of points represents ^{12}C particles (some beam contamination was present). Here it is assumed that,

$$V_T = V_T\ (LET_{350}). \qquad (2)$$

A point from an independent experiment utilizing 10 MeV/nucleon ^{16}O particles is also shown as is the bulk etch rate, $V_G = B/t_e$. The bulk etch rate represents the smallest value of V_T possible. From Figure 2, it is noted that V_T is a function of the etch time. This implies a depth dependence of V_T in the detector.

As can be seen from Figure 2, the measured response of the CN detector is such that charge identification of the CNO group of stopping particles is achieved.

The measured values of the $V_T(R)$ for ^{12}C and ^{14}N particles were also used to obtain the V_T vs. LET relationship for the CN detector. This is shown in Figure 3. The measured response shows a somewhat stronger dependence on LET than expected (2).

REFERENCES

1. Henke, R.P. and Benton, E.V., UCRL-20852 (1971).

2. Benton, E.V., USNRDL-TR-68-14 (1968).

FIGURE CAPTIONS

Figure 1. The stack configuration of plastic detectors and the etched track parameters.

Figure 2. The track etch rate, V_T, as a function of the average residual range, $\bar{R}$, for ^{12}C, ^{14}N and ^{16}O particles in the CN detector.

Figure 3. The measured track etch rate, V_T, as a function of LET_{350} in the CN detector.

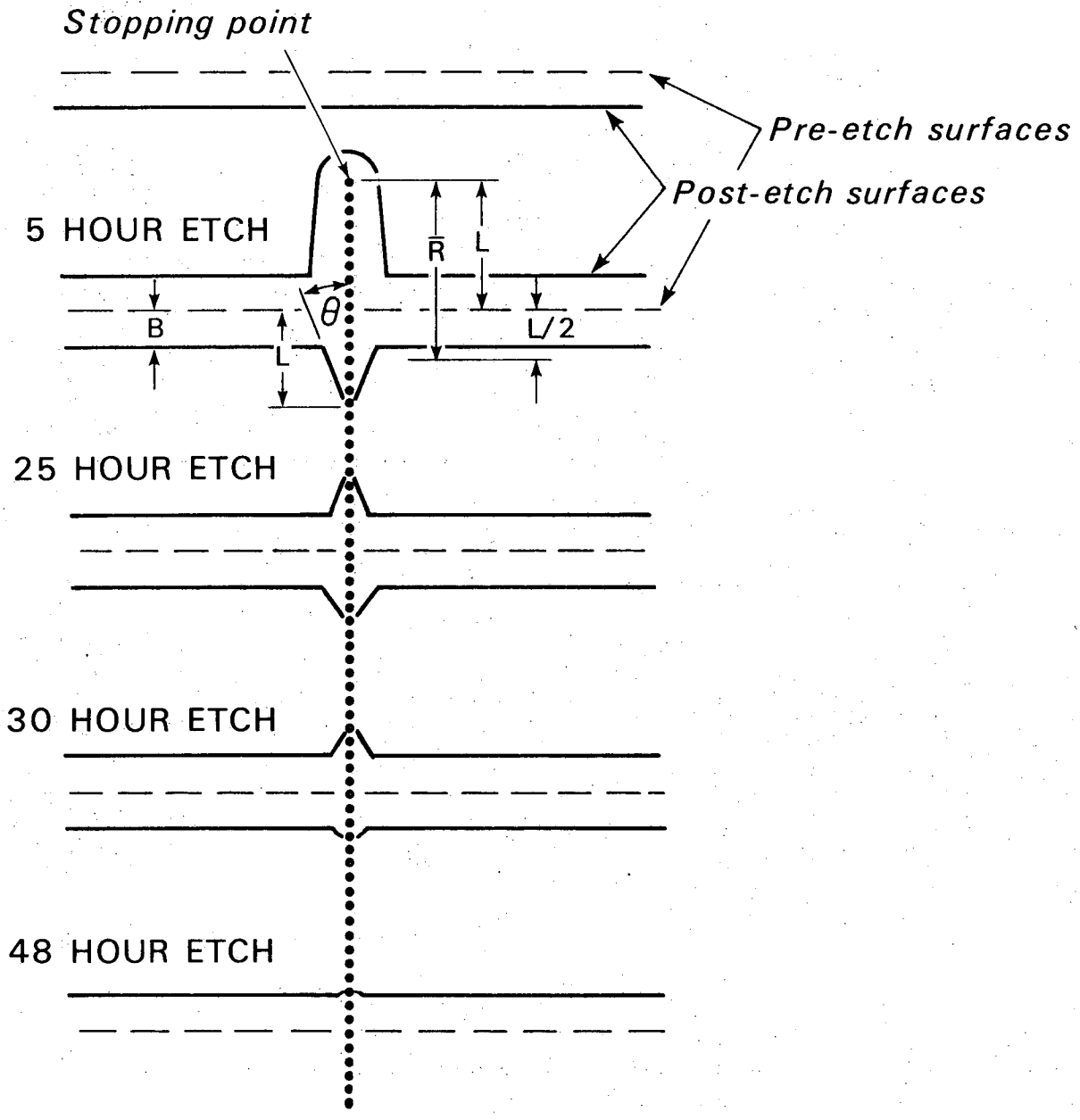

DBL 7112 6100

Fig. 1

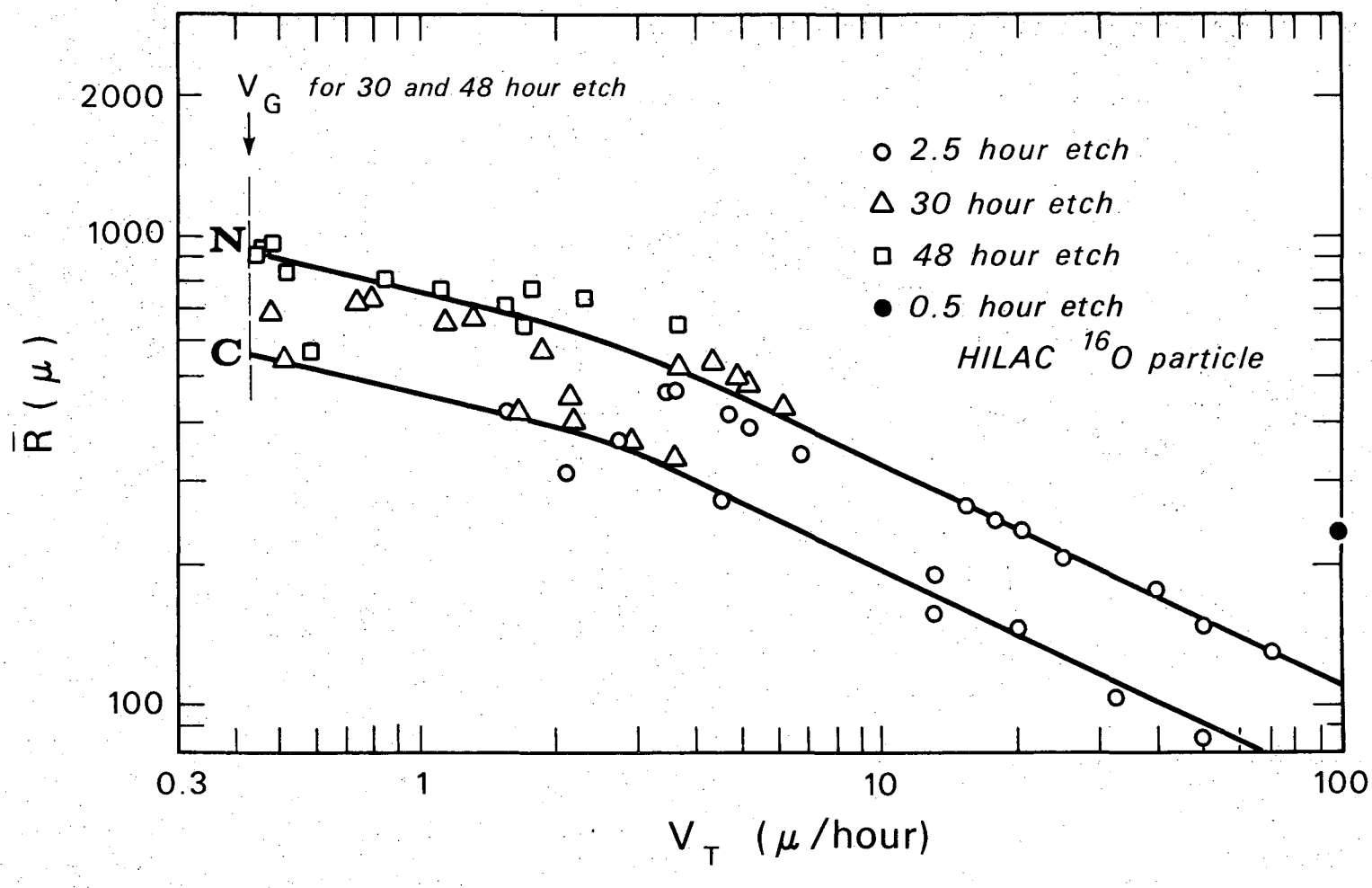

DBL 7111 6099

Fig. 2

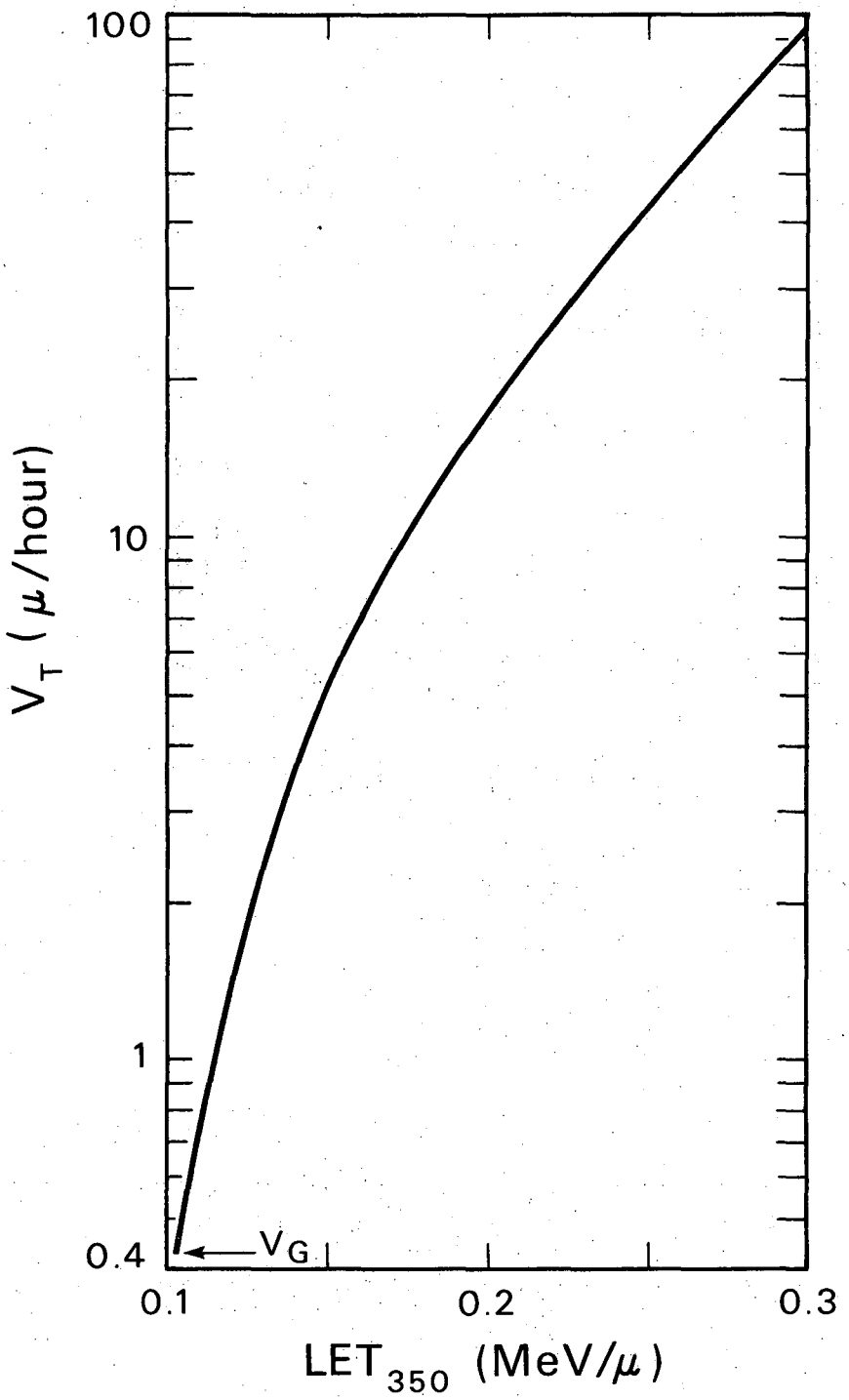

DBL 7112 6101

Fig. 2

VISUAL PERCEPTION OF ACCELERATED NITROGEN NUCLEI INTERACTING WITH THE HUMAN RETINA

by

T. F. Budinger, J. T. Lyman and C. A. Tobias

Abstract

Visual phenomena in the form of streaks and flashes induced by accelerated nitrogen (7^+) ions near the end of their range and passing through particular light-sensitive regions of the human retina are described.

During lunar spaceflight missions Apollo 11 to 15, American astronauts observed randomly occurring light flashes and streaks on a number of occasions (1). Among the explanations offered for these phenomena is the supposition that they are caused by direct interaction of fast, heavy primary cosmic rays with the retina (2, 3, 4, 5, 6). Other suggestions include the assumption that Cerenkov light from relativistic cosmic ray particles causes the effect (7,8), or that fluorescence of the lens plays a role (9). In earlier communications, we have demonstrated that light flashes are observed in single recoil events from fast neutrons in the hundred MeV energy domain (2, 3) or due to interactions in the eye by fast neutrons of 25 MeV maximum kinetic energy (6). Discrete flashes are generated by neutrons with energy ranges between 3 MeV and 8 MeV (10), but not by neutrons of fission spectrum energies (6).

More recently, in carefully controlled experiments with the Berkeley 184-inch cyclotron, it was demonstrated that flashes and streaks are seen when single fast helium ions (ca. 240 MeV kinetic energy) stop in or cross the retina of the human eye (11, 12). These particles, with a linear energy transfer greater than 10 keV per micron, were seen by two subjects (TFB and CAT) with a 40% detection efficiency in a 4-mm diameter beam of 10 particles per second.

Recently, high-energy nitrogen (7^+) beams up to 40 BeV became available at the Berkeley Bevatron (9). Using a nitrogen beam deflected at about 266 MeV/nucleon (or 3.72 BeV kinetic energy), we carried out a series of visual observations with three scientifically trained subjects (E. M. McMillan, a physicist, P. K. Chapman, a scientist-astronaut, and C. A. Tobias).

Figure 1 shows the general layout of the experiments carried out in beam channel No. 2. The nearly monoenergetic nitrogen particles were deflected in pulses of one millisecond duration, one pulse every four seconds. Initial calibration of the radiological physics characteristics of the beam was performed at beam intensities of 10^3 to 4×10^5 particles per pulse. The range of the particles in water was 11.9 cm. The depth penetration properties and Bragg ionization curve were measured in some detail (13), and it was shown that the beam was relatively pure, contaminated by less than 5% high-energy helium ions and protons (14). By the use of quadrapole focusing magnets, the deflected nitrogen particles formed a beam with about 0.5 degree convergence. The exposures were done near the focal point of the beam, where the horizontal and vertical dimensions were 3 mm and 20 mm respectively. Three modifications of the beam were made

for our experiments. First, the beam was detuned to decrease the number of particles to about 15 (0 to 50) per pulse (spill). This decrease was achieved by reducing the amplitude of the rf of the linear accelerator. Secondly, the nitrogen particles were slowed by an interposed variable water absorber to velocities so that the particles stopped in the vicinity of the eye or brain under study. This assured us, in the case of retinal exposures, that only one eye was exposed (the left eye in each case), and that the chance for a single particle entering the second eye, or any part of the brain, was negligibly small. Thirdly, the beam was collimated to a 6-mm diameter.

After passing through an ionization chamber and the variable absorber, the beam was limited to a diameter of 6 mm by a 5-cm-long brass aperture. The particles emerging from the aperture passed through a plastic scintillator approximately 3 mm in thickness. This scintillator counted the individual particles administered to the subjects; the ionization chamber gave measurable indication only if the beam pulse had more than 10^3 accidental overdose. Such a warning did not occur. The ionization chamber and scintillation paddle controlled a rapid, automatic beam plug as an added safety measure. Elective control of beam plug and Faraday cups was available to the biomedical group and the main Bevatron control group. Our committee on medical use of radiations suggested an allowable limit of 2,000 particles per person for the experiment--considerably fewer particles than the number of light flashes experienced by the astronauts in a single lunar flight. During our initial experiments with three subjects,

fluxes were 1100, 1500, and 1600. Biological effects have not been evaluated fully; however, we calculate the eye exposure was less than one rem.

The beam quality was ascertained at the low intensities in an independent experiment (15). A solid-state crystal spectrometer was used for measuring the passage and rate of energy loss of individual accelerated particles. From these measurements on the low-intensity extracted beam, we know that the beam remained "pure", except for an insignificant contamination of heavily ionizing particles that appeared to be either fast, heavy secondaries or accelerated ^{16}O (8^+) ions. The spectral measurements and additional calculations showed that, in the region where the nitrogen particles stopped, the beam composition was greater than 60% (N^{7+}) particles, with the remainder being fragmentation products of nitrogen (N^{7+}, C^{6+}, B^{5+}, etc.), fast protons, and helium ions. The heavy fragments stopped in the vicinity of the N^{7+} range, whereas the protons and helium ions had much greater penetration range. However, the scintillation monitor was biased in such a manner that 75% of the counts recorded by it were due to N^{7+}.

The subjects were dark-adapted prior to the experiment, except that one of the subjects (EMM) on a second exposure series was light-adapted before exposure to several nitrogen pulses, in order to determine the degree of dark adaptation necessary to see particle-induced light-flash events. After alinement of the portion of the eye or brain anatomy, pulse trains of two or three successive beam spills were given with an average of 15 (0 to 50) particles per spill. The exposures were terminated by reinserting the rapid beam plug and the Faraday cups; in addition, the subjects had the freedom of removing themselves from the beam between successive pulses by removing their

heads from the stationary alinement support (this method of exposure termination was not used). The subjects and observers wore film badges. The radiation background in the cave was negligible.

Exposure of the left eye. Figure 2 is a simplified anatomy of the left eye in horizontal section, showing the three regions where various beam positions intercepted visual and nervous structures. The positioning was achieved using a plastic mask and holder, previously custom-molded for each individual. This mask was mounted in a frame which allowed position changes with a precision of 0.2 mm; however, due to certain motional freedoms allowed to the subject, we estimate that the actual position accuracy is $\pm$ 2 mm. The subjects had a few seconds advance warning of oncoming beam pulses.

When the beam was passed through the vitreous body or the optic nerve, no streaks or flashes were seen by any of the subjects. On passage of the beam through the posterior globe of the eye, discrete bright flashes, sometimes in clusters and sometimes interspersed with streaks, were seen as diagrammed in Figure 3. The streaks were all horizontal, and most of the phenomena were observed in the upper visual field. The streaks or flashes appeared white. Because of the presence of nuclear fragments, we estimate more than 65% of the visual events were due to nitrogen ions. Twenty-five per cent of the flashes may have been due to various heavy fragments, helium ions, and stopping protons.

Two observers noted some character to individual streaks; mainly an intense ballooning-out on the right (Figure 3). The same two observers remarked that there was a sensation of motion, mostly from left to right, which was the trajectory of the beam. At this time,

we do not know what the psychological role of the observer's expectation of the particle path was in relation to his objectivity. One careful observer (EMM) did not note motion or shape to the nitrogen streaks, although in other respects his descriptions were similar to those of CAT and PKC.

The particles that transect the eye do so in a time period of 10^{-10} sec, many times faster than the response of the nervous system. The sense of motion in the perceived streaks was also reported by subjects (CAT and TFB) in the helium ion beam, and by five subjects in the Univ. of Washington neutron beams (6).

Throughout these experiments and prior experiments with helium ions, the beam had to be positioned in the posterior portion of the eye before visual phenomena were seen (Figure 2). In this position, the efficiency varies with observer, and probably with the atomic number of the particles and their velocity, as well as the flux density (11). In the nitrogen ion beam at 10 to 20 particles per pulse, observers reported a number of stars, flashes, or streaks equivalent to 40% of the number of particles in the beam path on entrance to the head. The efficiency is poorly known, as the beam was moved both in range and in position during the conduct of the experiments.

From interviews using lighted props with astronauts, we reconstruct the types of visual events seen by them in spaceflights as belonging to one of the classes, as follows:

1. Stars--minute, dim light-flashes.

2. Bright flashes--definite bright pinpoints of light that look like a star or a camera photoflash 100 meters distant, as described by Apollo 15 astronauts.

3. Streaks--pencils of light which varied from dim, thin lines to bright white lines across the visual field.

4. Supernovae--bright single flashes of slightly more than momentary duration surrounded by a hazy halo of less than half a degree in diameter. Supernovae is a term coined by astronauts on Apollo 14 in trying to describe what we think is the same type of phenomenon.

5. Luminous clouds--these events are diffuse, and resemble the appearance of actual clouds in the sky illuminated from behind by a luminous object; e.g., the moon.

These events are depicted in Figure 4. In the nitrogen beam, flashes and streaks similar to types (2) and (3) were seen. Two observers (EMM and CAT) noted interrupted streaks, sometimes also termed "coincidences" or "doubles" in the nitrogen beam. One observer (PKC) described an unusual event: a thick streak ending in several individual streaks. This type of event might have a relationship to nuclear fragmentation.

Careful attention was paid to the position of particles with respect to range in tissue; the best response was found when there was approximately 4.6 grams cm^{-2} of residual range (in water), which means that particles, after traversing the skin, zygomatic bone, and soft tissue, stop just past the center of the retina. When the beam was set to stop in the right portion of the left retina of PKC, phenomena appeared to be in the left visual field; and when the beam was stopped in the left retina, the appearance of the particles was in the center and right visual field, as expected. We were not able to consistently

produce this result in all observers, but none of them reported seeing flashes or streaks when the nitrogen particles were stopped prior to reaching the eye by the variable water absorber. No events were seen during waiting periods prior to the experiment or between beam pulses.

The flashes and streaks appeared bright, and were easily distinguishable from the weak phosphenes usually present in the field of vision of dark-adapted persons. One observer (CAT) thought that the events observed in the nitrogen beam were brighter than most of the events he had seen in a field of helium ions several months earlier (5). No color was observed.

One observer (EMM), who had previously noted these phenomena of nitrogen-induced flashes and streaks after over one hour dark adaptation, was re-exposed without dark adaptation. After entering the dark of the positioning mask, he received from 6 to 10 particles in three bursts separated by a few minutes, until he began to see the phenomena. Approximately 12 minutes elapsed between commencement of dark adaptation and the experience of light flashes. He reported these flashes as definitely dimmer than those he had seen when fully dark-adapted furing a previous experiment. During the remainder of this experiment, EMM noted an increase in brightness as he became more dark-adapted. This experience corroborates the experience with helium ions, and is consistent with astronaut findings on Apollo 15.

In one series of experiments, 800 particles in bursts of 3 to 40 were passed through the vitreous humor 1 cm anterior to the posterior portion of the eyeball of one subject (PKC), and no phenomena were seen. A separate experiment was performed for the study of fluorescence induced

by a beam of nitrogen particles in organic materials. Beam pulses of 10^4 particles each were passed through a quartz chamber containing various liquid materials including fresh rabbit vitreous fluid and freshly excised rabbit retina and lens. A photomultiplier tube was used to measure the yield of visual fluorescent quanta. The yields observed were so low (less than 2 photons per micron) as to make it unlikely that visual spectrum fluorescence of the vitreous fluid, lens, or of the retina as a whole could account for the human visual observations at accelerators or in space. However, ultraviolet photons from electronic excitations would not be detected by the physical experiment; thus, locally deposited ultraviolet photons are still candidates for the mechanism of flash phenomena.

Exposure of the visual cortex. Several regions of the brain participate in visual observations, including the optic nerves, the lateral geniculate bodies, and the visual cortex. In view of the fact that Penfield (16) and others have evoked visual phenomena in conscious patients by electrically stimulating the visual cortex during surgery, and that the cerebral cortex has been implicated in some cases of x-ray-induced phosphenes, we have explored the effect of nitrogen particles on the cortex of a single dark-adapted subject (CAT). The 6-mm particle beam was aimed at the visuosensory area located at the calcarine fissure of the left occipital lobe. The subject wore a dark-adaptation mask with a special water-filled plastic compartment (Figure 1) that allowed control of depth penetration of the beam into the brain when used in conjunction with the variable water-absorber mentioned above. Positioning of the beam was performed with the aid of x-ray diagnostic films

and bony landmarks on the skull. A total of 900 nitrogen particles were used in nine positions of various depths in the left occipital lobe. Throughout the exposures, the subject reported strong pressure phosphenes, but no star, flash, or streak events were seen correlated with the beam pulses. Thus, no radiation-induced visual phenomena were seen.

We conclude from these experiments that accelerated nitrogen (7+) ions near the end of their range cause bright streaks and flashes. In order to cause light flashes, the particles must cross light-sensitive regions of the retina at the posterior portion of the eye. Ionization and excitation, and possibly fluorescent light quanta in the immediate vicinity of the particle tracks, cause light sensation. Nitrogen particles passing through anterior portions of the retina and the vitreous body are not seen. The local energy deposition (linear energy transfer) necessary for this phenomenon, as determined with helium ions, appears to be greater than 10 keV/micron (stopping power of 10^8 eV gm^{-1} cm^2). Light flashes and streaks caused by single particles are well localized and are different from the diffuse light sensation reported in fields of diagnostic x-ray machines, or in a mu meson field (8).

Some degree of dark adaptation is necessary for perception of helium and nitrogen nuclei. This is an indication that the outer segments of rods and cones are involved in the visual observation of fast charged particles somewhat similar to observations of light phenomena. Electrical and magnetic produced phosphenes, which are caused by currents, do not require dark adaptation (17).

Exploratory work with nitrogen nuclei passing through and stopping in the visual cortex (calcarine fissure region of the occipital cortex) gave negative results.

Acknowledgments

Professor E.M. McMillan and Dr. P.K. Chapman, astronaut-scientist, were volunteer observers. We are indebted for many valuable discussions with them. The experiments were made possible due to co-operation of Dr. H.A. Grunder and the Bevatron crew. The vital assistance of J. Howard, R.E. Walton, Dr. R. Thomas of the Lawrence Berkeley Laboratory, and L.S. Pinsky of the Manned Spacecraft Center is acknowledged. Dr. Webb Haymaker aided in the exposure of the cerebral occipital lobe. This work was done under the auspices of the U.S. Atomic Energy Commission and the National Aeronautic and Space Administration.

REFERENCES

1. Chapman, P, Pinsky, L. Benson, R. and Budinger, T. Proc. Nat. Symp. Natural and Manmade Radiation in Space (in press).

2. Tobias, C.A., Budinger, T.F., Lyman, J.T., Fourth International Congress of Radiation Research; Evian, France, June 1970 (Gordon & Breach, Washington, D.C., 1971).

3. Tobias, C.A., Budinger, T.F., and Lyman, J.T., Nature 230, 596 (1971).

4. Charman, W.N., Dennis, J.A., Fazio, G.G. and Jelly, J.V., ibid., 230, 522 (1971).

5. Charman, W.N. and Rowlands, C.M., ibid., 232,574 (1971).

6. Budinger, T.F., Bichsel, H. and Tobias, C.A., Science 172, 868 (1971).

7. Fazio, G.G., Jelley, J.V., and Charman, W.N., Nature 228, 260 (1970).

8. McNulty, P.J., ibid., 234, 110 (1971).

9. McAulay, I.R., ibid., 232, 421 (1971).

10. Fremlin, J.H., New Scientist 47, 42 (1970).

11. Tobias, C.A., Budinger, T.F., and Lyman, J.T., Proc. Nat. Symp. Natural and Manmade Radiation in Space (in press).

12. Budinger, T.F., Tobias, C.A., Lyman, J.T., Chapman, P.K., Pinsky, L.S., Bichsel, H., Denney, J.D., and Nelp, W.B., Proc. Colloquium Space Biology Related to Post-Apollo Programme, (Eur. Space Res. Org., Paris, 1971), p. 235.

13. Tobias, C.A., Lyman, J.T., Chatterjee, H.J., Maccabee, H.D., Raju, J.R., Smith, A.R., Sperinde, J.M., and Welch, G.P., Science (in press).

14. Grunder, H.A., Hartsough, W.D., and Lofgren, E.J., Science (in press).

15. Maccabee, H.D. and Lyman, J.T. Lawrence Berkeley Laboratory Report No. 528 (1971).

16. Penfield, W., Proc. Roy. Soc. London, Ser. B, 134, 329 (1947).

17. Barlow, H.B., Kohn, H.I., and Walsh, E.G., Am. J. Physiol., 148, 732 (1947).

FIGURE CAPTIONS

Fig. 1. Human eye and brain exposure–experimental configuration. Nitrogen ions, after final stripping, are injected into the Bevatron, accelerated to 266 MeV/nucleon, and stopped in known parts of the eye and brain.

Fig. 2. Left eye horizontal section showing three nitrogen beam paths. Visual phenomena seen in middle position only.

Fig. 3. Representation of visual phenomenas seen by three dark-adapted observers in a nitrogen ion beam. Duration of flashes is very short without after-images.

Fig. 4. Representation of visual phenomenon seen by Apollo astronauts and us, in ion beams. Cloud phenomenon is similar to x-ray, magnetic, or electrical phosphenes.

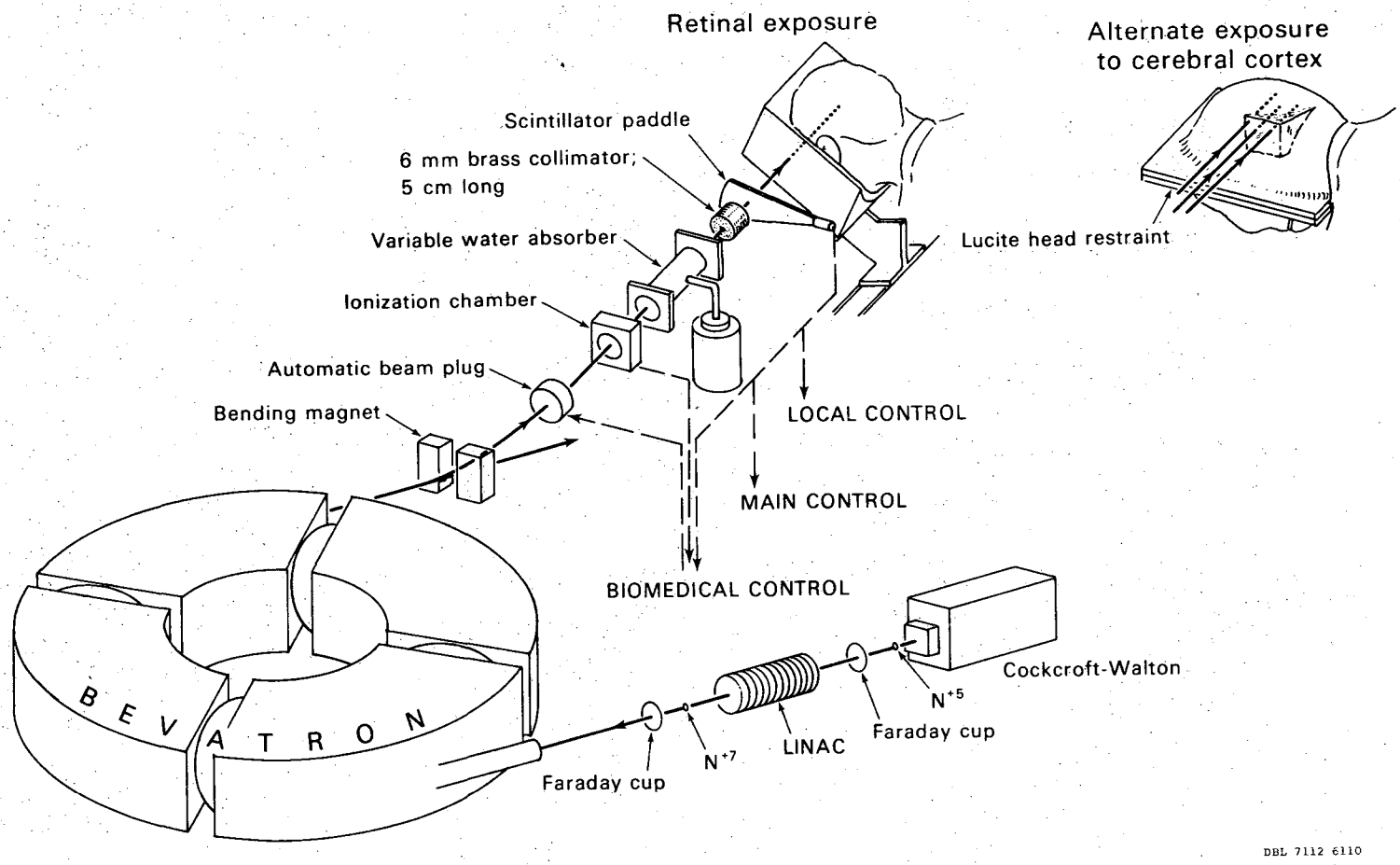
Retinal exposure
Alternate exposure
to cerebral cortex
Scintillator paddle
6 mm brass collimator;
5 cm long
Variable water absorber
Ionization chamber
Automatic beam plug
Bending magnet
Lucite head restraint
LOCAL CONTROL
MAIN CONTROL
BIOMEDICAL CONTROL
BEVATRON
Faraday cup
N+7
LINAC
Faraday cup
N+5
Cockcroft-Walton
DBL 7112 6110

Fig. 1

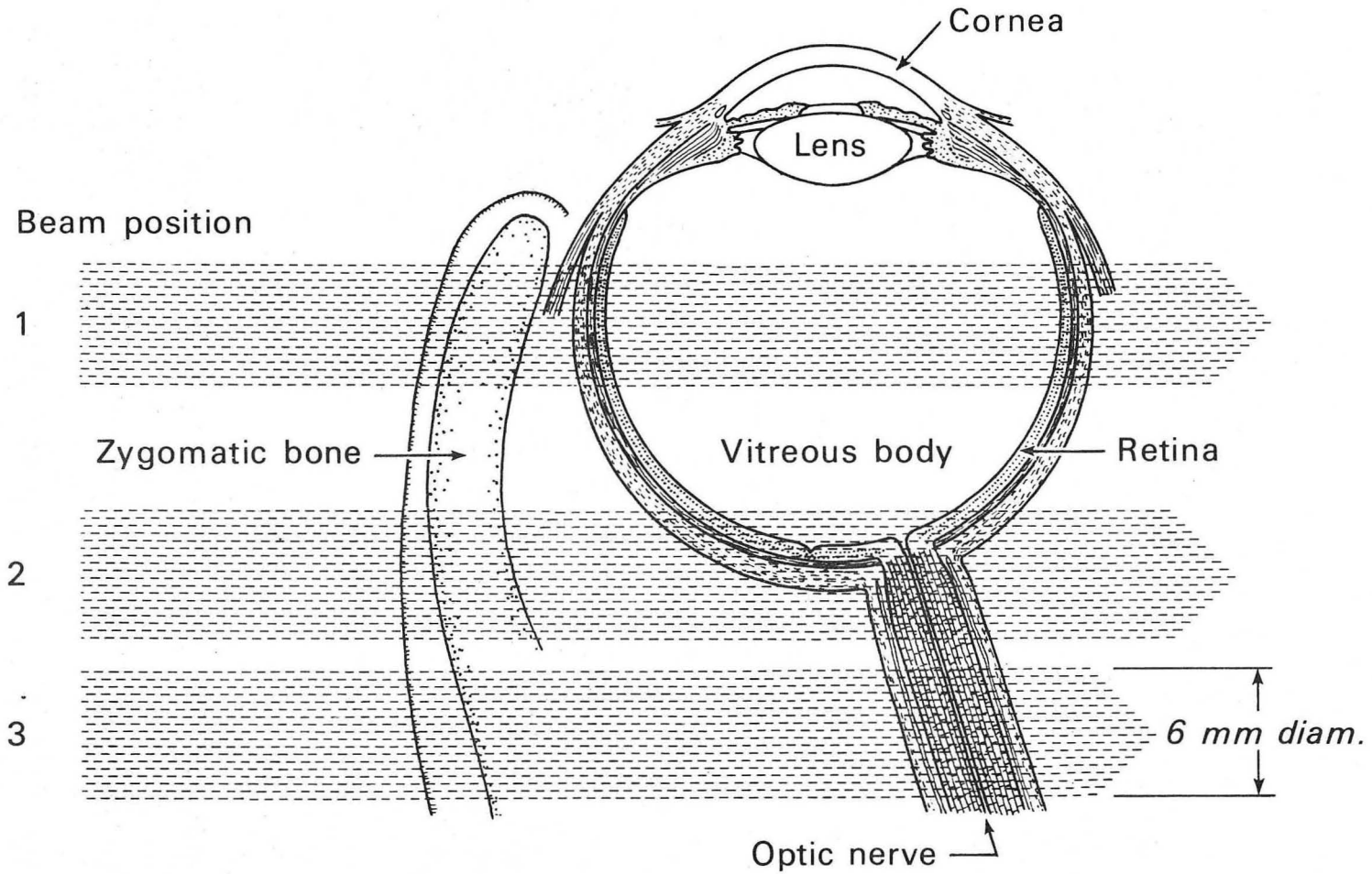
Cornea
Lens
Beam position
1
Zygomatic bone
Vitreous body
Retina
2
3
6 mm diam.
Optic nerve
DBL 717-5921

Fig. 2

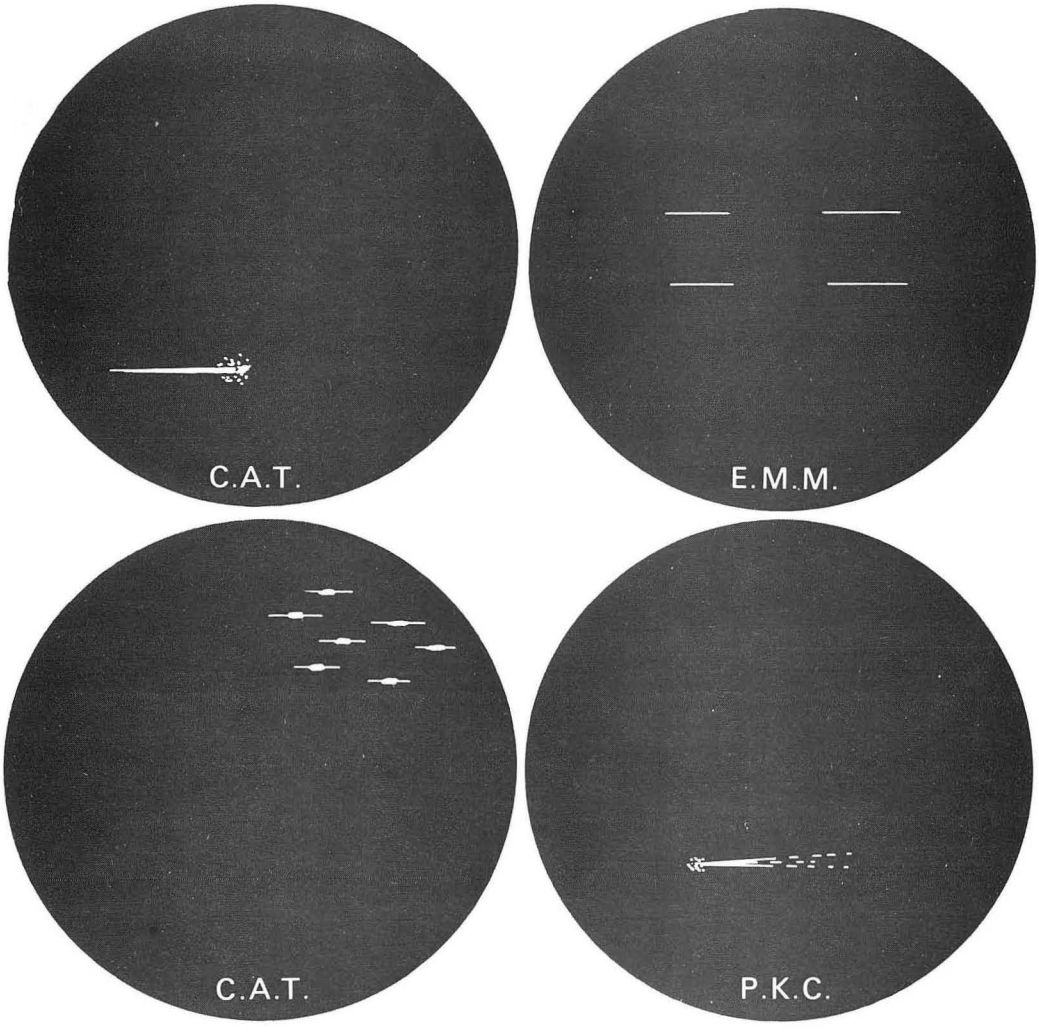

XBL 719-1392

Fig. 3

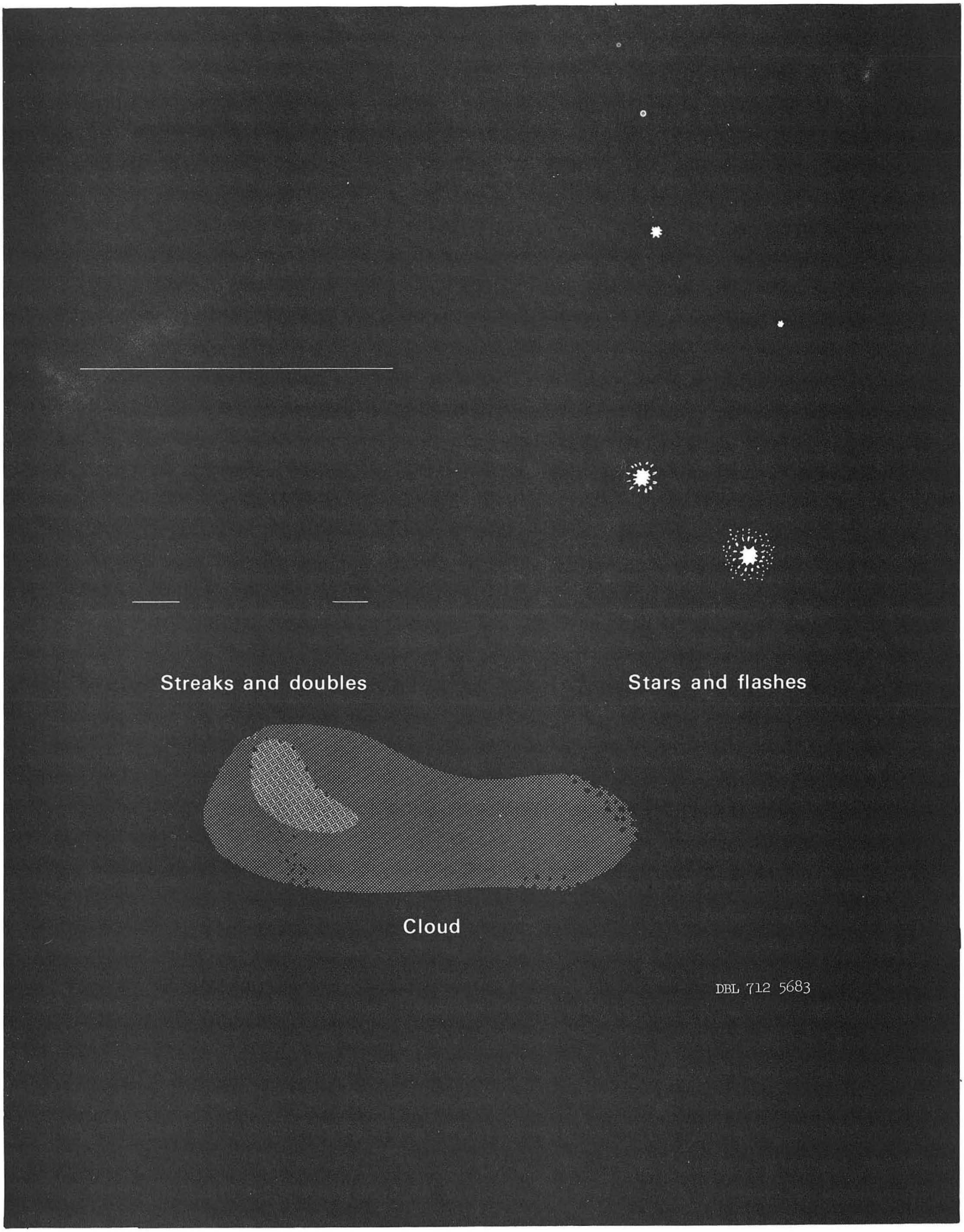

Fig. 4

INITIAL STUDIES ON VERTEBRATE RETINAL INTERACTION WITH THE NITROGEN BEAM

by

by Y. Y. Zeevi,* C. A. Tobias and E. R. Lewis**

Abstract

The interaction of heavy nuclei with the retina may result in pathological damage. The preliminary experiments reported here indicate that gross morphological damage due to a dose of 10^7 particles/cm^2 is confined to the receptor outer segments. This conclusion should, however, await further confirmation.

Introduction

It was first suggested by Tobias in 1952 (1) that the interaction of heavy particles with the retina may produce a visual response. Such responses, in the form of light flashes and streaks were, in fact, reported by astronauts on lunar missions(2). Subsequently, simulations of the presumed interactions of the human eye with cosmic particles, through exposure of human subjects to ion beams, have confirmed the validity of the hypothesis about the nature of light flashes seen by the astronauts (3).

An important question regarding the interaction of heavy galactic nuclei with the retina, as well as with any other nervous tissue, is: what are the longterm effects? In view of the fact that a dark-adapted

* Dr. Zeevi was a pre-doctoral fellow in Biophysics, on PHS-5 T01 GM00829-10; he is now a post-doctoral fellow on PHS-5 T1 GM1418-07 in Bioengineering.

** Dr. Lewis is with the Department of Electrical Engineering & Computer Sciences.

human rod can be stimulated by the absorption of a single photon (4), it is not surprising that high-energy ions elicit a similar response. However, whereas the photon is presumably absorbed by a single molecule of rhodopsin, the interaction with a heavy particle may alter the permeability of disc and plasma membranes and the process of macromolecular synthesis at the inner segment of the rod (Figure 1). This, in turn, may result in a structural deformation of the outer segment. It has been previously established (5) that the outer segments of retinal rods are continuously renewed by the process of assembling new discs (Figure 1) at the base of the outer segment, and the migration of the discs toward the apex of the outer segment where older disc material is being removed. The protein constituents for the discs are synthesized in the inner segment. It is known that high doses (more than several hundred rads) of x-rays, γ-rays or neutrons cause permanent degeneration of the outer segments of rods. If bombardment of the retina with a small ionic beam results in similar damage, then we should be able to detect it with microscopic techniques, especially with scanning electron microscopy.

To investigate such possible pathological effects, we have chosen the mudpuppy, Necturus maculosus, as a preparation for our first series of experiments. The principles of both structural and functional organization of the Necturus retina are similar to those of other vertebrates (6). It consists of five types of nerve cells organized in a layered manner (Figure 5). Synapses in the retina are confined to two plexiform layers. Compared to other retinal

neurons, the cell bodies in the Necturus retina are much larger, having an average size of 30μ in diameter. It is possible, therefore, to record intracellular responses from all five types of neurons (7). That is why the mudpuppy is currently the subject of a concerted effort to understand the functional organization of a vertebrate retina. With respect to the photoreceptors, their gross morphology and fine structure have been studied in detail by light and electron microscopy (8). Recently, two of us have developed new techniques for neural architectural studies with scanning electron microscopy and have applied it to the Necturus photoreceptors (9). It has been shown that, with respect to the surface topography, the results obtained by scanning electron microscopy are identical to those inferred from transmission electron microscopy. Thus, the Necturus retina is clearly an ideal preparation for the investigation of the pathological effects in question.

Materials and methods

Live adult animals were used in the reported experiments (obtained from Schattle Biologicals, Stillwater, Minnesota). Prior to the experiment, a Necturus was anesthetized by immersion in 0.02% ethyl m-aminobenzoate methanesulfonate (TMS) for about 15 minutes. The animal chamber was placed in the nitrogen beam path, oriented so that the animal medial plane formed a 45° angle with the beam axis. The right eye was centered in the beam pathway with the aid of an aligned pointer and was monitored on a closed circuit TV. The doses used were in the range of from 10^5 particles/cm^2 to 10^7 particles/cm^2

of nitrogen^{7+} at an energy of about 250 Mev/nucleon. The animals exposed to the beam were kept in cold water for 15 days before they were sacrificed.

To isolate the retina, the eye was dissected, the vitreous and the lens were removed, and the posterior portion of the eyeball was immersed in cold 2% buffered glutaraldehyde and kept in the dark for three minutes. This procedure helps to separate the retina from the pigment epithelium. The retina was then sectioned, fixed for five hours in 5% buffered glutaraldehyde and dehydrated with a series of ethanol solutions. About one third of the retina was prepared for light microscopy, utilizing Toluidine Blue and periodic acid-Schiff (PAS) techniques, which stain the cell bodies and the plexiform layers respectively. A few sections from the rest of the retina were air dried, and others, critical point dried (10). The dried sections were coated with a thin film of gold and placed in the scanning electron microscope for observation.

Results

In the initial experiments reported here, we exposed six animals to the nitrogen beam. For reasons unrelated to the experiment and probably due to fungus infection, most of the animals (both irradiated and nonirradiated groups) died prior to the time of sacrifice. Our results are limited, therefore, to microscopical studies on retinas of just two animals. We prepared both retinas of both these animals, one which was exposed to the nitrogen beam, and the other which was

used as a control for these two specimens. There appeared to be consistency in the results, using both light and scanning electron microscopy.

Gross morphological damage was confined to the outer segments of the retinas exposed to the beam. Compared to normal retinal receptors, outer segments of most of the irradiated receptor cells appear to have lost part of their volume; some of them either shrank or collapsed (Figure 3). The surface texture of the irradiated receptors was coarse and irregular, whereas the surface of the outer segments in the control eyes appeared to be normal. A topographical view from the top of a field of several hundred retinal receptors (located in the back of the retina) exhibited in the irradiated retinas regions depleted of outer segments (Figure 4). Abnormal outer segments such as those shown in Figure 3 were observed only in the irradiated retinas. We assume, therefore, that damage was induced by the nitrogen particles. However, because of the limited number of specimens, such a conclusion should await further confirmation.

As a byproduct of these experiments, we have been able to obtain scanning electron micrographs demonstrating the three-dimensional structure of the retina. Figure 5 provides an example of a micrograph of two adjacent sections of Necturus retina prepared fifteen days after the exposure to nitrogen^{7+} particles. It exhibits the layered organization of the nerve cells and the synaptic layers, and the glial cell that extends across the retina. Such micrographs,

as far as can be determined, have not been obtained previously.

Discussion

The initial studies reported here were designed as a pilot for future experimentation. To confirm our preliminary observations, we plan to repeat the experiments with larger numbers of specimens. In the next series of experiments, the animals will also be exposed to higher numbers of particles and will be sacrificed at various stages after the exposure to the beam. For comparison, some animals will be exposed to an equivalent dose of x-rays. Functional studies are planned.

Whereas scanning electron microscopy is sufficient for gross morphological studies, it is not adequate for ultrastructural observations. Furthermore, scanning electron microscopy is limited (in the secondary electron mode) to observations of surface topography. Therefore, in order to obtain information about changes in the structure of the outer segment discs and possible pathological damage in the plexiform layers, we plan to supplement our study by transmission electron microscopy.

Acknowledgments

We thank Mrs. L. Jackson, Mrs. T. Scott, and Mr. B. Roesch for technical assistance.

The scanning electron microscope used in this study is located in the Electronics Research Laboratory, University of California, Berkeley. The operation of the microscope is supported by NIH Grant No. GM-17523-02.

REFERENCES

1. Tobias, C.A., J. Aviation Med. 23, 345 (1952).
2. Budinger, T.F. et al, UCRL Report LBL-31 (1971).
3. Tobias, C.A., Budinger, T.F. and Lyman, J.T., UCRL Report UC-48 (1970).
4. Hecht, S., Shlaer, S. and Pirenne, M. M., J. Gen. Physiol 25, 819 (1942).
5. Young, R.W., J. Cell. Biol. 33,61 (1967).
   Young, R.W., J. Cell. Biol. 42, 392 (1969).
6. Dowling, J.E. and Werblin, F.S., J. Neurophysiol. 32, 315 (1969).
7. Werblin, F.S. and Dowling, J.E., J. Neurophysiol. 32, 339 (1969).
8. Brown, P.K., I.R. Gibbons and Wald, G., J. Cell. Biol. 19, 79 (1963).
9. Lewis, E.R., Zeevi, Y.Y. and Werblin, F.S., Brain Res. 15, 559 (1969).
10. Cohen, A.L., Marlow, D.P. and Gardner, G.E., J. Microsc. 7, 331 (1968).

FIGURE CAPTIONS

Figure 1. Schematic diagram of a sagital section through a Necturus retinal rod. Rod outer segment (os) is about 12 μ in diameter and 30 μ long and consists of a stack of about 1100 discs (d) (8). The upper portion of the inner segment, the ellipsoid (el), is densely packed with mitochondria (m). Also illustrated are the ribosomes (r); nucleus (n) which is situated in the paraboloid (p); and the synaptic terminal with its synaptic vesicles (sv) and synaptic ribbon (sr). Two or three processes of horizontal and bipolar cells may be associated with one ribbon (6).

Figure 2. Diagram of the animal chamber and its orientation relative to the beam axis.

Figure 3. Comparison of outer segments for a retina exposed to the nitrogen beam (10^7 particles/cm^2) and from the control eye:
a) scanning electron micrograph Necturus receptors prepared 15 days after exposure to nitrogen^{7+} particles;
b) scanning electron micrograph from the control eye prepared at the same time and by the same technique as the retina exposed to the beam.

Figure 4. A field of retinal receptor cells in a retina exposed to the nitrogen^{7+} beam (10^7 particles/cm^2) compared to a field of receptor cells in the control eye:
a) exposed retina;
b) retina from the control eye.

Figure 5. Scanning electron micrograph of two adjacent sections of Necturus retina prepared 15 days after exposure to nitrogen^{7+} particles. The top layer demonstrates the presumed pathological characteristics of damage induced by the beam. Each cross section exhibits the geometric organization of the retina. Viewing the micrograph from top to bottom, one sees first the receptor outer segments and inner segments, then the outer nuclear layer, outer plexiform layer, inner nuclear layer, inner plexiform layer and ganglion cell layer. Periodically, a Müller cell [glial retinal cell (M)] extends across the retina. Cleavage occurs along the cell surfaces. For example, as indicated by the arrows, an amacrine cell is missing in the top cross section, while it is present in its counterpart.

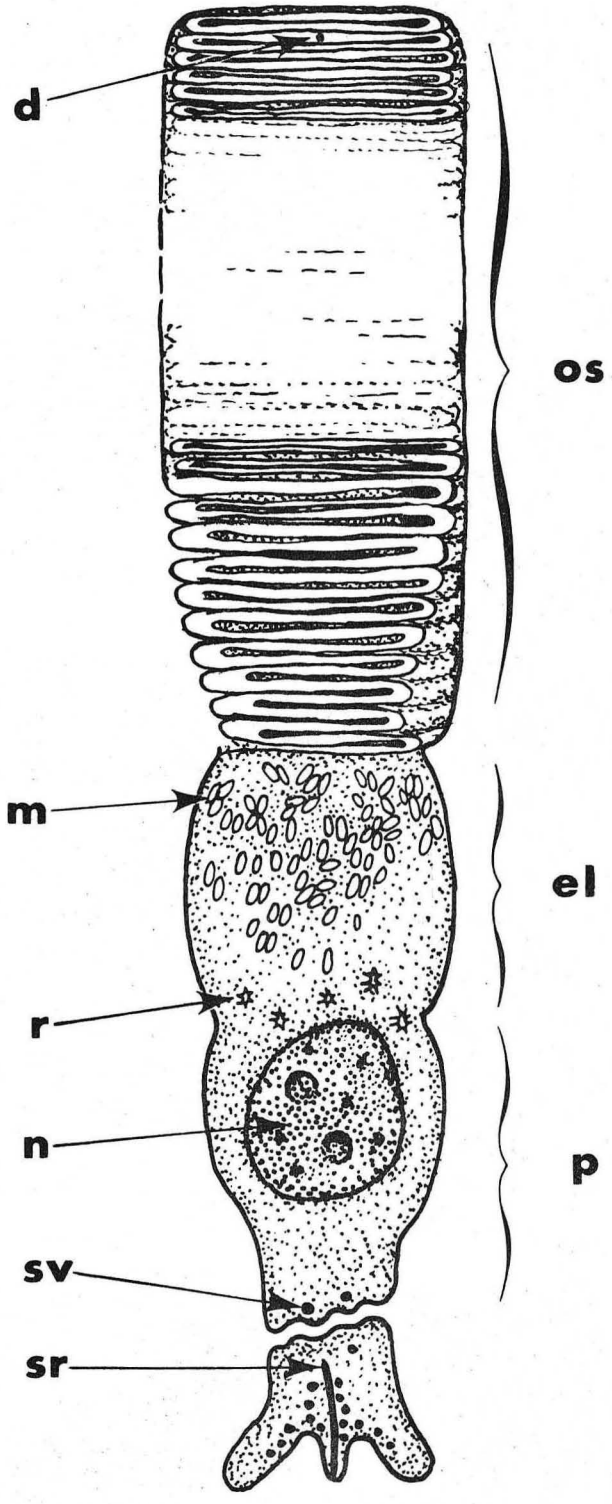

DBL 721 5100

Fig. 1

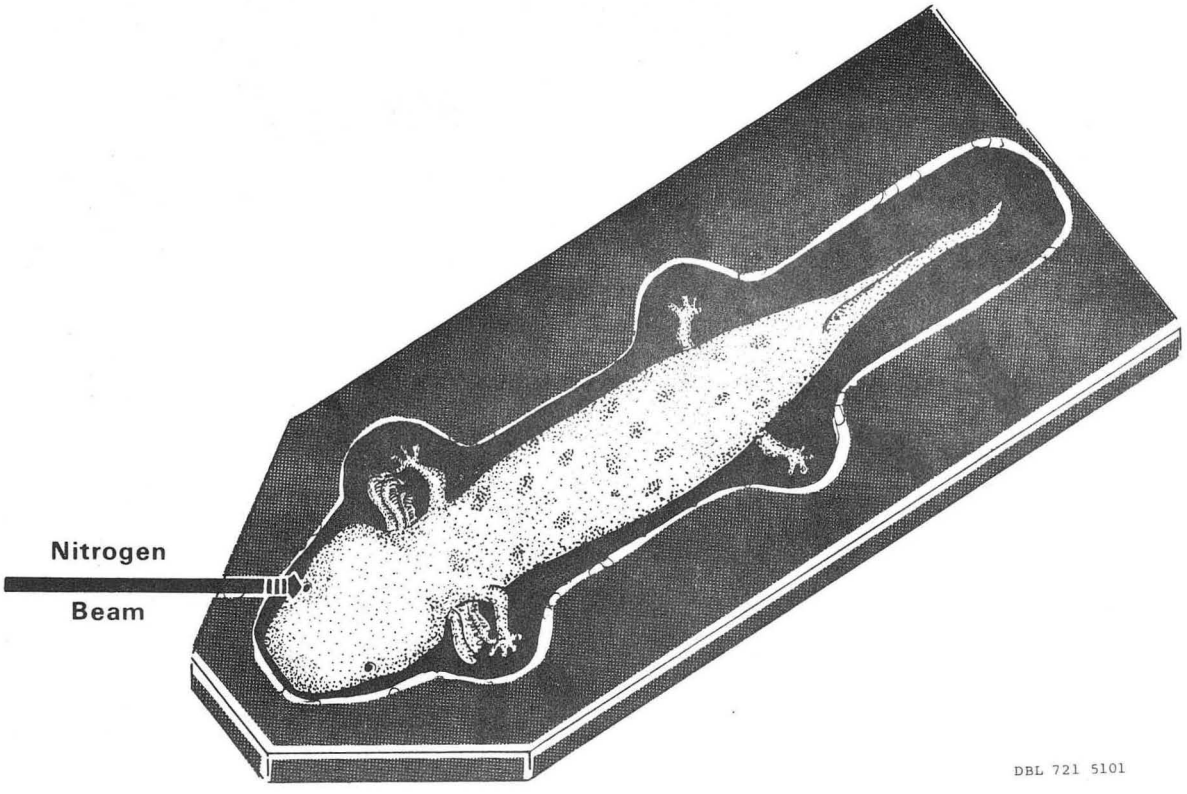

Fig. 2

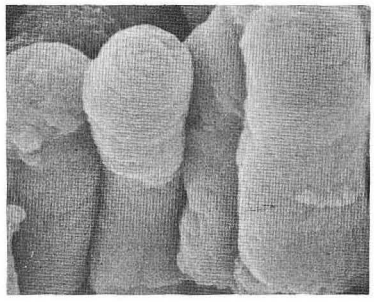

Fig. 3(a)

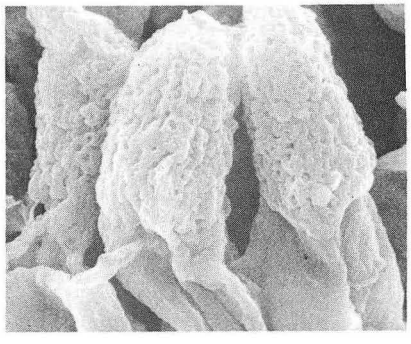

Fig. 3(b)

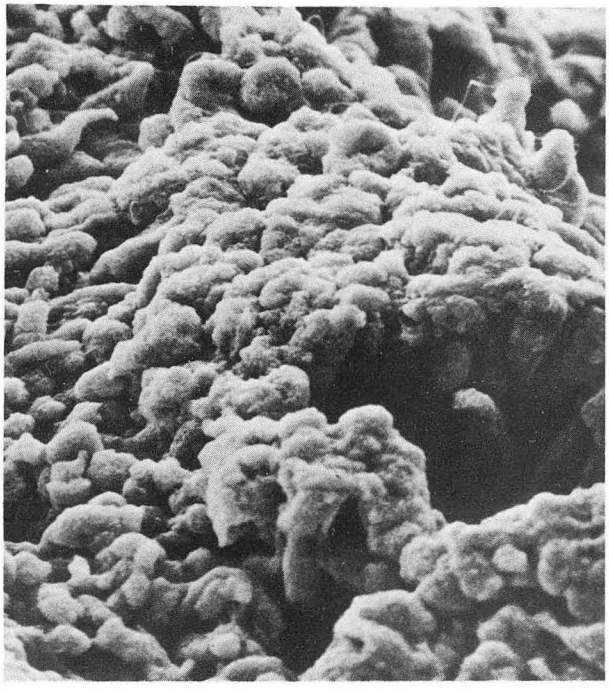

Fig. 4(a)

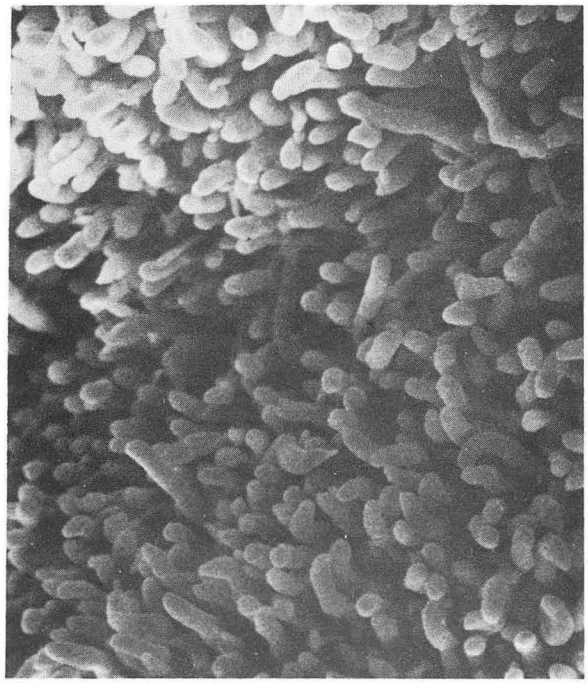

Fig. 4(b)

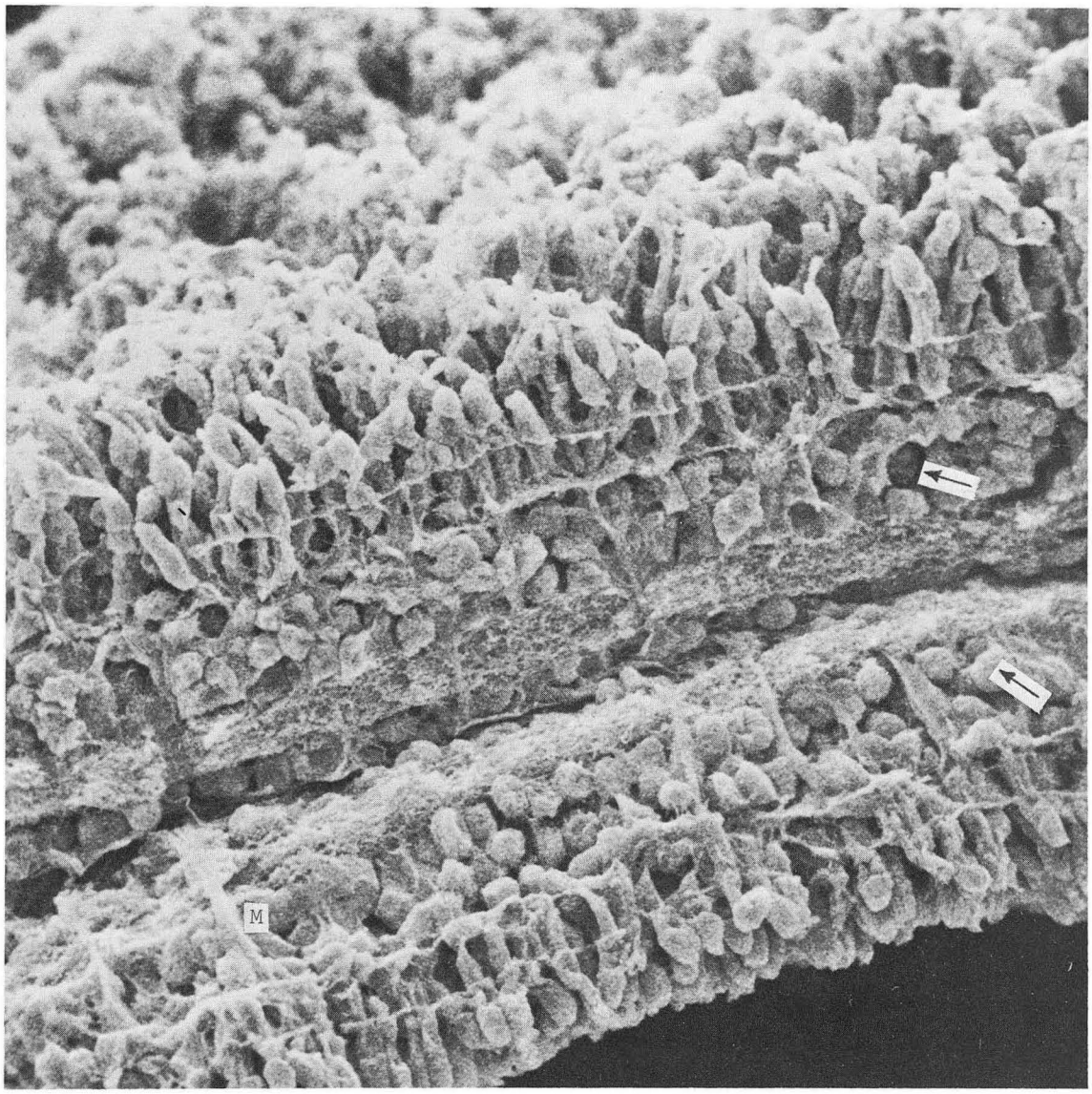

Fig. 5

STUDY OF THE EFFECTS OF A N^{7+} ION BEAM ON THE SURVIVAL OF CULTURED HUMAN KIDNEY CELLS (T-1) IN THE PRESENCE OF AIR AND NITROGEN

by

B. Martins, R. Roisman, M. Raju and C.A. Tobias

Abstract

Cultured human kidney cells (T-1) were exposed in the presence of air or nitrogen at the plateau and the peak of the depth dose distribution curve of a 266 MeV/nucleon N^{7+} ion beam.

The experimentally obtained values for the fractional survival are compared with theoretical curves based on three different models, depending on the radius of the dense ionization tracks. Although the data scatter a good deal, due to difficult experimental conditions, still there is a clear trend in favor of the model, which assumes energy deposition of heavy ion tracks results in a very dense region of ionization of about 21 Å radius.

More detailed experiments are necessary and are being planned. Preliminary data, however, do indicate that the beam may be useful in cancer therapy.

Introduction

Recently a N^{7+} ion beam was successfully accelerated at the Berkeley Bevatron to 266 MeV/nucleon. Several experiments were carried out to study the physical and biological effects of this

N^{7+} ion beam by Tobias et al (1).

This paper deals with the experiments on the survival of cultured human kidney cells exposed, in the presence of air or nitrogen, at the plateau and peak, on a N^{7+} depth dose distribution curve. Such experiments are helpful in assessing radiotherapeutic potentials of heavy ion beams.

We already have many detailed data on the RBE and OER of heavy ion beams at low kinetic energy of less than 10 MeV/nucleon, due to the work of Todd (2) and Bird & Burki (3) of this laboratory, and of Barendsen and others (4) elsewhere. However, when heavy ions are moving at high speeds, the distribution of ionizing events in their tracks is changed; the delta rays have a different energy distribution. For this reason, it is important to carry out experiments with heavy ions at various velocities and atomic numbers.

This was the first time a heavy ion beam was accelerated at the Bevatron, and, because of low dose rate and inconsistency of operation, the experiments could not be performed under ideal conditions. The results presented here are preliminary and qualitative in nature.

Materials and methods

The dosimetry setup as described by Tobias et al (1) was used in this experiment. The beam was monitored with an ionization chamber as well as a plastic scintillation counter. A remotely controlled variable thickness water absorber was placed in the beam path. The dose as a function of depth in water was measured using a parallel plate ionization chamber.

The depth dose distribution of the N^{7+} ion beam is shown in Figure 1. Exposures were made at position 1 when the N^{7+} ion had about 255 MeV/nucleon kinetic energy, and at position 2 when the kinetic energy was about 15 MeV/nucleon.

The beam intensity was low and the beam was focused to a small elliptical spot (0.5 cm x 1.5 cm). Because of these limitations, the classical radiobiological techniques used for obtaining survival curves could not be employed; hence, a modified technique developed by Raju et al (5) and described below, was used.

A 16-hr -old culture of T-1 cells was trypsinized and suspended in fresh medium to give about 10^6 cells/ml. Then 0.03 ml of this cell suspension was plated onto 35-mm plastic dishes, care being taken to confine the cells to a 0.5-cm diameter area in the center of the dish. The dishes were then incubated at 37°C for $1\frac{1}{2}$ hours, after which, 2 ml of medium was added per dish and the dishes were re-incubated. At the time of the experiment, the medium was removed from the dishes, and two layers of thin sterile gauze were placed over the cells and the gauze wetted with L-15 medium. The dishes were exposed in Lucite boxes, through which moist air or nitrogen was passed.* This technique kept the cells moist and at the proper pH.

Each dish was pregassed with N_2 or air for at least $1\frac{1}{2}$ hours and then exposed, with the gas flowing during exposure. After exposure, the cells were removed from the dishes by trypsinizing for 5-10 min at 37°C with 0.03% trypsin (Worthington Biochemicals) in Puck's Saline A(1X), and a cell count was made in a Coulter counter. Suitable dilutions were then made and appropriate aliquots of cell

*Using a Hersh cell, we have estimated the oxygen content of the N_2 gas as being less than 50 ppm.

suspensions plated, so that there would be about 100 clonogenic cells per dish. Ten dishes were plated per dose point. After 12-14 days, the colonies were stained by adding 2-3 drops of 1% aq. methylene blue solution to each dish, and the number of visible colonies per dish was counted.

Results and discussion

Due to the experimental conditions, the cells were kept in exposure boxes for periods of time varying from one to four hours; however, it can be seen from Figure 2 that the plating efficiency of unirradiated cells that were maintained under these stressed conditions for different times did not vary significantly from that of incubator controls, indicating that the cells were not damaged significantly by this treatment. We had previously shown that $1\frac{1}{2}$ hours of pregassing with N_2 is adequate to make cells sufficiently hypoxic (5), except for a possible effect of the plastic support.

The data obtained were compared to theoretical curves derived from quantitative analysis of previous survival curves of Todd (2) and a model for the dependence of cross section on LET developed by Tobias (6).

Three sets of theoretical curves are plotted (Figure 3). The first set assumes that the energy deposition of heavy ion tracks results in a very dense region of ionization of about 21 Å radius, according to the calculations of Chatterjee et al (7); it is this ion dense region that gives rise to the special effects of heavy ions. The second model assumes that the distribution of the initial and

perhaps the secondary ionization events is within a radius of about 150 Å around the track. Finally, in the third model, it is assumed that the 266 MeV/nucleon N^{7+} particles behave just like x-rays. The three models give the following RBE and OER values at the 10% survival level.

	Track Structure	RBE in Air	OER (N_2/air)
I	56% of energy in 24 Å radius	1.2	1.9
II	65% of energy in 150 Å radius	1.3	2.2
III	like x-rays	1.0	2.9

As can be seen from Figure 4, the data scatter a good deal, and the highest dose was not sufficiently high. Also, as indicated in the figure, there were errors in the dose measurements themselves; nevertheless, there is a clear trend in favor of Model 1.

The significance of this, if proved in a more detailed experiment, is that, even at high energy, there is a substantially dense ionization column at the center of heavy ion tracks. This accounts in a major way for the high RBE and low OER of heavy ions. However, the data are sufficiently inaccurate to indicate the final answer may fall between Models I and II.

At the lower energy, near the Bragg peak, the OER is 1.2± 0.2, indicating that this beam may be useful in cancer therapy.

The experimental technique used by us had certain limitations that could have affected the OER values.

Cells were exposed in plastic dishes, under which conditions, it is not possible to obtain maximum OER values (8).

Due to the fluctuating and low dose rate and the breakdown in the Bevatron operation during exposures, samples were exposed at different dose rates and often received multiple fractionated doses. Also, the exposures were made at room temperature, and the amount of moisture in the dishes was not strictly controlled.

These variables could have affected differently, cells exposed to different doses and in N_2 or in air.

We are planning to repeat these experiments using specially made glass dishes in aluminium holders for better control on the moisture content and the pregassing. We are also planning to expose cells bathed in medium which can be maintained at any desired temperature.

We are indebted to Dr. H. John Burki for supplying the mammalian cells and for his general support.

REFERENCES

1. Tobias, C.A., et al, Radiological physics characteristics of the extracted heavy ion beams of the Bevatron, Science 174, 1131-1134 (1971).

2. Todd, P.W., Reversible and irreversible effects of ionizing radiations on the reproductive integrity of mammalian cells cultured in vitro, Ph.D. Thesis, UCRL-11614 (1964).

3. Bird, R. and Burki, H.J., Sensitivity of synchronized Chinese hamster cells to high-LET radiation, presented at Radiat. Res. Soc. mtg. (May, 1971).

4. Barendsen, G.W., Walter, H.D.M., Fowler, J.F. and Bewley, D.K., Effect of ionizing radiations on human cells in tissue cultures. III. Experiments with cyclotron-accelerated alpha particles and deuterons, Radiat. Res. 18, 106-119 (1963).

5. Raju, M.R., Gnanapurani, M., Martins, B.I., Richman, C. and Barendsen, G.W., RBE and OER of π^- - mesons for damage to cultured T-1 cells of human kidney origin, UCRL-20669 (1971) (to be published in Brit. J. Radiol.).

6. Tobias, C.A, Physical energy transfer and biologic effect, in Advances in Medical Physics (Ed., J.S. Laughlin), (Second Int'l. Conf. on Medical Physics, Inc., Boston, Mass., 1971).

7. Chatterjee, A., Tobias, C.A., and Maccabee, H., Radial cutoff LET and radial cutoff dose calculations for heavy charged particles in water, presented at Radiat. Res. Soc. mtg. (May, 1971).

8. Boag, J.W., Crookall, J.O., Chapman, J.D. and Sturrock, J., Factors affecting the oxygen tension around cells growing in plastic petri dishes, Int. J. Radiat. Biol. 17, 305-328 (1970).

FIGURE CAPTIONS

Figure 1. Bragg curve for the 266 MeV/nucleon N^{7+} ion beam showing the positions 1 and 2 where the samples were exposed.

Figure 2. Plating efficiency of T-1 cells as a function of degassing time in air and in nitrogen.

Figure 3. Theoretical survival curves for T-1 cells exposed to N^{7+} ion beams in air or in nitrogen.

Figure 4. Experimental data points and theoretical survival curves for T-1 cells exposed to N^{7+} ions and x-rays or gamma-rays in air or in nitrogen.

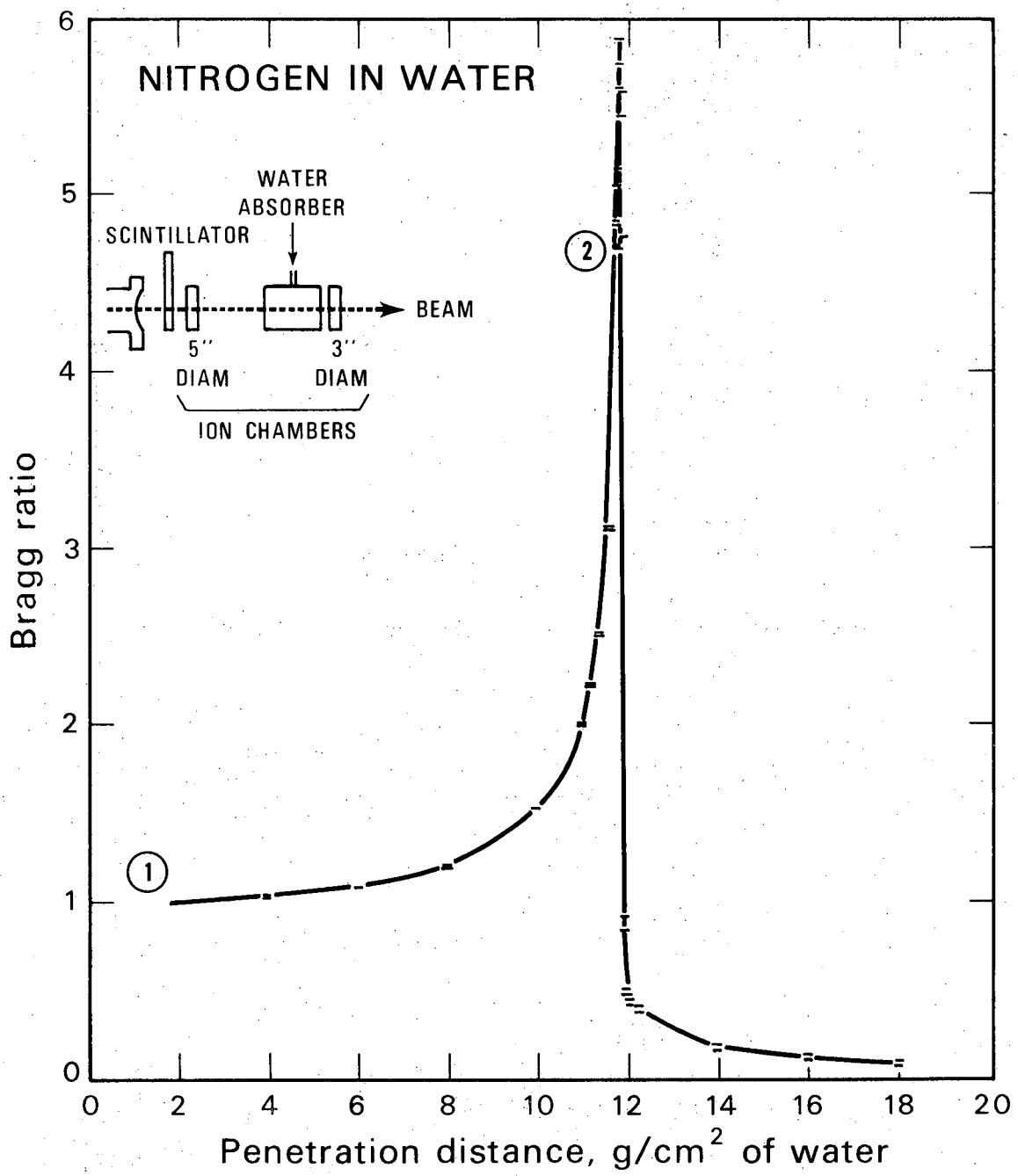

DBL 721 5109

Fig. 1

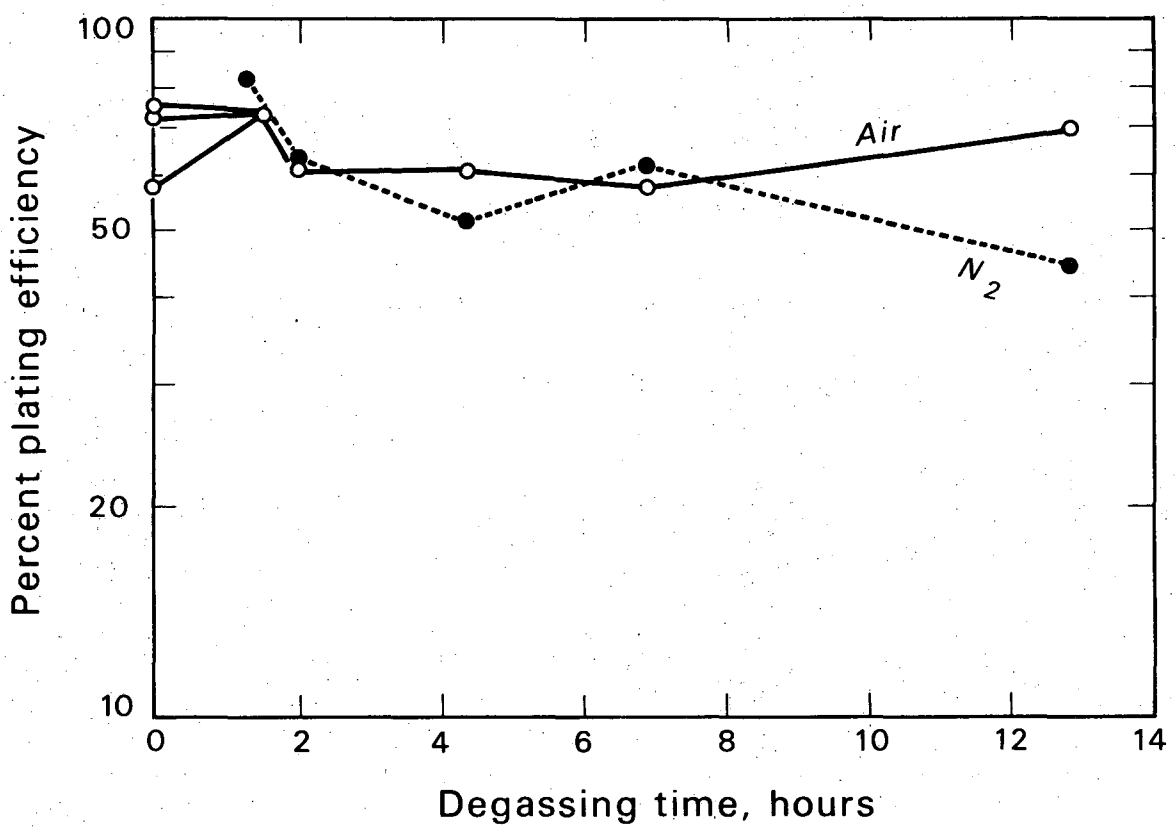
100
50
20
10
Percent plating efficiency
0
2
4
6
8
10
12
14
Degassing time, hours
Air
N_2
DBL 721 5118

Fig. 2

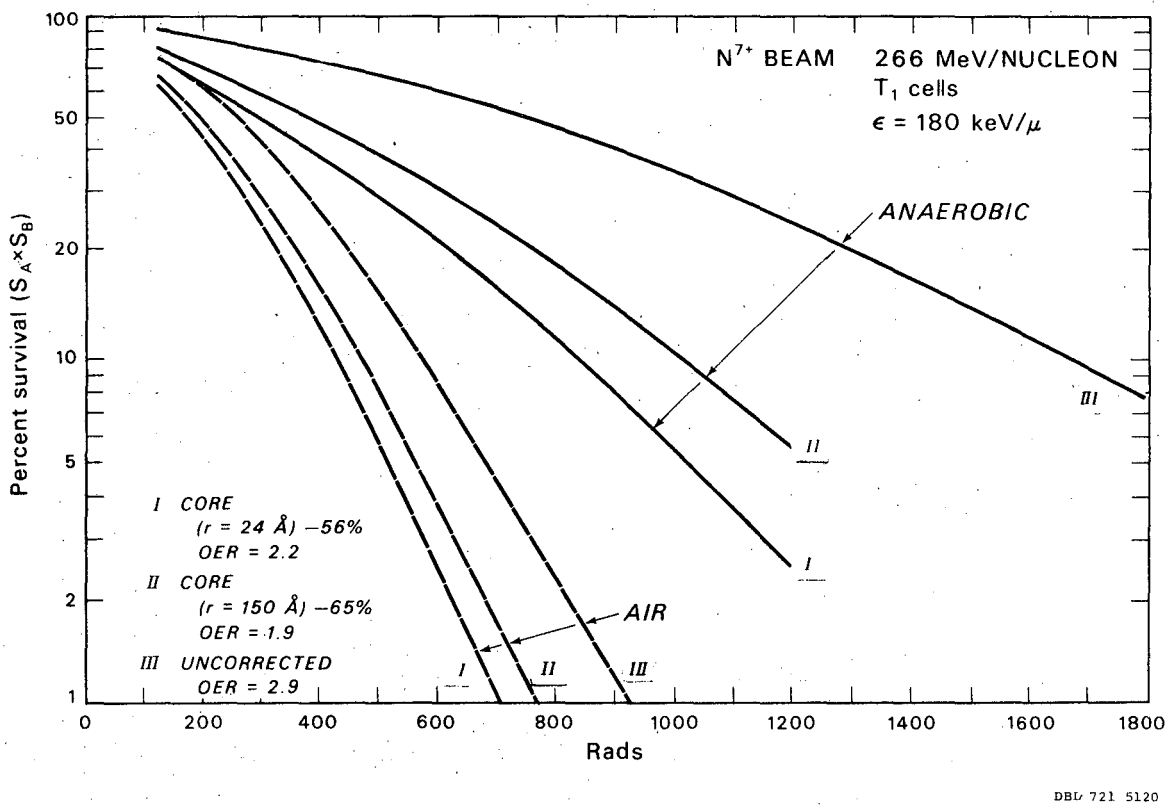

Fig. 3

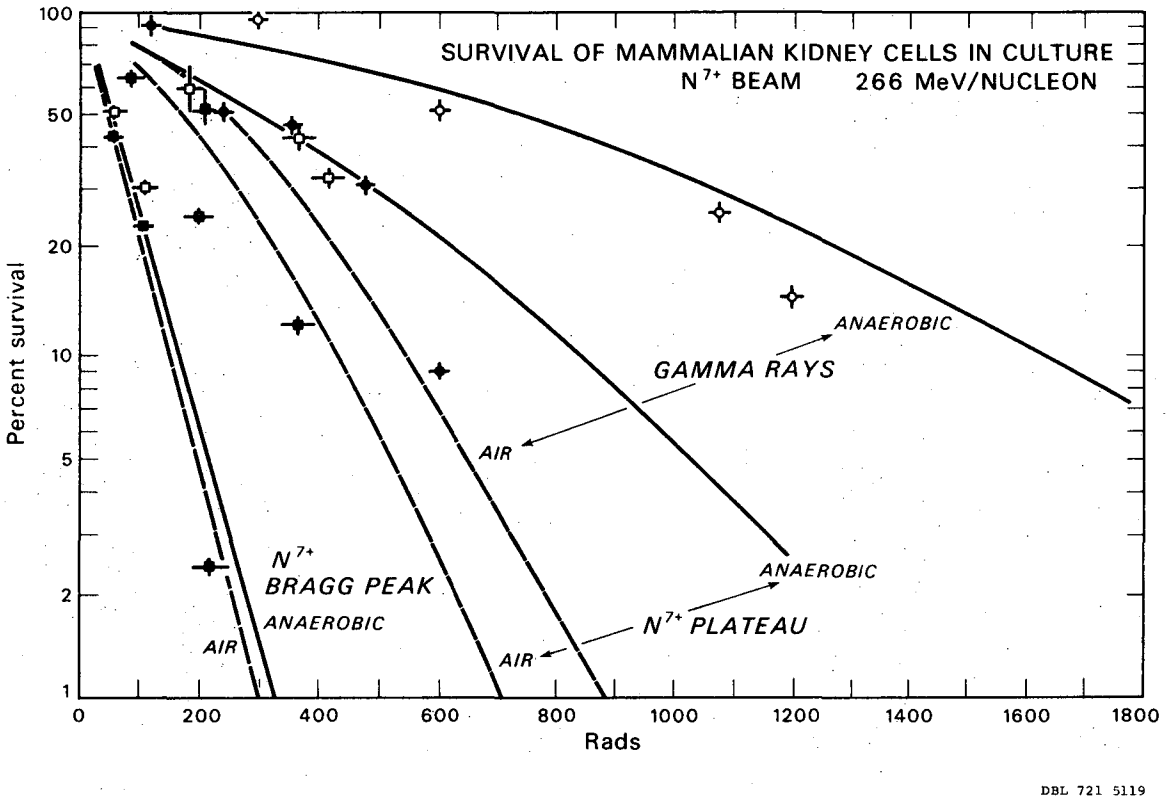
SURVIVAL OF MAMMALIAN KIDNEY CELLS IN CULTURE
N7+ BEAM 266 MeV/NUCLEON
Percent survival
Rads
100
50
20
10
5
2
1
0
200
400
600
800
1000
1200
1400
1600
1800
ANAEROBIC
GAMMA RAYS
AIR
ANAEROBIC
N7+ PLATEAU
AIR
N7+
BRAGG PEAK
ANAEROBIC
AIR
DBL 721 5119

Fig. 4

HEAVY ION IRRADIATION OF ZEA MAYS--A SEARCH FOR BIOLOGICAL ENDPOINTS

by

W. J. Heinze, L. Craise, and J. Howard

Abstract

The attempt to determine biological endpoints showing the effects of very low doses of nitrogen ions on corn seed, Zea mays, is described. The endpoints of per cent germination, germination period, and growth rate showed no effects. The endpoint of per cent developmental abnormalities showed that 6.0% of the nitrogen ion treated seeds showed abnormalities, compared to 4.2% for the cobalt treated seeds, and 2.7% for the untreated seeds, and therefore seems promising for further study.

Introduction

The purpose of this experiment was to find biological endpoints showing the effects of very low doses of heavy ions (in this experiment, nitrogen ions) on dry corn seed, Zea mays. Per cent of germination, length of germination period, growth rate, and per cent of developmental abnormalities were the endpoints assessed. Past studies have investigated x-rays (1,4,9), gamma-rays (5,6), fast neutrons (8), and heavy ions (2,7) to determine their effect on dry corn seed. The biological endpoints of growth rate (4), chromosomal breakage (8), lethality (5), and developmental abnormalities (7) have been assessed. Most studies using x-rays or gamma-rays have employed doses in the

range of 1,500 to 30,000 rads, although doses of fast neutrons in the range of 32 to 126 rads have been used (8). Two studies which involved cosmic rays (2,7) presumably involved much lower doses.

Materials and methods

1. Plant material. Hybrid maize seed, Hybrid 3567 T (Pioneer Hi-Bred Corn Co.), from a single cross between two highly inbred lines, were used in these experiments. These hybrids have the advantages of having no genetic variance while possessing a large percentage of heterozygous loci (3). Any variation between plants and/or treatment groups can be assumed to reflect differences between environments and/or treatments: Group I - no ionizing radiation, Group II - ^{60}Co gamma-rays, or Group III - nitrogen ions.

Before treatment the seeds were placed in two layers (15 seeds to a layer) in 35 mm plastic petri dishes. The seeds were oriented with the long axis of the embryos perpendicular to the axis of the gamma-ray or nitrogen ion beams (See Figure 1).

All seeds were sown in a greenhouse in flats (18" x 24" x 3"), 15 seeds per flat. The greenhouse conditions during a 24-hr period were 16 hrs of light at approximately 25°C and 8 hrs of dark at approximately 23°C. During one period of four days, the ambient temperature rose to 36°C due to a heat wave. Each flat was given a code number and arranged in a completely randomized experimental design. Planting and scoring of seeds were done by separate individuals; the scorer did not know what group was being scored in order to eliminate scorer bias.

2. Cobalt source. The gamma-rays were generated by a ^{60}Cobalt source. The petri dishes were exposed to 1 rad gamma-rays at 3 rads/minute.

3. Nitrogen ion source. The nitrogen ion beam was generated at the Bevatron. For a full description of the beam parameters, see Tobias, et al (10). The petri dishes were exposed to the nitrogen beam and irradiated at the Bragg peak.

Results

1. Assumptions.

a. The beam width was the same as the width of the petri dish, 35 mm.

b. The nitrogen particles were evenly distributed over the area of the petri dish.

c. The area of the embryo was 20% the area of the maize kernel, the remaining 80% is endosperm.

d. 300,000 nitrogen ion particles equal 1 rad.

2. Calculations.

a. The area of the petri dish is approximately 110 sq. mm.

b. The area of a maize kernel is approximately 7.3 sq. mm.

c. The area of a maize embryo is approximately 1.5 sq. mm.

d. Approximately 1% of the particle flux is absorbed by a given embryo, the remaining 99% is absorbed by the endosperm or other kernels. These calculations are valid if the above assumptions are valid.

3. Unirradiated controls. To establish base line values for biological endpoints, 220 seeds were sown. Growth rate and length of

germination were unobtainable for the three groups because of a heat wave. 97.27% of the seeds germinated and 2.7% of the seeds showed developmental abnormalities. The developmental abnormalities were subdivided into four categories:

a. Whole-plant abnormalities (see Figure 2);

b. Primary-leaf abnormalities (see Figures 3 and 4);

c. Secondary-leaves abnormalities (see Figures 5 and 6); and

d. Deficient plant growth, "dwarf".

Table 1 summarizes the results.

4. Gamma-ray treatments. For comparison with controls and nitrogen ion irradiation, 120 gamma-irradiated seeds were sown. 95% of the seeds germinated and 4.2% of the plants showed developmental abnormalities. Table 1 summarizes the different types of abnormalities.

5. Nitrogen ion treatment. In this group different particle fluxes were used, ranging from 5,344 particles (0.018 rad). Table 1 summarizes the results for the group as a whole. 97.18% of the seeds germinated and 6.0% of the seeds showed developmental abnormalities. Table II summarizes the results for different particle fluxes.

Discussion

While no conclusions can be drawn concerning growth rate or length of germination period, the available data weakly supports the conclusion that there are no treatment differences in these two parameters, which is not unexpected due to the low doses utilized. The guaranteed percentage of germination given by the seed company was 95%, and all groups equalled or exceeded that value; therefore, this parameter does not seem promising for further study.

The endpoint of developmental abnormality seems quite promising. Group III had the highest percentage of the three groups. Due to the small number of seeds planted and the small differences between groups, too much reliance, at this time, must not be placed on this fact. A larger number of seeds are being planted which may strengthen the belief that plant abnormalities are suitable endpoints to assess the effects of low doses of heavy ions.

Further studies are being contemplated using the endpoint of chromosomal breakage (8), and using stocks with five or more heterozygous markers, each in a different linkage group.

REFERENCES

1. Bianchi, A. and Contin, M., Effects of Ionizing Radiations on Seeds, International Atomic Energy Agency, Vienna, 359-369 (1961).
2. Curtis, H. and Smith, H., Science 141, 158-160 (1963).
3. Falconer, D., Methodology in Mammalian Genetics, (Holden-Day, San Francisco, 1963), p. 193-216.
4. Notani, N., Effects of Ionizing Radiations on Seeds, International Atomic Energy Agency, Vienna, 475-484 (1961).
5. Pfahler, P., Radiat. Bot. 10, 329-335 (1970).
6. Sarvella, P. and Grogan, C., Radiat. Bot. 7, 107-111 (1967).
7. Slater, J. and Tobias C., Radiat. Res. 19, 218 (1963).
8. Smith, H. et al., Biological Effects of Neutron Irradiation, International Atomic Energy Agency, Vienna, 233-248 (1963).
9. Smith, H. et al., Neutron Irradiation of Seeds, International Atomic Energy Agency, Vienna, 3-8 (1968).
10. Tobias, C. et al., LBL-345 Preprint (In press).

Table I. Treatment Groups and Biological Endpoints.

				Abnormality Types			
Group	No. seeds	% germination	% abnormalities	I	II	III	IV
I	220	97.27	2.7	0	3	1	2
II	120	95.0	4.2	0	4	1	0
III	248	97.18	6.0	1	5	3	6

Table II. Particle Flux and Plant Abnormalities.

				Abnormality Types			
Dish	Particles	Dose	Particles/embryo	I	II	III	IV
57	5,344	.018	80	0	0	0	1
56	13,427	.045	201	0	1	0	1
55	23,339	.078	350	0	1	0	0
45	30,315	.101	455	0	1	0	1
54	46,693	.156	700	1	0	3	0
47	59,980	.200	900	0	1	0	1
49	99,611	.332	1494	0	0	0	0
53	104,350	.348	1565	0	1	0	2

FIGURE CAPTIONS

Figure 1. Possible seed orientations.

Figure 2. Whole plant deformity following N^{14} irradiation.

Figure 3. Embryonic leaf abnormality following N^{14} irradiation--1.

Figure 4. Embryonic leaf abnormality following N^{14} irradiation--2.

Figure 5. Third leaf abnormality following N^{14} irradiation--1.

Figure 6. Third leaf abnormality following N^{14} irradiation--2.

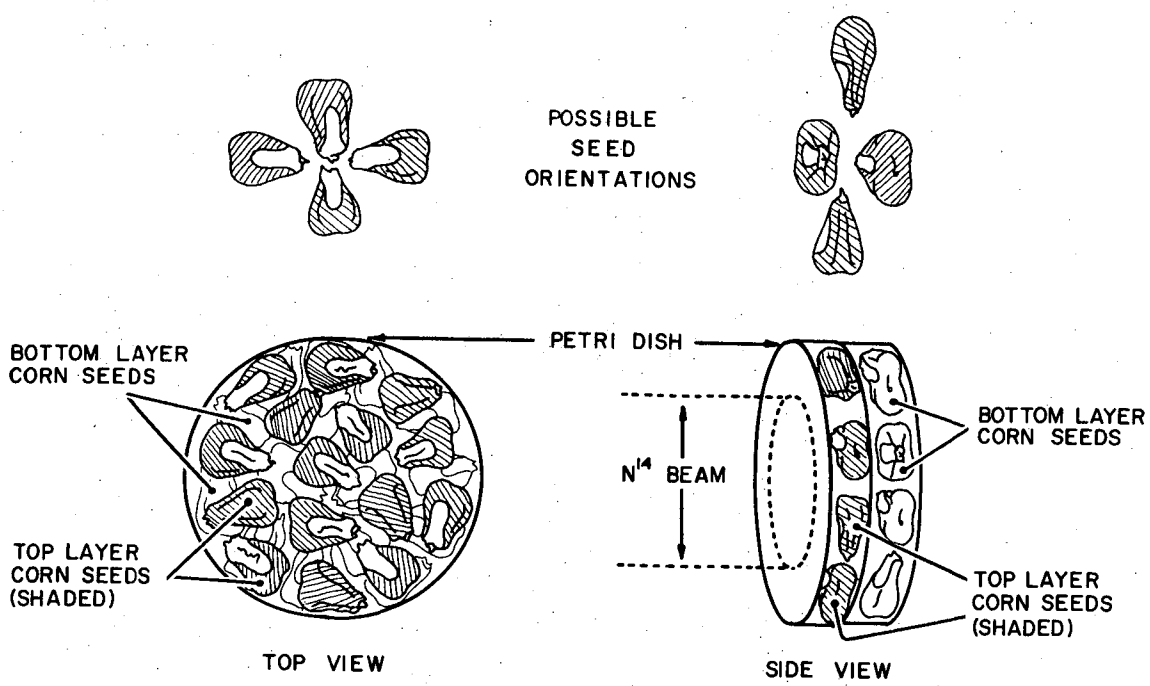
POSSIBLE
SEED
ORIENTATIONS
BOTTOM LAYER
CORN SEEDS
TOP LAYER
CORN SEEDS
(SHADED)
PETRI DISH
N14 BEAM
BOTTOM LAYER
CORN SEEDS
TOP LAYER
CORN SEEDS
(SHADED)
TOP VIEW
SIDE VIEW
XBL 721-17

Fig. 1

VIEW 1 VIEW 2

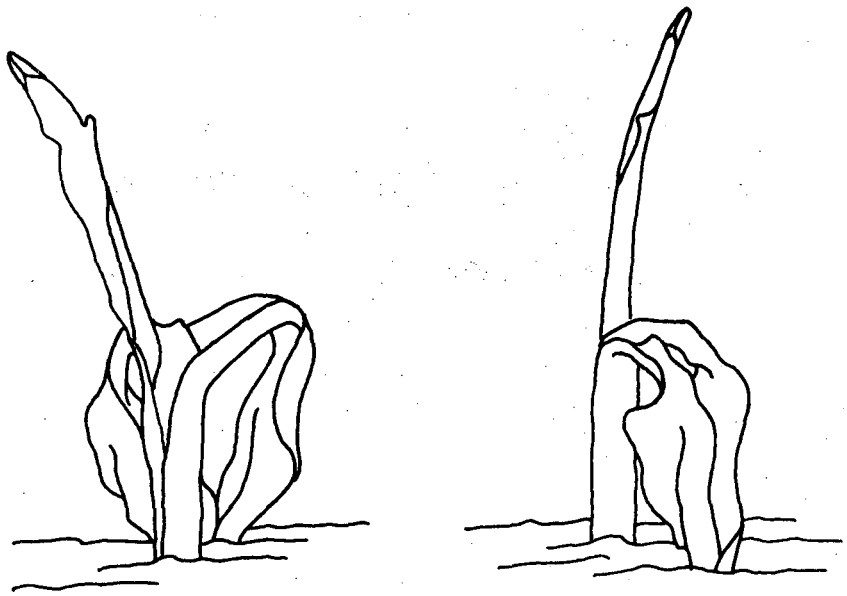

WHOLE PLANT DEFORMITY
FOLLOWING N^{14} IRRADIATION

VIAL: 54 PLANT: 21

XBL 721-18

Fig. 2

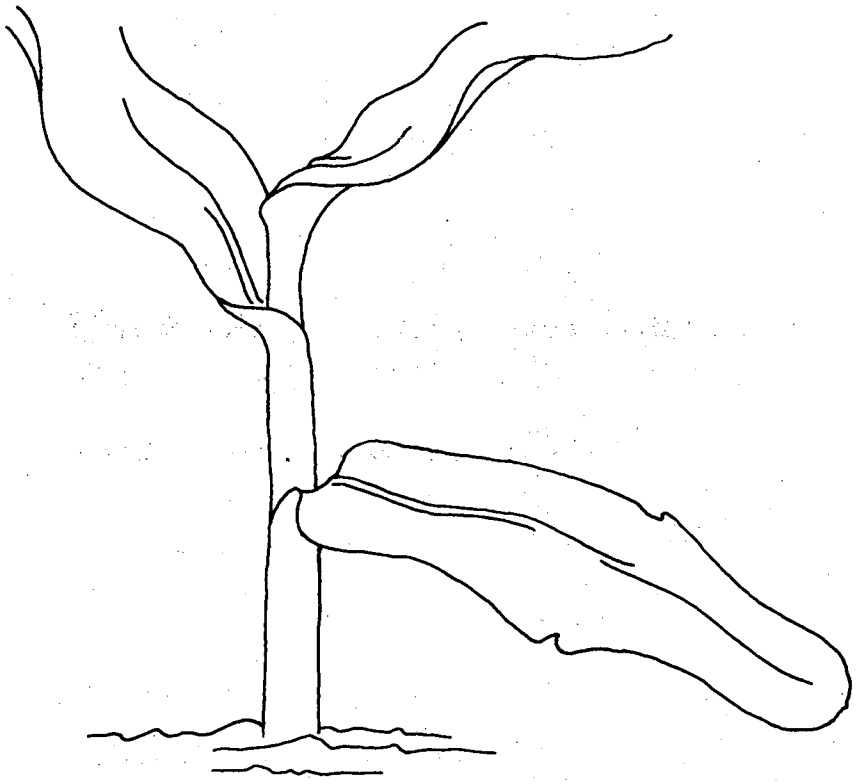

EMBRYONIC LEAF ABNORMALITY
FOLLOWING N^{14} IRRADIATION

VIAL: 47 PLANT: 17

XBL 721-19

Fig. 3

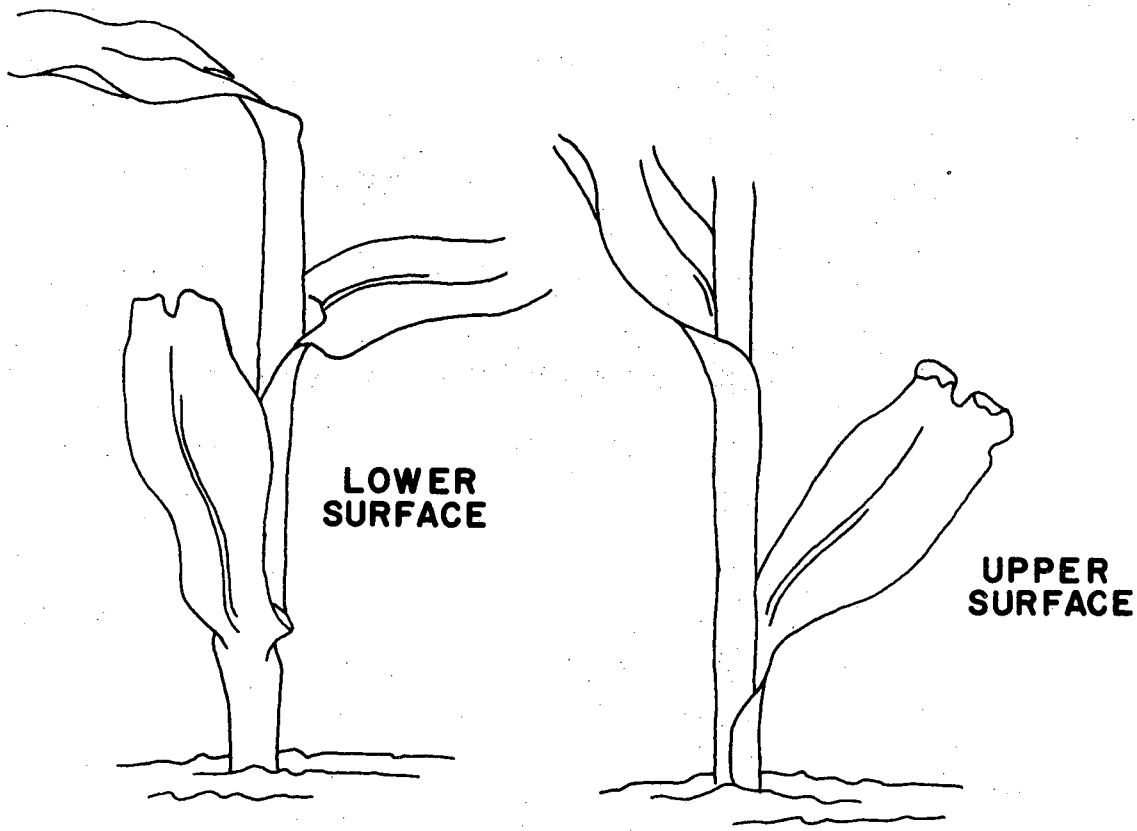

EMBRYONIC LEAF ABNORMALITY
FOLLOWING N^{14} IRRADIATION

VIAL: 45 PLANT: 1

XBL 721-20

Fig. 4

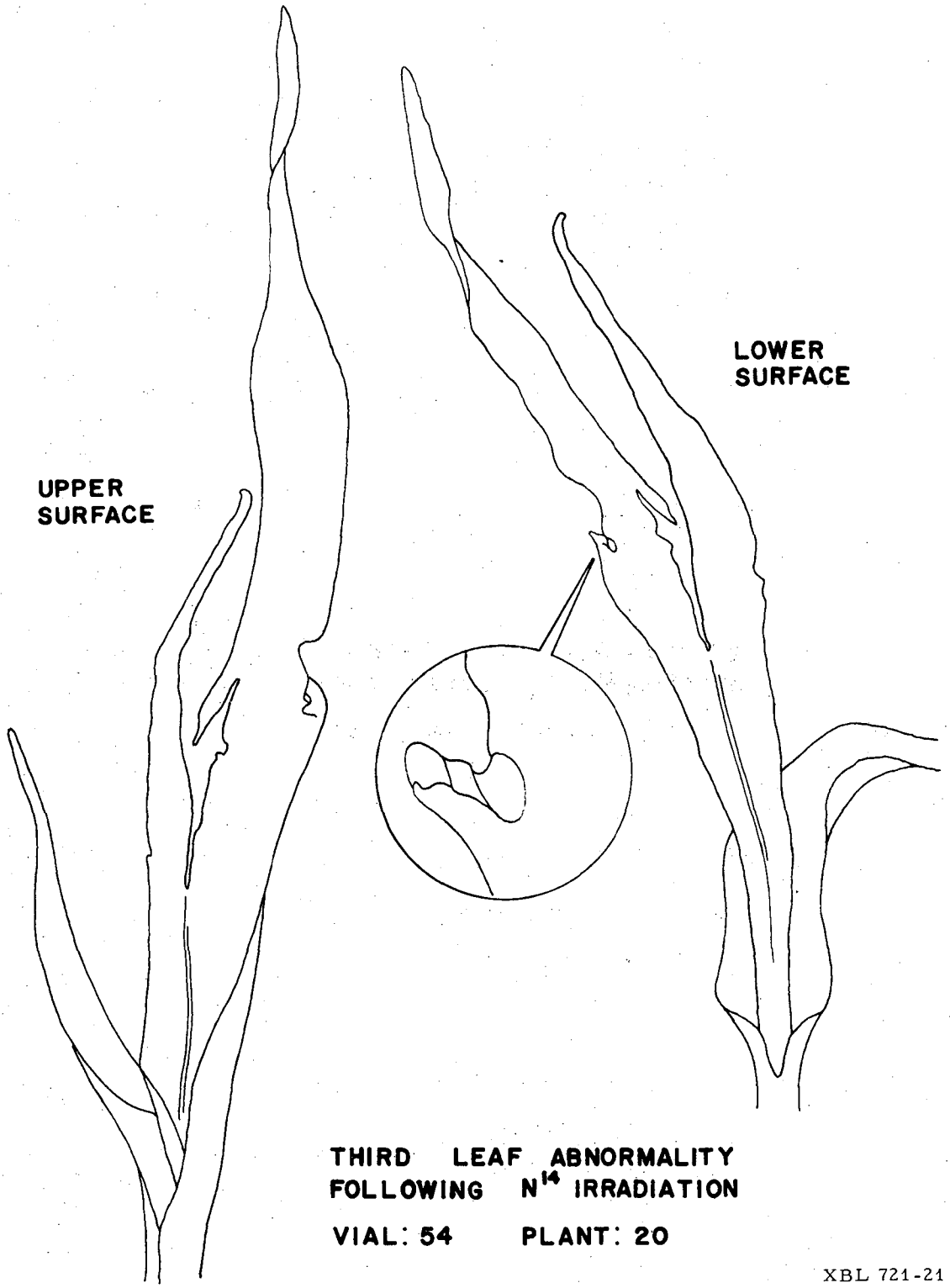
LOWER
SURFACE
UPPER
SURFACE
THIRD LEAF ABNORMALITY
FOLLOWING N^{14} IRRADIATION
VIAL: 54 PLANT: 20
XBL 721-21

Fig. 5

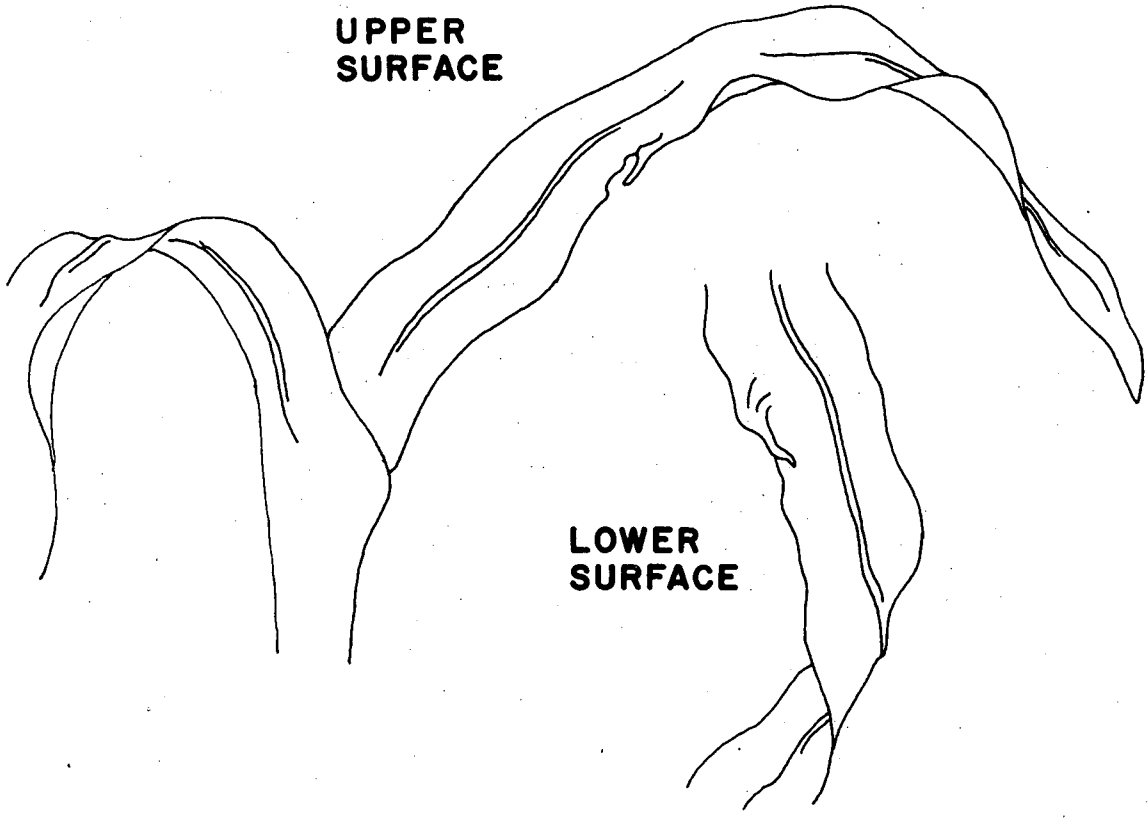

THIRD LEAF ABNORMALITY
FOLLOWING N^{14} IRRADIATION

VIAL: 54 PLANT: 16

XBL 721-22

Fig. 6

EFFECT OF NITROGEN IONS ON BIOLOGICAL DEVELOPMENT

by

T.C. Yang, Beverly D. Heinze, H. Maccabee and G. Welch

Abstract

In this study, Tribolium confusum eggs were exposed to small doses, at different ages, and the effects of nitrogen ions on early embryo development and on late metamorphosis were investigated. Results indicate that some irreparable damage was induced by nitrogen ions and that normal development of Tribolium was obstructed.

Introduction

The influence of ionizing radiation on biological development has been observed and examined by radiation physicists and biologists since soon after the discovery of x-rays. In general, radiation has a harmful effect on organisms, especially when it is given at an early developmental stage. Most studies, however, have been performed with x-rays or gamma radiation, and information about the effect of heavy ion particles on the development of organisms is quite lacking. In the past several years, efforts have been made at this laboratory to examine the relative biological effectiveness in plants, including Arabidopsis (1) and maize (2). Recently, Tribolium confusum eggs were used to study the effect of heavy ions on animal development, since they are very sensitive to ionizing radiation, small in size, and easy to handle.

Materials and methods

The general methods of collecting Tribolium eggs have been reported elsewhere (3). For this experiment, Tribolium eggs were collected during eight hours at 30°C from 1-month-old adults. Under a dissecting microscope, one hundred healthy looking eggs were chosen and placed in a clean glass capillary tube with I.D. of 1.0 mm. Eggs, kept at room temperature before and during exposure to radiation, were irradiated at the Bevatron with a nitrogen beam of 241 Mev/nucleon. The last cm of range of the particles was used in this experiment.

One-day-old eggs were divided into irradiated and nonirradiated groups, and both groups were treated with low temperature, 4°C, for different intervals. After being exposed to low temperature, eggs were transferred into a 30°C incubator, R.H. 30%, and the hatchability, percentage of pupation and eclosion, and abnormalities in adults were checked. The irradiated 2-day-old eggs were put into a 30°C incubator directly after exposure and received no low temperature treatment.

Results and discussion

A total of 1500 1-day-old eggs (25°C) were used in this experiment, and 700 of them received a dose of about 1307 particles/egg at room temperature. All eggs were subsequently treated with low temperature for different intervals to amplify the damage induced by nitrogen ions. Results that are depicted in Figure 1 show that about 10% more

embryonic development failure occurred in the irradiated group when eggs were exposed to 4°C for more than two days. This difference in hatchability is statistically significant, since 100 eggs were used for each data point.

The possible explanation for this result is that the radiation dose used was not high enough to destroy a sufficient number of cells in the egg, which was at late blastoderm and early primitive pit formation stage, in time to stop a successful embryonic development. The subsequent low temperature treatment could increase the number of cell deaths to a critical point and, thus, cause development failure. The increase of the incidence of chromosome breaks and of chromosome constriction of the erosin type (break-constriction) in human lung cells due to low temperature (3°C) treatment has been demonstrated by Hampel and Levan (4).

Although the injury produced by heavy ions was not enough to prevent the embryonic development, this injury was expressed at subsequent developmental stages. In the irradiated group with no low temperature treatment, for example, the percentage of eclosion was about 2% less than in the nonirradiated control group. Also, the percentage of pupation dropped significantly, from 100% to 82.67%, in the group irradiated and kept at 4°C for one day, as shown in Table 1. Some Tribolium adults showed interesting abdominal abnormalities, as depicted in Figure 2. The percentage of abdominal abnormalities, however, was not significantly different between the irradiated and nonirradiated groups. Apparently, low temperature promotes abdominal malformation, so possibly, eggs injured significantly by heavy ions were blocked from developing into adults by

early metamorphosis. This may have prevented us from seeing more in the irradiated group.

Eggs irradiated with nitrogen particles at two days old showed no change in hatchability, but a decrease in percentage of pupation and in that of eclosion was found, as shown in Table 1. Adults with abnormal antennae were observed, as shown in Figure 2. This malformation is definitely induced by nitrogen ions, for at two days old, the body segments of the embryo within the egg were already formed, as shown in Figure 3, and the most observable body structure injury could be seen in the antennae only. Our studies with x-rays also showed that adults irradiated at the 2-day-old stage frequently developed abnormal antennae (3), whereas we do not find this abnormality present in nonirradiated control group.

Results from this experiment suggest that nitrogen ions can induce irreparable injuries in cells, even at a very low dose rate and with a very small dose, since: (a) a synergistic effect of radiation and low temperature treatment was observed; (b) some Tribolium irradiated at the egg stage failed to develop into final adult stage; and (c) abnormalities were observed in adults irradiated at the 2-day-old stage.

For insects having completed metamorphosis, the early stages (i.e., egg, larval and pupal stages) can be considered as an embryonic stage for the adults, and many adult structures (e.g., antennae) are developed from anlages--a group of embryonic cells. Since a higher percentage of developmental failure was observed in the irradiated group in this experiment, it seems likely that embryonic cells in mammals with a

potential for differentiation, e.g., erythroblast, crypt cells, gonad cells, etc., will be very sensitive to heavy ion irradiation. More studies with heavy ion particles, therefore, are needed in the interests of radiotherapy, space biology and fundamental radiobiology alike.

Acknowledgments

We thank Miss Laurie M. Craise for her excellent technical help and drawings.

REFERENCES

1. Hirono, Y., Smith, H.H., Lyman, J.T., Thompson, K.H., and Baum, J.W., Radiat. Res. 44, 204-223 (1970).

2. Slater, J.V. and Tobias, C.A., Radiat. Res. 19, 218 (1963).

3. Yang, T.C., Silver, I.L. and Heinze, B.D., Tribolium Information Bulletin 13, 90-93 (1970).

4. Hampel, K.E. and Levan A., Hereditas 51, 315-343 (1964).

Table 1. Effects of ^{14}N particles on the development of Tribolium confusum.

Dose (particles/egg)	Age of eggs at irradiation	No. eggs	Days at 4° C	Hatchability (%)	Pupation (%)	Eclosion (%)	Abnormalities (%)	Types of abnormality
0000	1-day old (25° C)	100	0	73	100	100	0.00	---
			1	78	100	98.72	2.60	abdomen
			2	65	92.30	100	0.00	---
			3	46	95.65	100	11.36	wing
			4	36	97.22	94.28	18.18	abdomen, wing
			5	36	86.11	96.77	10.00	abdomen, wing
			6	28	57.14	87.50	21.43	abdomen
1307	1-day old (25° C)	200	0	83	100	98.19	0.00	---
		100	1	75	82.67	100	0.00	---
			2	53	92.45	95.91	2.13	abdomen
			3	38	71.05	100	15.15	abdomen, wing
			4	22	95.45	95.23	15.00	wing
			5	19	94.73	100	11.11	wing
4297	2-day old (25° C)	200	0	74	91.22	98.51	0.75	antenna
8594	2-day old (25° C)	125	0	81.6	97.06	96.96	2.08	antenna

FIGURE CAPTIONS

Fig. 1. Synergistic effects of nitrogen ion irradiation and low temperature treatment on the embryonic development of 1-day-old Tribolium confusum eggs. Number of nitrogen particles per egg = 1307.

Fig. 2. Abnormalities of Tribolium adults exposed in Bevatron experiment.

1. Fused antennal segments of adult irradiated with 8594 nitrogen particles at 2-day old egg stage.
2. Dislocated antennal segment of adult irradiated with 4297 nitrogen ions at 2-day-old egg stage.
3. Twisted abdomen of adult irradiated with 1309 nitrogen ions and exposed to 4° C for 3 days.
4. Twisted abdomen of adult exposed to 4° C for 5 days at 1-day-old egg stage.
5. Fused abdominal segments of adult exposed to 4° C for 1 day at 1-day-old egg stage.

Fig. 3. Embryonic development of T. confusum egg.

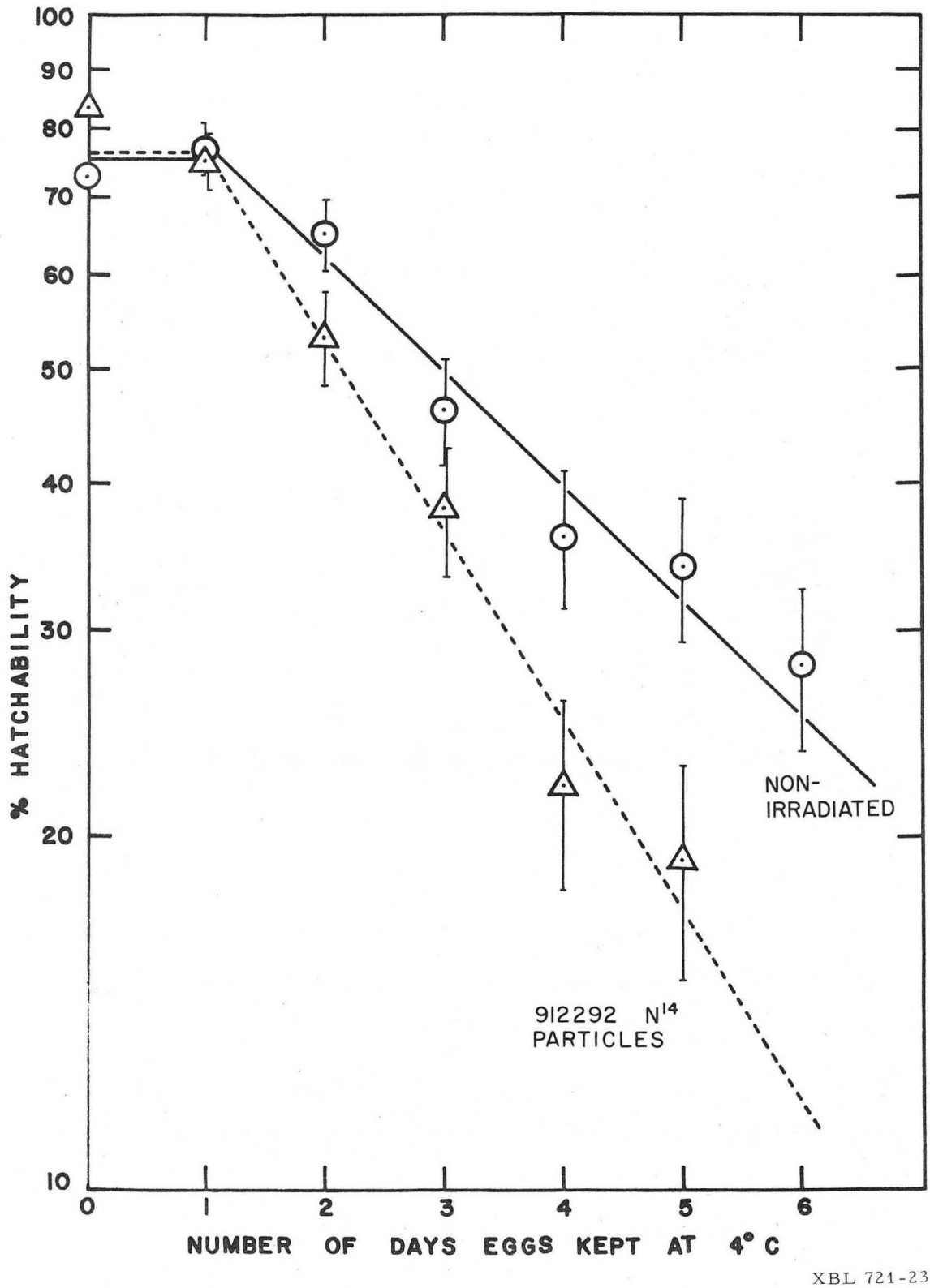

Fig. 1

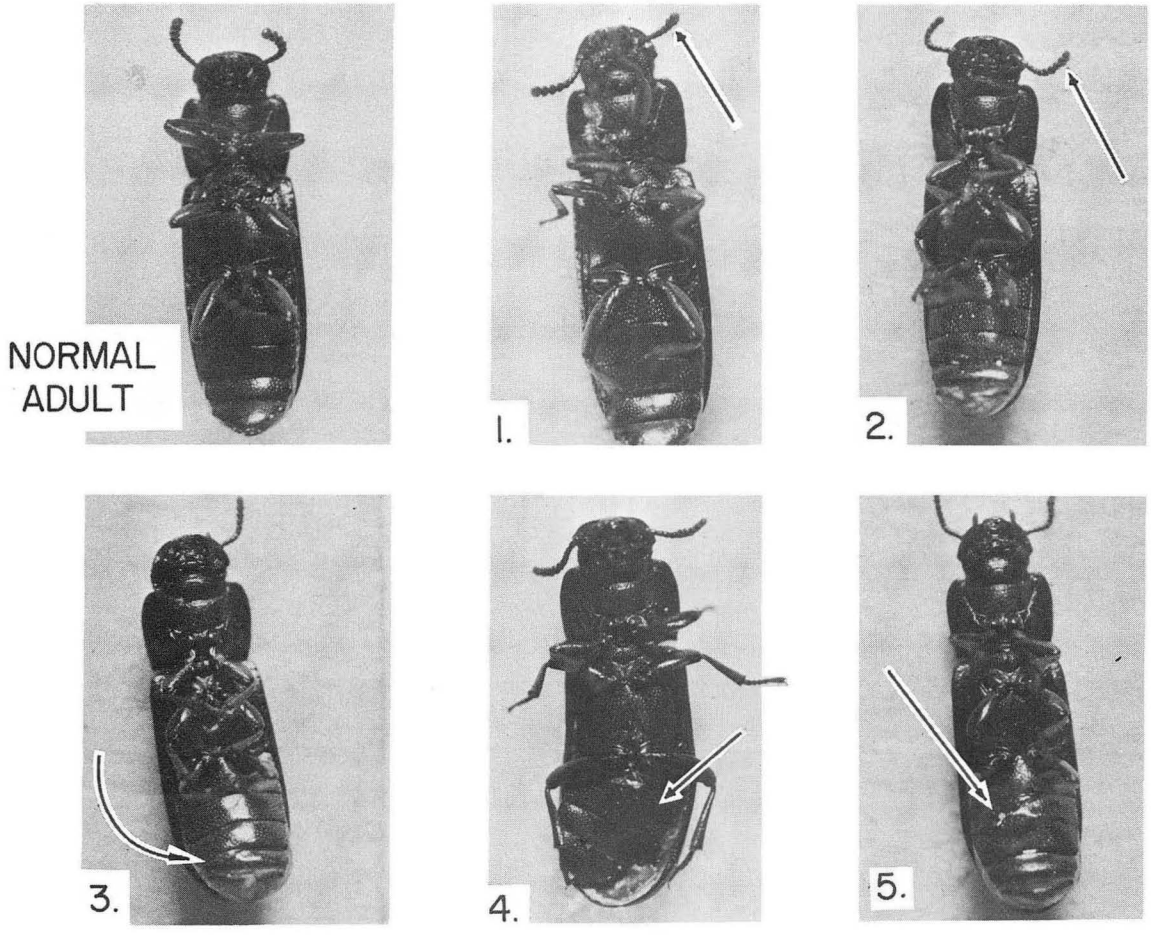

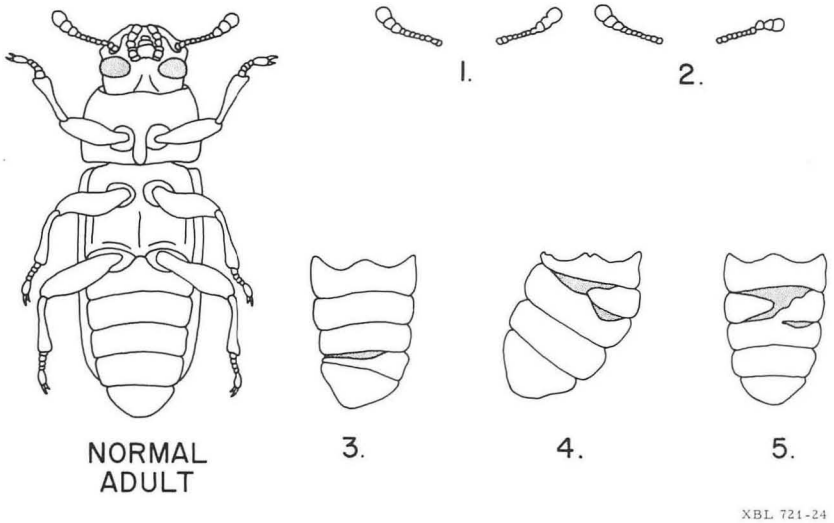

Fig. 2

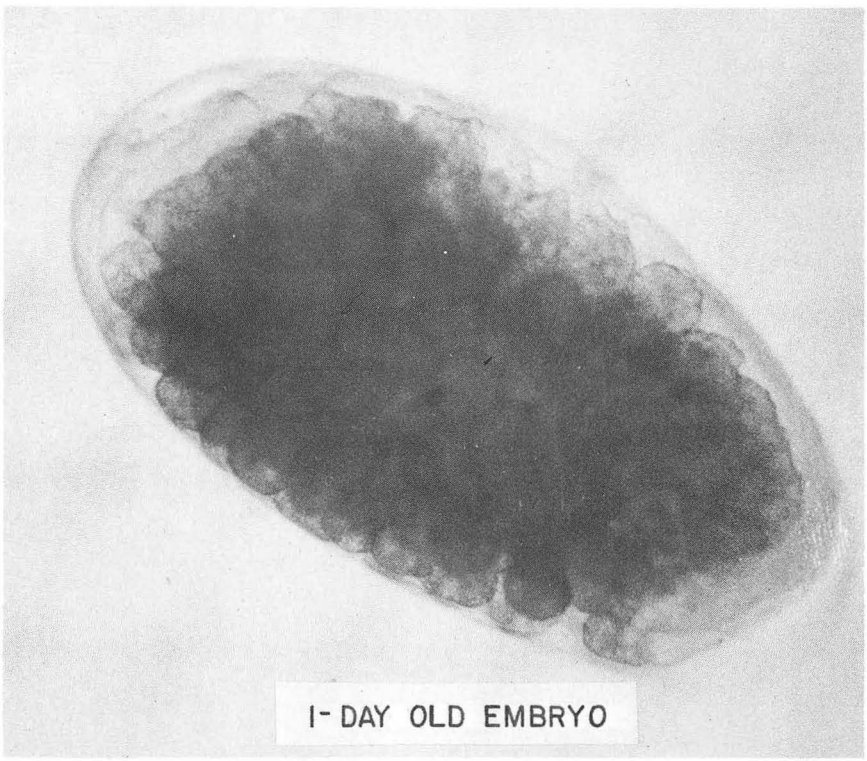

Fig. 3(a)

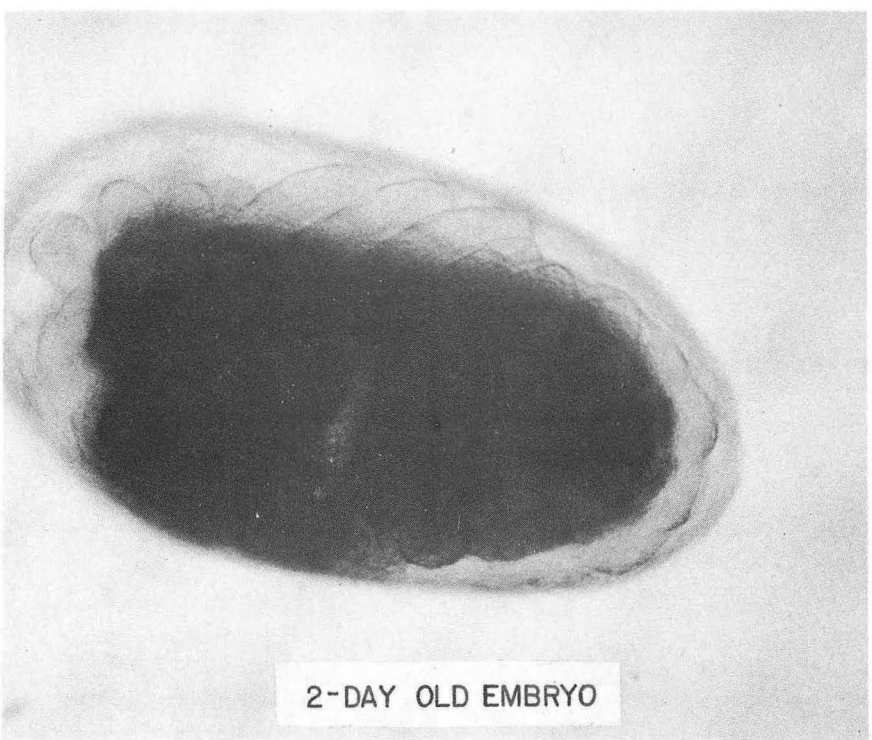

Fig. 3(b)

EFFECTS OF ACCELERATED NITROGEN IONS ON THE HAIR OF MICE

by

J.T. Leith, W.A. Schilling, G. Welch

Abstract

Skins of C57Bl male mice were irradiated with N^{7+} ions at three different particle flux levels. A significant hair depigmentation was seen at the highest particle flux level.

Introduction

Exposure of resting hair follicles in the skin of mice to ionizing radiation results in the production of hair depigmentation seen in subsequent generations of growing hair. This phenomenon, known as the greying effect, appears to have an approximate threshold of 250 rads with progression to complete (100 per cent) hair depigmentation at about 1000 rads with conventional radiations (1-4). This effect is due to radiation damage to the melanocyte population of the hair follicle germinal bulb.

The purpose of this experiment was to examine the effects of accelerated heavy ions, nitrogen $^{7+}$ particles, on the greying response of mouse skin hair follicles. Due to the much greater linear energy transfer of the accelerated heavy ions, it is reasonable to assume that the greying response should be greater than with x- or gamma-ray irradiation for equivalent amounts of radiation. Another consideration

is that exposure of personnel in space to heavy cosmic ray primaries ($Z \geq 6$) is a potential hazard, as the effects of such heavy primaries on mammalian somatic cells is not known.

Materials and methods

Male C57Bl/6J mice obtained from the Jackson Laboratories, Bar Harbor, Maine, were used in the experiment. Mice were 70 days old at irradiation, and were anesthetized immediately prior to exposure. The hair was plucked from the back approximately 1 hour prior to exposure to the nitrogen ion beam to ensure that the hair follicles were in a resting (catagen) stage. After irradiation, the mice were housed singly and were observed daily throughout the regrowth period. Animals received Feedstuffs Lab Chow and chlorinated water ad libitum.

Thirty days after irradiation, on regrowth of the first generation of new hair, hair was plucked from the irradiated area and hair samples were dispersed in a small volume of water containing a surface active agent to ensure separation of the individual hairs. An aliquot was then spread on slides with Permount, allowed to dry, and covered with a coverslip. Observations were made using a 40 x microscope. Each hair was examined along its entire length and was scored as either white, black, or mosaic (partly white). The mosaic category was included in the white category for expression of results.

Radiation techniques

The nitrogen ion Bragg curve in water is shown in Figure 1 (5). A variable water absorber was used to reduce the residual range of the

nitrogen ion beam to 1.2 cm in tissue. That portion of the Bragg curve which irradiated the skin of the mice is shown in the shaded area of Figure 1. The height of the Bragg curve on beam entrance into the skin is approximately 1.85 times the Bragg curve value of the beam before any degradation with water absorbers. As the Bragg ratio rises to a maximum of about 5.82, with the ratio rising sharply through its residual range in mouse skin, the tissue dose will also vary widely. The incident nitrogen ion beam passed in a posterior-anterior direction along the skin of the back of the mouse is also shown schematically in Figure 1.

The cross-sectional geometry of the nitrogen ion beam was 0.6 x 1.5 cm^2 at its apex. This noncircular geometry presents important considerations when evaluating the response of irradiated skin, which may be considered as a flat sheet intersecting the major axis of the nitrogen ion beam in a perpendicular fashion.

As all of the nitrogen ion particles of the incident beam were counted by the available dosimetric instruments (i.e., ionization chambers and fast scintillation counters), it is necessary to make a correction for the fraction of total particles that would be seen by the target in question, the skin.

We have considered the skin to be a flat sheet of 0.05 cm thickness. Therefore, if the total number of particles in the beam spot for the entire beam is counted by ion chambers (i.e., 0.6 x 1.5 cm^2), the biologically important particle fraction, assuming a homogeneous distribution of particles, is 0.6 x 0.05 cm^2, or 0.03 cm^2. The fraction of the total particle flux seen by the skin is then 3.3 per cent of the total flux as seen by dosimetric instruments.

Results

Figure 2 is a photograph of control and irradiated mouse skin 13 days after irradiation. Visually, a number of distinctly white hairs may be seen in the irradiated animal, while none of the control animals show any such effect. This irradiated animal received about 4.13×10^4 nitrogen particles.

In Table 1 are presented those values obtained from nitrogen ion irradiation of the C57Bl/6J mice for controls and three levels of particle flux differing by factors of ten. There appears to be a tendency for the per cent of white hairs to increase with increasing particle flux. However, there is much interanimal variation, and there are not enough animals per flux level to justify any definitive conclusions. Still, using a t-test for a single sample as compared to control values, there appears to be a statistical increase in hair whitening significant at the 0.05 level of probability for the single animal that received 100 pulses of radiation (6).

It is instructive to perform an analysis of the particle flux with regard to the number of hair follicles per unit area of irradiated skin and to the cross-sectional area occupied by such hair follicles. Assuming that the follicles are evenly distributed in the skin of the back at a density of 5×10^3 follicles/cm^2 as the nitrogen beam penetrates the full thickness of the skin, the skin surface irradiated is approximately 1.2×0.5 cm^2, or 0.6 cm^2. Given the previous follicle density, this would yield about 0.6 $cm^2 \times 5 \times 10^3$ follicles/cm^2, or 3×10^3 follicles per irradiated skin area at any particle flux level.

In the last column of Table 1 are listed approximate numbers of hits by nitrogen ion particles that might have been sustained by each hair follicle. In derivation of this number of hits/hair follicle, we have assumed that the cross-sectional area of each hair follicle is about 0.005 x 0.0075 cm^2, or 37.5 x $10^{-6} cm^2$. Only for the animal that received 100 pulses of radiation would it appear that the nitrogen ion density/hair follicle is great enough to produce a noticeable degree of melanocytic hair follicle damage, and, indeed, this appears to be the situation.

Discussion

As the actual dose in rads received by the mice in these irradiations is very small (i.e., about 2 rads at 100 pulses of radiation), there follows the suggestion that the greying response of mouse skin hair follicle melanocytes after irradiation may represent a sensitive, nonthreshold situation in that even the smallest amount of heavy particle irradiation has a distinct possibility of damaging melanocytes. In this regard, it must be mentioned that the linear energy transfer in skin, at the entrance to skin (i.e., residual range 1.2 cm) is about 47 KeV/μ and rises rapidly thereafter. A radiation response for skin greying has also been observed with low energy carbon ions some years ago at the Lawrence Berkeley Laboratory Heavy Ion Linear Accelerator, in cooperation with Herman Chase and group from the University of Rhode Island (7). That work was not brought to quantitative conclusion, since the short range of carbon particles at that time made estimation of depth penetration to the hair follicles uncertain.

In conclusion, the tentative results presented would suggest that the nitrogen ions accelerated at the Lawrence Berkeley Laboratory Bevatron have a significantly greater biological effect than previously obtained literature suggests for this particular biological assay following conventional irradiations.

Pigmentation of hair depends on the action of several pigment cells. The results suggest that the action of a single nitrogen^{7+} particle is sufficient to cause lack of pigmentation, whereas in an x-ray beam, many secondary electrons are necessary to accomplish a similar result.

REFERENCES

1. Galbraith, D.B., Response of hair types in mice to higher doses of x-rays, J. Morph. 118, 589-596 (1966).

2. Chase, H.B. Greying of hair. I. Effects produced by single doses of x-rays in mice, J. Morph. 84, 57-80 (1949).

3. Chase, H.B. and Rauch, H. Greying of hair. II. Response of individual hairs in mice to variations in x-radiation, J. Morph. 87, 381-392 (1950).

4. Curtis, H.J., The effect of a deuteron microbeam on greying of hair, Radiat. Res. 18, 510-515 (1963).

5. Tobias, C.A., et al, Radiological physics characteristics of the extracted heavy ion beams of the Bevatron, Science 174, 1131-1134 (1971).

6. Sokal, R.R. and Rohlf, F.J., Biometry (W.H. Freeman and Co., San Francisco, 1969).

7. Tobias, C.A. Personal communication.

Table I

Number of Bevatron nitrogen ion pulses as measured by scintillators	Number of nitrogen ion particles per animal	Number of particles seen by irradiated skin	Number of animals per exposure level	Per cent white hairs 30 days after irradiation	Approximate number of particles per hair follicle
0	---	---	6	0.40 ± 0.57(1) (0.0, 0.8, 1.2,(2) (0.0, 0.0)	0.01
1	4.26×10^3	1.40×10^2	3	1.53 ± 2.26 (3.8, 0.0, 0.8)	0.14
10	4.13×10^4	1.36×10^3	4	2.18 ± 1.04 (3.4, 2.5, 2.0, 0.8)	0.14
100	4.24×10^5	1.40×10^4	1	6.00 ± 2.60 (6.0)	1.46

(1) Control animals were plucked on the same day and in the same conditions as the irradiated animals.

(2) Figures in parentheses indicate the white hair percentages for the individual mice.

FIGURE CAPTIONS

Fig. 1. Bragg ionization curve for the 270 MeV/nucleon ^{14}N beam. Sketch also shows the penetration of the residual beam in mouse skin and the change in the Bragg ratio over this penetration in skin.

Fig. 2(a). Photograph of regrowing control mouse hair 13 days after plucking. There are no white hairs visible. The lighter background of the incompletely covered skin is also visible.

(b). Photograph of regrowing mouse hair 13 days after irradiation. There are distinctly white hairs visible. The animal received approximately 4.13×10^4 nitrogen ions.

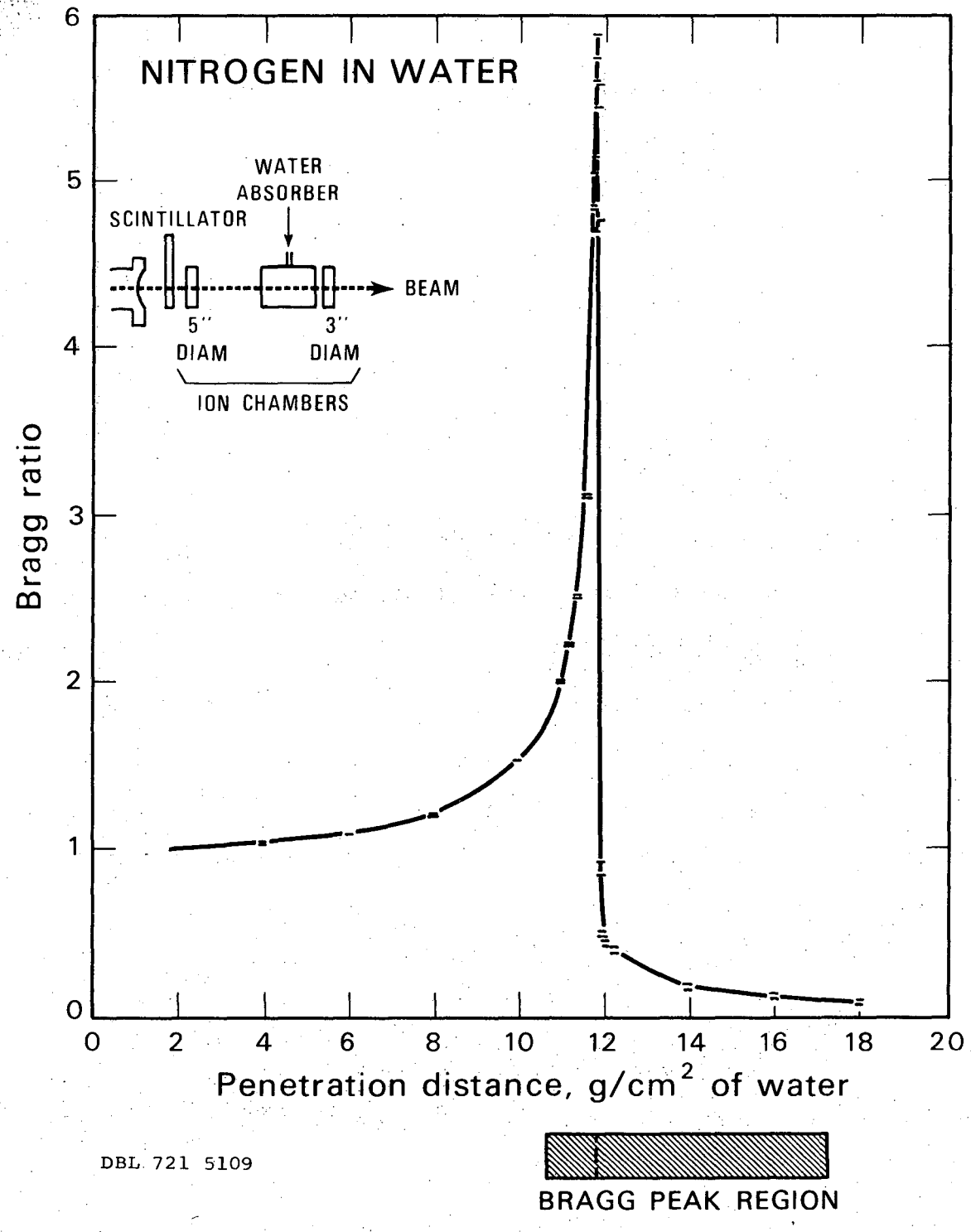
NITROGEN IN WATER
WATER
ABSORBER
SCINTILLATOR
BEAM
5"
DIAM
3"
DIAM
ION CHAMBERS
Bragg ratio
Penetration distance, g/cm² of water
DBL 721 5109
BRAGG PEAK REGION

Fig. 1

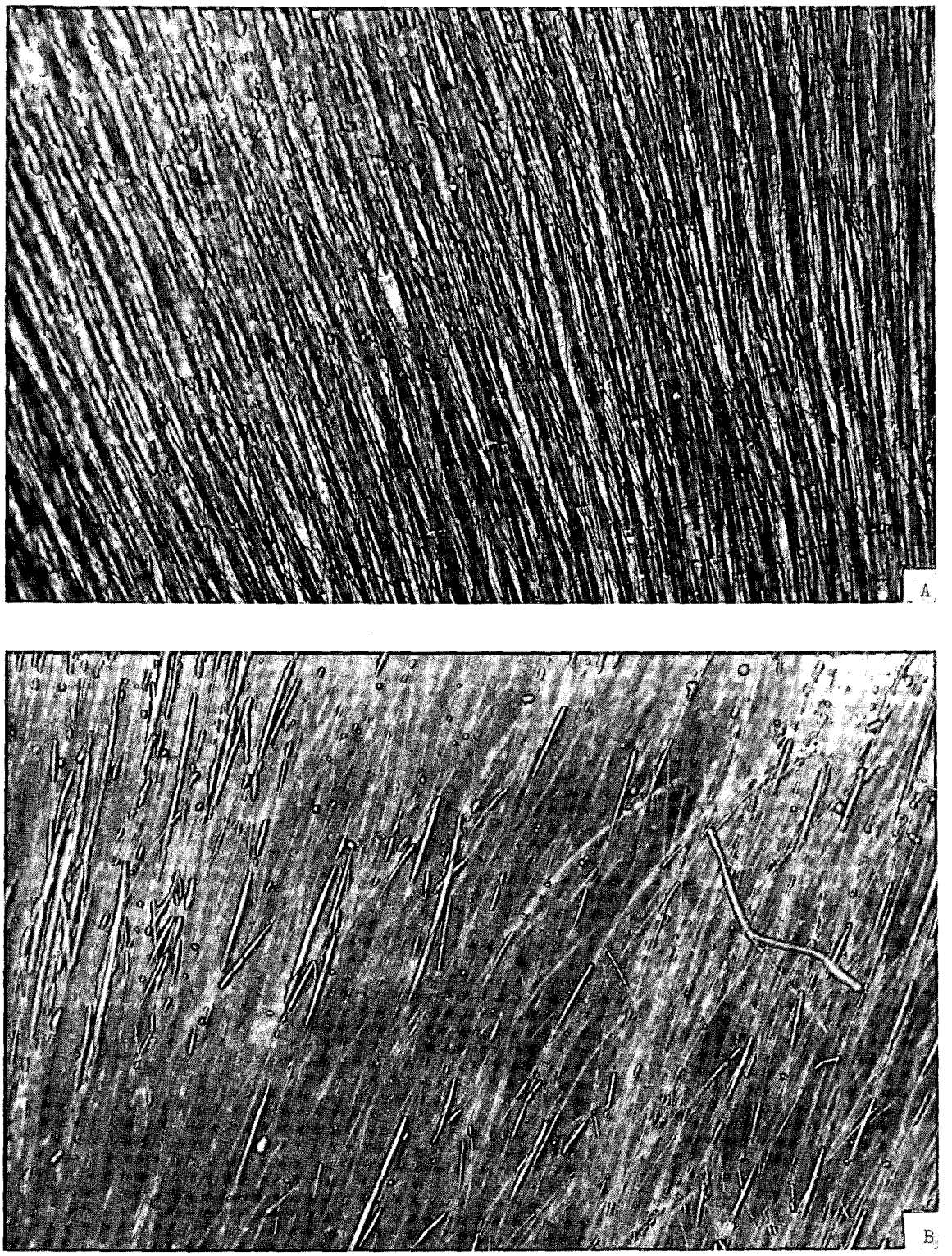

Fig. 2

TECHNICAL INFORMATION DIVISION
LAWRENCE BERKELEY LABORATORY
UNIVERSITY OF CALIFORNIA
BERKELEY, CALIFORNIA 94720